

Faculdade de Engenharia da Universidade do Porto



Traction Control in Electric Vehicles

Tiago Oliveira Bastos Pinto de Sá

Dissertation prepared under the
Master in Electrical and Computers Engineering

Major Automation

Supervisor: Adriano Carvalho

July 2012

A Dissertação intitulada

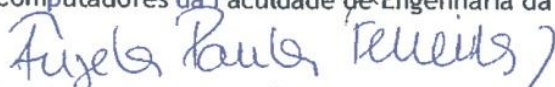
“Traction Control in Electric Vehicles”

foi aprovada em provas realizadas em 20-07-2012

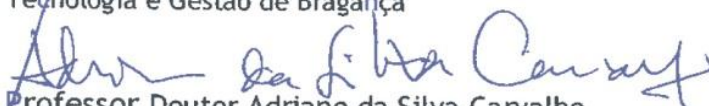
o júri



Presidente Professor Doutor António José de Pina Martins
Professor Auxiliar do Departamento de Engenharia Electrotécnica e de
Computadores da Faculdade de Engenharia da Universidade do Porto



Professora Doutora Ângela Paula Barbosa da Silva Ferreira
Professor Adjunto do Departamento de Electrotecnia da Escola Superior de
Tecnologia e Gestão de Bragança



Professor Doutor Adriano da Silva Carvalho
Professor Associado do Departamento de Engenharia Eletrotécnica e de
Computadores da Faculdade de Engenharia da Universidade do Porto

O autor declara que a presente dissertação (ou relatório de projeto) é da sua exclusiva autoria e foi escrita sem qualquer apoio externo não explicitamente autorizado. Os resultados, ideias, parágrafos, ou outros extratos tomados de ou inspirados em trabalhos de outros autores, e demais referências bibliográficas usadas, são corretamente citados.



Autor - Tiago Oliveira Bastos Pinto de Sá

Faculdade de Engenharia da Universidade do Porto

To my mother and grandma

Resumo

O sector dos transportes é um dos maiores setores industriais hoje em dia. Desde o desenvolvimento do motor de combustão interna e da sua aplicação ao setor dos transportes, as pessoas estão cada vez mais dependentes de uma forma económica e confortável de viajar.

Com o aumento do preço dos combustíveis fósseis causado pela sua procura excessiva, e com as recentes preocupações ambientais relativas à emissão de gases poluentes gerados pela queima do combustível, a existência de uma alternativa é fulcral. A forma de transporte alternativo mais comum num ambiente urbano é o autocarro. É mais barato, mais conveniente em determinados casos e produz menos poluição *per capita* do que um carro próprio. No entanto, continua a poluir.

Com isto em mente, e com a recente eminência dos motores elétricos no setor dos transportes, é analisado o controlo de motores síncronos de ímanes permanentes, em particular a aplicação de um de 150kW num autocarro elétrico. O objetivo deste documento é analisar o domínio do controlo na mobilidade elétrica e discutir o projeto do controlador que alimenta o motor, permitindo o seu acionamento e travagem, com a possibilidade de regenerar a energia da travagem, recarregando dessa forma as baterias. O sistema deverá ser capaz de funcionar sem sensores de velocidade ou posição.

Pretende-se validar os resultados obtidos na simulação aplicando um motor menos potente do que o objetivo final, de forma a poder validar laboratorialmente esses mesmos resultados. O propósito final deste trabalho é ser implementado num autocarro elétrico da empresa CaetanoBus, melhorando desta forma o sistema de tração já existente.

Abstract

Transportation sector is one of the biggest industrial sectors nowadays. Since the development of the internal combustion engine and its application in the transportation sector, people are becoming more dependent on a more economic and comfortable way of traveling.

With the constant increase in fossil fuels' price caused by the excessive demand, and with recent environmental concerns relatively to toxic gases emissions, the search of alternative ways of locomotion becomes crucial. Urban buses are the most common alternative to the usage of own vehicle. However, they still produce toxic gases.

Having this in consideration and taking advantage of the recent eminence of electric motors on transportation sector, it is analyzed the control of permanent magnet synchronous motors, in particular an application of a 150kW motor on an electric bus. This document aims at analyzing the control domain in electric mobility and discussing the design of the controller that drives the motor, allowing its driving and braking, with the ability to regenerate braking energy for recharging the batteries. The system should be capable of working without speed or position sensors.

It is intended to validate the simulation results applying a less powerful motor than the one to be used as the final objective, in order to achieve a laboratorial validation of those results. The final purpose of this work is to be applied in an electric bus from the company CaetanoBus, enhancing the traction control already existent.

Acknowledgments

I would like to express my gratitude to my supervisor Adriano da Silva Carvalho for his guidance and suggestions along the development of this work.

I wish to thank my teammate and friend Ricardo Soares who also collaborate in the development of the work, for his constant high motivation level and exchange of ideas.

I want to give my most special thanks to my lovely girlfriend Cátia Albergaria for being there every time I needed and for her constant encouragement.

To all my friends and comrades for all the great moments provided all over the years, for the help and motivation given in the worst times, for the knowledge sharing and essentially for being part of my life. It has been a pleasure.

Finally, to my family I would like to sincerely thank, specially my brother who always supported me, and my mother and grandmother who have always been there in every stage of my life and made possible the journey of the last 5 years in this University. To them I dedicate this thesis.

Contents

RESUMO	V
ABSTRACT	VII
ACKNOWLEDGMENTS	IX
CONTENTS.....	XI
LIST OF FIGURES.....	XIII
LIST OF TABLES.....	XV
ABBREVIATIONS AND SYMBOLS.....	XVII
CHAPTER 1	1
INTRODUCTION.....	1
1.1. Motivation.....	1
1.2. About the Project	2
1.3. Document Structure	2
CHAPTER 2	5
ELECTRICAL TRACTION IN THE POWER TRAIN	5
2.1. System Overview	5
2.2. System Requirements.....	8
2.3. Electronic Power Converters (EPC).....	9
2.3.1. “High Efficiency” Converters	9
2.3.2. DC/DC ZVS Bidirectional Converter with <i>Phase-Shift</i> + PWM	11
2.3.3. Improved DC/DC <i>buck/boost</i> Bidirectional Converter.....	12
2.3.4. Isolated Full Bridge Converter	12
2.3.5. Three-phase Inverter.....	13
2.4. Types of Control	13
2.5. Market Research	17
2.5.1. Selling of the Regenerative Braking System	17
2.5.2. Electric Vehicles With Regenerative Braking	17
2.6. Summary	18
CHAPTER 3	19
PERMANENT MAGNET SYNCHRONOUS MOTOR	19
3.1. Introduction.....	19
3.2. Types of Permanent Magnet Synchronous Motors	20
3.3. PMSM Modeling.....	22
3.4. Definitions of Torque Angle.....	26

3.5. Relations Between Torque Angle, Current and Air-gap Flux	28
3.5.1. Torque dependability on I_s and λ_s	28
3.5.2. Torque dependability on θ_T	29
3.6. Used Motor's Parameters and Simulation	29
3.7. Summary	30
CHAPTER 4	31
CONTROL OF THE PMSM	31
4.1. Introduction.....	31
4.2. Control Strategy	32
4.2.1. Control Methods	32
4.2.2. Control Signal Generation for the Inverter.....	36
4.2.3. Controllers' Tuning	41
4.3. Controller platform.....	45
4.4. Partial Results Analysis.....	47
4.4.1. Stator current vector angle (θ_i) at 90 degrees with sine-PWM.....	48
4.4.2. Air-gap flux vector angle (θ_λ) at 90 degrees with sine-PWM.....	49
4.4.3. MTPA with sine-PWM	50
4.4.4. MTPA with SVM.....	52
4.5. System Behavior Based on Power Balance.....	53
4.5.1. Power definitions	53
4.5.2. Mathematical Expressions	54
4.5.3. P-Q Theory	56
4.5.4. Power Control	57
4.6. Summary	60
CHAPTER 5	63
SYSTEM SENSORLESS CONTROL.....	63
5.1. Introduction.....	63
5.2. Sensorless Techniques Comparison	63
5.2.1. Back-EMF Estimator	64
5.2.2. State Observer.....	64
5.2.3. Sliding-mode Observer	65
5.2.4. High-frequency Signal Injection.....	65
5.2.5. PLL-based Estimator	66
5.3. Sensorless Control Results	68
5.4. Summary	71
CHAPTER 6	73
SYSTEM VALIDATION.....	73
6.1. Introduction.....	73
6.2. Regenerative Braking	73
6.3. System Performance Detailed Analysis	77
6.4. Hardware Implementation	81
6.5. Summary	83
CHAPTER 7	85
CONCLUSION.....	85
7.1. Final Conclusions	85
7.2. Future Work	87
REFERENCES	89

List of Figures

FIG 2.1 – SCHEMATIC OF A GENERIC ELECTRIC VEHICLE’S COMPONENTS WITH POSSIBLE SOLUTIONS [1].	5
FIG 2.2 – RELATIONAL SCHEMATIC OF GENERIC ELECTRIC VEHICLE COMPONENTS [1].	6
FIG 2.3 – BLDC AND PMSM STATOR FLUX LINKAGE AND BACK-EMF WAVEFORMS [2].	7
FIG 2.4 – SEVERAL HIGH EFFICIENCY SWITCHING CONVERTERS’ TOPOLOGIES [3].	10
FIG 2.5 – IMPROVED HIGH EFFICIENCY CONVERTERS TOPOLOGIES: UNIDIRECTIONAL (FROM A TO C) AND BIDIRECTIONAL (D) [3].	11
FIG 2.6 - DC/DC ZVS BIDIRECIONAL CONVERTER [4].	11
FIG 2.7 – IMPROVED DC/DC BUCK/BOOST BIDIRECTIONAL CONVERTER [5].	12
FIG 2.8 – ISOLATED FULL BRIDGE CONVERTER.	12
FIG 2.9 - THREE-PHASE INVERTER TO BE USED, WITH BRAKING CHOPPER AND DC LINK FILTER.	13
FIG 2.10 - REPRESENTATION OF λ_s , i_s AND v_s , AS THEIR dq COMPONENTS AND ANGLES RELATIONS AT A RANDOM POINT OF OPERATION. MODULES MUST NOT BE CONSIDERED.	15
FIG 3.1 – ROTOR ARRANGEMENTS OF PMSM: A) SURFACE MOUNTED (SPM), B) INSET SURFACE MOUNTED AND C) INTERIOR MOUNTED (IPM) [6].	20
FIG 3.2 – IPM ROTOR WITH FOUR POLES WITH A) TANGENTIALLY MAGNETIZED PMs AND B) RADIALLY MAGNETIZED PMs [6].	21
FIG 3.3 – MAGNETIC FLUX PATHS IN A) SPM MOTOR AND B) IPM MOTOR [7].	22
FIG 3.4 – REPRESENTATION OF THE THREE REFERENCE FRAMES: THREE-PHASE, dq AND ab . d -AXIS ALIGNED WITH ROTOR FLUX. a -AXIS ALIGNED WITH PHASE-A.	24
FIG 3.5 – d AND q REPRESENTATION CIRCUITS OF A PMSM.	25
FIG 3.6 – DLL MODEL OF PMSM IN PSIM SOFTWARE.	30
FIG 4.1 - PSIM CONTROL SCHEME WITH i_s VECTOR AT 90 DEGREES METHOD.	34
FIG 4.2 - PSIM CONTROL SCHEME WITH λ_s AT 90 DEGREES METHOD.	35
FIG 4.3 - PSIM CONTROL SCHEME WITH MTPA METHOD.	36
FIG 4.4 - SVM STATES ACCORDING TO INVERTER’S TRANSISTORS STATE.	38
FIG 4.5 - SVM SEQUENCE FOR ODD SECTOR.	40
FIG 4.6 - SVM SEQUENCE FOR EVEN SECTOR.	40
FIG 4.7 – SVM MODEL DESIGNED IN PSIM WITH DIFFERENT STEPS HIGHLIGHTED.	40
FIG 4.8 – SIMPLIFIED BLOCK DIAGRAM OF THE SYSTEM.	43
FIG 4.9 – SIMPLIFIED SYSTEM IMPLEMENTED IN SIMULINK.	43
FIG 4.10 – REPRESENTATION OF FPGA ARCHITECTURE.	46
FIG 4.11 – TORQUE REFERENCE AND LOAD TORQUE PATTERN. EXPECTED SPEED BEHAVIOR.	47
FIG 4.12 - RESULTS FOR i_s AT 90° WITH SINE-PWM. TOP GRAPHIC: TORQUE PRODUCED, LOAD TORQUE AND ROTOR ANGULAR SPEED; BOTTOM GRAPHIC: i_d AND i_q .	48
FIG 4.13 - RESULTS FOR i_s AT 90° WITH SINE-PWM. TOP GRAPHIC: STATOR CURRENT ANGLE θ_i AND AIR-GAP FLUX ANGLE θ_λ ; BOTTOM GRAPHIC: i_s AND λ_s (x1000) MODULES.	49
FIG 4.14 - RESULTS FOR λ_s AT 90° WITH SINE-PWM. TOP GRAPHIC: TORQUE PRODUCED, LOAD TORQUE AND ROTOR ANGULAR SPEED; BOTTOM GRAPHIC: i_d AND i_q .	49
FIG 4.15 - RESULTS FOR λ_s AT 90° WITH SINE-PWM. TOP GRAPHIC: STATOR CURRENT ANGLE θ_i AND AIR-GAP FLUX ANGLE θ_λ ; BOTTOM GRAPHIC: i_s AND λ_s (x1000) MODULES.	50
FIG 4.16 - RESULTS FOR MTPA WITH SINE-PWM. TOP GRAPHIC: TORQUE PRODUCED, LOAD TORQUE AND ROTOR ANGULAR SPEED; BOTTOM GRAPHIC: i_d AND i_q .	51

FIG 4.17 - RESULTS FOR MTPA WITH SINE-PWM. TOP GRAPHIC: STATOR CURRENT ANGLE θ_I AND AIR-GAP FLUX ANGLE θ_Λ ; BOTTOM GRAPHIC: I_S AND Λ_S (x1000) MODULES.....	51
FIG 4.18 - RESULTS FOR MTPA WITH SVM. TOP GRAPHIC: TORQUE PRODUCED, LOAD TORQUE AND ROTOR ANGULAR SPEED; BOTTOM GRAPHIC: I_D AND I_Q	52
FIG 4.19 - RESULTS FOR MTPA WITH SVM. TOP GRAPHIC: STATOR CURRENT ANGLE θ_I AND AIR-GAP FLUX ANGLE θ_Λ ; BOTTOM GRAPHIC: I_S AND Λ_S (x1000) MODULES.....	52
FIG 4.20 – POWER TRIANGLE	55
FIG 4.21 – SENSORLESS CONTROL BASED ON POWER BALANCE. TOP LEFT: ELECTROMAGNETIC TORQUE CALCULUS; TOP RIGHT: DYNAMIC FILTER GAIN; BOTTOM LEFT: ACTIVE POWER CALCULUS; BOTTOM RIGHT: REACTIVE POWER CALCULUS.....	58
FIG 4.22 - BODE DIAGRAM OF A FIRST-ORDER LOW-PASS FILTER. $f_c = 5\text{Hz}$	59
FIG 4.23 – BODE DIAGRAM OF A SECOND-ORDER LOW-PASS FILTER. $f_c = 5\text{Hz}$	60
FIG 5.1 – PLL-BASED ESTIMATOR LOGIC [8].	66
FIG 5.2 - PLL-BASED SENSORLESS SPEED AND POSITION ESTIMATOR IMPLEMENTED IN SIMULINK.	69
FIG 5.3 - SENSORLESS OPERATION. TOP GRAPHIC: TORQUE PRODUCED AND LOAD TORQUE. BOTTOM GRAPHIC: I_D AND I_Q . ..	70
FIG 5.4 – SENSORLESS OPERATION. TOP GRAPHIC: ROTOR ELECTRICAL ANGULAR SPEED (ω_r – ESTIMATED; ω_{r_real} – MEASURED); BOTTOM GRAPHIC: ROTOR ELECTRICAL POSITION (θ – ESTIMATED; θ_{real} – MEASURED).....	71
FIG 6.1 – PLL-BASED SPEED AND POSITION ESTIMATOR IMPLEMENTED IN PSIM.	74
FIG 6.2 - SENSORLESS OPERATION WITH REGENERATIVE BRAKING. TOP GRAPHIC: TORQUE CALCULATED AND TORQUE PRODUCED. BOTTOM GRAPHIC: I_D AND I_Q	75
FIG 6.3 - SENSORLESS OPERATION. TOP GRAPHIC: ROTOR ELECTRICAL ANGULAR SPEED (ω_r – ESTIMATED; ω_{r_real} – MEASURED); BOTTOM GRAPHIC: ROTOR ELECTRICAL POSITION (θ – ESTIMATED; θ_{real} – MEASURED).....	75
FIG 6.4 – DETAIL OF THE ESTIMATED POSITION ERROR.	76
FIG 6.5 - DC-BUS AVERAGE CURRENT I_{DC} IN TRACTION AND BRAKING, WITH SENSORLESS OPERATION.....	76
FIG 6.6 – RIPPLE DETAIL OF (TOP) TORQUE AND (BOTTOM) STATOR CURRENT, WITH SINE-PWM AT 10kHz.	77
FIG 6.7 - RIPPLE DETAIL OF (TOP) TORQUE AND (BOTTOM) STATOR CURRENT, WITH SVM AT 10kHz.....	78
FIG 6.8 – STATOR CURRENT VECTOR ANGLE θ_I AND AIR-GAP FLUX VECTOR ANGLE θ_Λ	79
FIG 6.9 – TORQUE ANGLE DETAIL FOR POSITIVE TORQUE.	79
FIG 6.10 – TORQUE ANGLE DETAIL FOR NEGATIVE TORQUE.	80
FIG 6.11 – BACK-EMF PRODUCED BY THE MOTOR.....	80
FIG 6.12 – REGENERATIVE FEATURE LIKE CRUISE-CONTROL. TOP: TORQUE PRODUCED AND LOAD TORQUE; MIDDLE: ROTOR ANGULAR SPEED; BOTTOM: DC-BUS CURRENT.....	81
FIG 6.13 – BLOCK DIAGRAM OF INFINEON HYBRID KIT FOR HYBRIDPACK™1 [9].....	82
FIG 6.14 – INFINEON IGBT DRIVER MODULE FOR HYBRIDPACK™1.	83

List of Tables

TABLE 1.1 – DISSERTATION STRUCTURE	3
TABLE 2.1 - SUBJECTIVE COMPARISON BETWEEN DIFFERENT TYPES OF MOTORS FOR ELECTRIC VEHICLES APPLICATION (0 TO 5 SCALE) [1].	6
TABLE 3.1 – NOMINAL VALUES OF THE PMSM USED IN SIMULATION.	29
TABLE 3.2 – PARAMETERS OF THE PMSM USED IN SIMULATION.	29
TABLE 4.1 – SWITCHING VECTORS COMBINATIONS.	38
TABLE 4.2 – EXAMPLE OF A SVM TABLE FOR TRANSISTOR T1.....	40
TABLE 4.3 – ZIEGLER-NICHOLS METHOD.	42
TABLE 4.4 – INFLUENCE OF INCREASING CONTROLLER PARAMETER IN RESPONSE BEHAVIOR.	44
TABLE 4.5 – I_d PI GAINS.....	44
TABLE 4.6 – TORQUE PI GAINS.	44
TABLE 5.1 – SENSORLESS PLL PI GAINS.	69
TABLE 6.1 – INFINEON SINGLE DRIVER 1ED020I12-FA.	82
TABLE 6.2 - CONCEPT DUAL-CHANNEL DRIVER 2SC0108T.....	82

Abbreviations and Symbols

Abbreviations (alphabetical order)

ABS	Anti-lock Braking System
AC	Alternating Current
ADC	Analog-to-Digital Converters
ANN	Artificial Neural Networks
BLDC	Brushless DC Motor
BMS	Battery Management System
CPU	Central Processing Unit
DC	Direct Current
DLL	Dynamic-Link Library
DSP	Digital Signal Processor
DTFC	Direct Torque and Flux Control
DTC	Direct Torque Control
ELO	Extended Luenberger Observer
EKF	Extended Kalman Filter
EMF	Electromotive force
EPC	Electronic Power Converter
EV	Electric Vehicle
FOC	Field-Oriented Control
FPGA	Field Programmable Gate Array
HRB	Rexoroth's Hydrostatic Regenerative Braking system
ICE	Internal Combustion Engine
IGBT	Insulated Gate Bipolar Transistor
INFORM	Indirect Flux detection by On-line Reactance Measurement
IPM	Interior mounted Permanent Magnets
MMF	Magnetomotive force
MTPA	Maximum Torque Per Ampere
OTD	One Time Programmable
p.u.	per-unit
PI	Proportional Integrative Controller

PID	Proportional Integrative Derivative controller
PLL	Phase-Locked Loop
PM	Permanent Magnet
PMSM	Permanent Magnet Synchronous Motor
PWM	Pulse-Width Modulation
QRAS	Quasiresonant Regenerating Active Snubber
RMS	Root Mean Square
SAZZ	Snubber Assisted Zero Voltage and Zero Current Transition
SPM	Surface mounted Permanent Magnets
SRAM	Static Random-Access Memory
SRM	Switched Reluctance Motors
SVM	Space Vector Modulation
TCS	Traction Control System
VHDL	VHSIC hardware description language
VHSIC	Very High Speed Integrated Circuit
ZCT	Zero-Current Transition
ZVT	Zero-Voltage Transition
ZCS	Zero-Current Switching
ZVS	Zero-Voltage Switching

Symbols

∂	Differential operator
θ	Rotor angular position
θ_i	Stator current angle
θ_λ	Air-gap flux angle
θ_T	Torque angle
λ_α	α -axis flux component
λ_β	β -axis flux component
λ_d	Direct-axis flux component
λ_{ds}^r	Direct-axis flux component
λ_f	Rotor magnetic flux
λ_q	Quadrature-axis flux component
λ_{qs}^r	Quadrature-axis flux component
λ_s	Air-gap flux vector
ξ	Damping factor
ξ	Saliency (or anisotropy) ratio
φ	Power-factor angle
ω_c	Cut-off frequency
ω_e	Rotor electrical angular speed

ω_r	Rotor angular speed
B	Friction coefficient
e_d	Direct-axis back-EMF component
e_q	Quadrature-axis back-EMF component
f_1	Reference signal fundamental frequency
f_{tri}	Carrier signal frequency
F_p	Power factor
$i(t)$	Instantaneous current
$\mathbf{i}_{\alpha\beta}$	Current vector on $\alpha\beta$ reference frame
i_α	α -axis current component
i_β	β -axis current component
$i_{a,b,c}$	a,b,c phase current
i_{as}	Stator phase a current
i_{bs}	Stator phase b current
i_{cs}	Stator phase c current
i_{dc}	DC-bus current
i_d	Direct-axis stator current
i_f	Stator current flux component
i_q	Quadrature-axis stator current
i_T	Stator current torque component
I_s	Stator current vector
I_{sn}	Normalized stator current
J	Moment of Inertia
K_p	Proportional gain
K_d	Derivative gain
K_i	Integral gain
L_d	Direct-axis Inductance
L_q	Quadrature-axis Inductance
L_s	Stator phase inductance
m_a	Modulation index
m_f	Frequency index
p	Number of poles
p	Instantaneous active power
$p(t)$	Instantaneous useful power
P	Active power
$P_{winding}$	Winding losses
q	Instantaneous reactive power
Q	Reactive Power
Q_G	Gate Charge
R_s	Stator phase resistance
s	Complex power

$t_d \text{ OFF}$	Turn-OFF delay time
$t_d \text{ ON}$	Turn-ON delay time
t_f	Fall time
t_r	Rise time
T_b	Base (nominal) torque
T_d	Derivative time constant
T_{em}	Electromagnetic torque
T_{emn}	Normalized electromagnetic torque
T_i	Integrative time constant
T_L	Load torque
T_m	SVM modulation period
$v_{\alpha\beta}$	Voltage vector on the $\alpha\beta$ reference frame
v_α	α -axis voltage component
v_β	β -axis voltage component
$v(t)$	Instantaneous voltage
$v_{a,b,c}$	a,b,c phase voltages
V_d	Direct-axis stator voltage
V_{dc}	DC-bus voltage
V_{GES}	Gate-emitter Peak Voltage
V_{Geth}	Gate Threshold voltage
V_q	Quadrature-axis stator voltage
V_{Ref}	Reference signal amplitude
V_s	Stator Voltage vector
V_{tri}	Carrier signal amplitude
$W(t)$	Electric energy
x_d	Synchronous reactance

Chapter 1

Introduction

This dissertation is prepared to analyze control methodologies in electric mobility and within the scope of a project whose objective is to design an electronic power converter control to be applied in an electric urban bus, which should be capable of driving and braking it with the possibility of reuse the braking energy. The electric motor is a 150kW permanent magnet synchronous motor which pulls a CaetanoBus' electric urban bus.

The development of the work was done together with Ricardo Soares [10] whose core of the dissertation is within the same domain but with different scopes, and with the supervision of Adriano Carvalho.

1.1. Motivation

Transportation is one of the most important social sectors nowadays. Travelling from one point to another is now easier than ever and in some developed countries going from home to work every day by foot is not even a possibility. This was only possible with the invention and development of the internal combustion engine, which provided a new perspective over the transportation. However, besides all the benefits and comfort that it brings, the abusive use of fossil fuels and environmental concerns led to a new form of mobility made possible nowadays: the electric motor. This opens doors to a new era in transportation, more efficient, cleaner and cheaper.

Being the autonomy of electric vehicles one of the biggest obstacles to their production nowadays, an efficient regenerative braking system is an important approach to the development of more and better economic and ecological transportation solutions. So and motivated by the prominence and immediacy of the subject, it is proposed a work whose goal is to model an electronic power converter control, in order to enable bidirectional power flow, allowing the drive of an urban bus' electric motor with the possibility of recover energy from regenerative braking operation to recharge the batteries. The model should be later implemented in a prototype which will prove the results obtained in simulation.

With this project it is expected a contribution to the development of the traction control system to the CaetanoBus electric urban bus, more efficient and safer, increasing the range of the batteries and capable to satisfy CaetanoBus' demands.

1.2. About the Project

The approach to this problem assumes that the electric motor already exists and that is a 150kW permanent magnet synchronous motor. All of the vehicle's traction system is already functional. However, although its functionality is unknown because it is property of CaetanoBus, some imperfections are identified. Therefore, the proposed problem where this project is inserted consists in developing a traction control system with capability of regenerative breaking that would be more efficient than the actual one, with safety warranties and whose functionality is completely transparent to the driver, allowing the inclusion of the electric bus in any fleet already existent.

This document pretends to demonstrate the development process through modeling and functional testing of the described system. Initially, a literature review within the scope of energy reuse to recharging of the batteries in electric vehicles is presented. The solutions presented are the result of a research in several scientific articles, engineering books and Internet in general. Here, some issues beyond the specific scope of the project will be discussed as they concern electric mobility. These issues are essential to a better understanding of the content in which they're inserted, but they will not be detailed for the same reason. Among them are the power electronic converters, responsible to ensuring the interface between batteries and DC bus. Then, a brief explanation and comparison of existing electric motors is done, followed by the modeling and functional explanation of the motor used. Control methods are then described where some important considerations are made. The results of several simulations are shown and analyzed and conclusions are drawn. The simulation software products to be used are PSIM from PowerSim and MatLab Simulink from Mathworks. At the end, the designed controller will be prototyped and tested with a scalable motor - 50kW motor - than the real one.

Regarding the boundaries of this project, their limits are the virtual implementation of the traction control system for the permanent magnet synchronous motor with regenerative breaking, with the possibility of creating its scalar prototype. The project does not include any other sub-system of the bus power train, neither any other sub-system of the vehicle itself. However, it is possible that some issues may be discussed in relation with the main subject-matter, thus allowing a better understanding of this project.

1.3. Document Structure

This document is divided in 7 chapters. Chapter 2 shows an overview of what is currently done in electric traction.

Chapter 3 describes the modulation of the motor as well as some considerations about the types of permanent magnets synchronous motors existent.

Chapter 4 details the procedures of the control design, explaining each step and discussing the results obtained in simulation tests.

Chapter 5 shows the sensorless position and speed control techniques known nowadays and describes the technique used in this work, with results analysis and discussion.

In Chapter 6 the system validation is done with the detailed analysis of the motor operation, including regenerative braking with sensorless system.

Lastly, in Chapter 7 final conclusions are drawn and some suggestions about future developments based on the work here described are given.

Table 1.1 - Dissertation structure

Chapter 1 - Introduction
Chapter 2 - Electrical Traction in the Power Train
Chapter 3 - Permanent Magnet Synchronous Motor
Chapter 4 - Control of the PMSM
Chapter 5 - System Sensorless Operation
Chapter 6 - System Validation
Chapter 7 - Conclusions

Chapter 2

Electrical Traction in the Power Train

2.1. System Overview

In this section it is pretended to summarize the components that are part of a generic electric vehicle (EV). For each component potential implementation solutions are presented, according to different perspectives: for the electronic controller, several software and hardware solutions are presented; for the electronic power converter, different transistors are described, as some topologies made with them; finally, for the electric motor, some types of motors are shown as well as simulation possibilities. Fig 2.1 schematizes the approach to subsystems of EV powertrain.

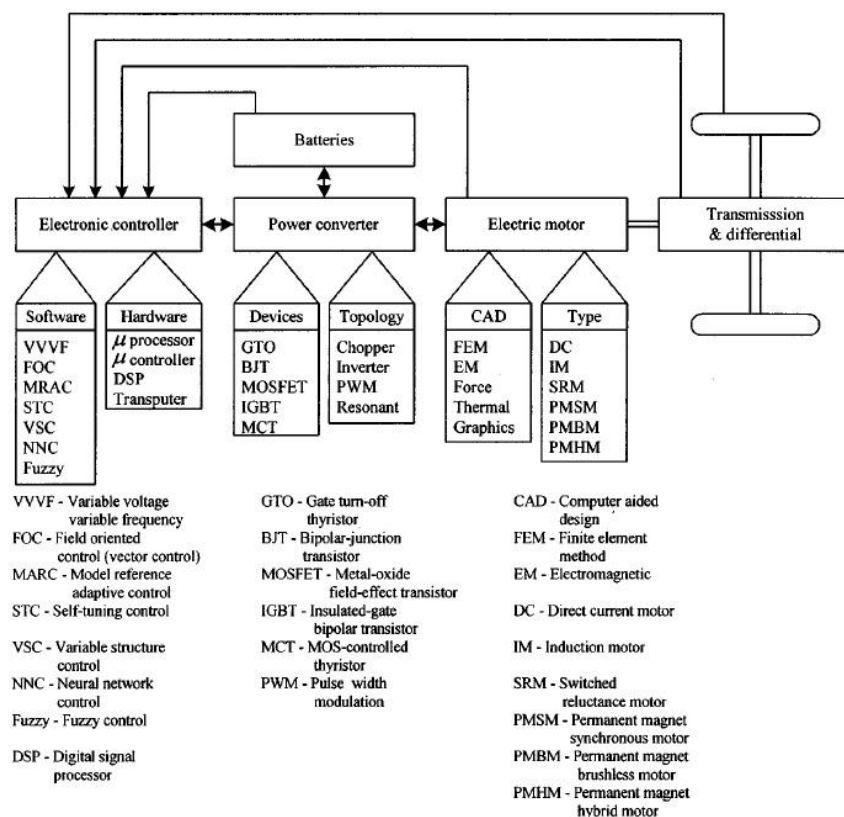


Fig 2.1 - Schematic of a generic electric vehicle's components with possible solutions [1].

Fig 2.2 describes with more detail the elements that are associated to an electric vehicle, establishing a relation among them, without any solution suggestion. This schematic pretends to show more precisely what is involved in electric vehicles traction and the relations between subsystems. It should be noted that the block “Auxiliary subsystem” will not be considered in this work, however it has to be considered at designing this sort of vehicles.

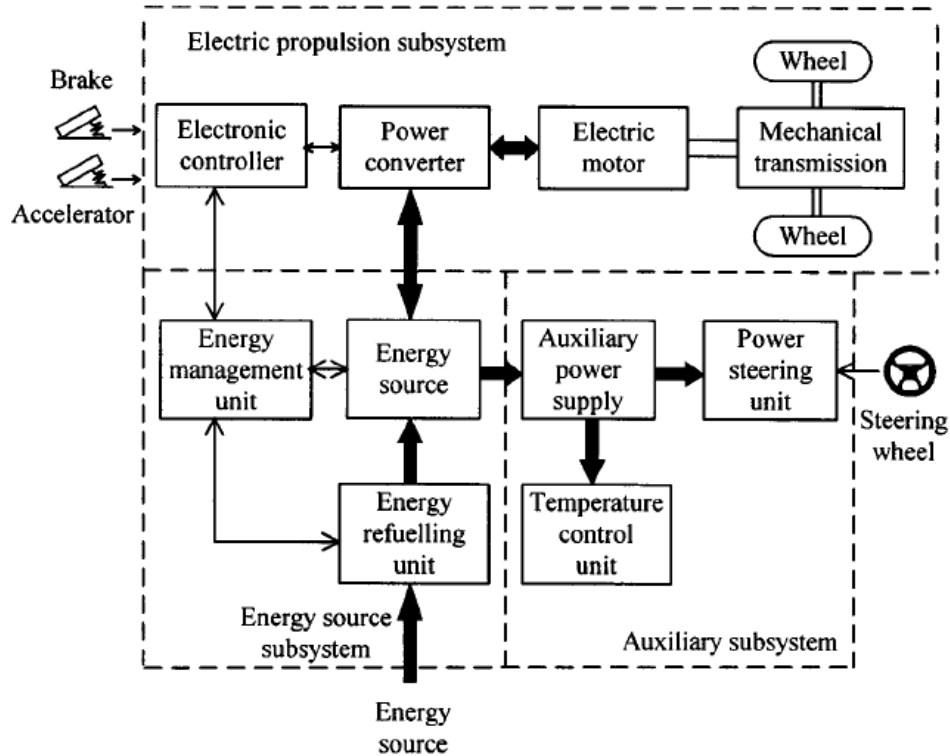


Fig 2.2 - Relational schematic of generic electric vehicle components [1].

Next a table with a qualitative and comparative evaluation of five types of electric motors is presented. It is noteworthy the Permanent Magnet Brushless Motor which, despite not having the best grades, has two main characteristics that are important when discussing about electric vehicles: power density and efficiency. Therefore, it would be a good choice.

Table 2.1 - Subjective comparison between different types of motors for electric vehicles application (0 to 5 scale) [1].

	DC motor	Induction motor	PM brushless motor	SR motor	PM hybrid motor
Power density	2.5	3.5	5	3.5	4
Efficiency	2.5	3.5	5	3.5	5
Controllability	5	4	4	3	4
Reliability	3	5	4	5	4
Maturity	5	5	4	4	3
Cost	4	5	3	4	3
Total	22	26	25	23	23

Permanent magnet synchronous motors can be classified according to the back electromotive forces they generate. This differentiation is a consequence of the way the wiring is connected, which creates sinusoidal or trapezoidal back electromotive forces. If they're sinusoidal the motor is called Permanent Magnet Synchronous Motor (PMSM). Against, if they are trapezoidal the motor is called Permanent Magnet Brushless DC (BLDC) [11]. This difference is graphically represented in Fig 2.3.

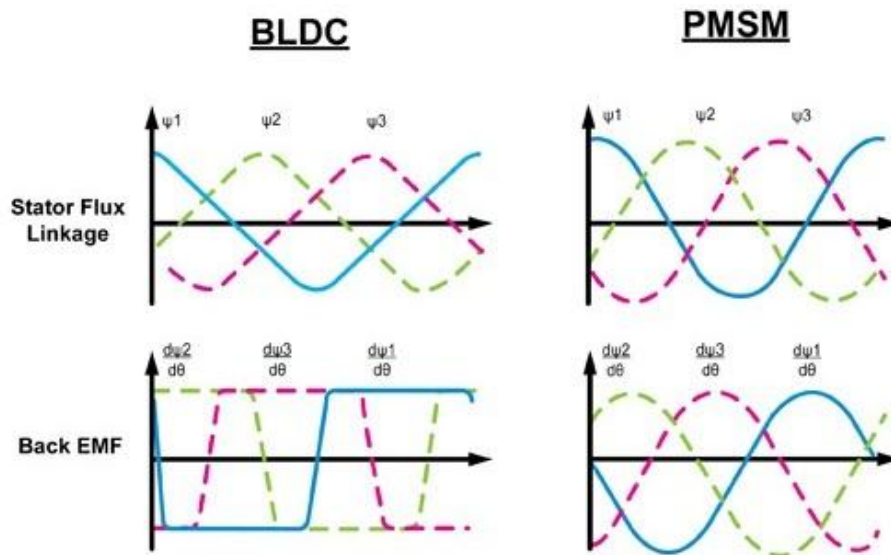


Fig 2.3 - BLDC and PMSM stator flux linkage and back-EMF waveforms [2].

Even concerning the BLDC motor, some advantages compared to the induction motors are noteworthy. This comparison is legitimate because permanent magnet synchronous motors have been replacing induction motors in many applications, since they have better efficiency, a better torque/size ratio and cover a wider range of speed and power [2].

- Since magnetic field is generated by permanent magnets of high energy density, the weight and the volume are reduced dramatically which leads to a higher power density;
- Because the rotor has no winding, there are no Joule effect losses in it, leading to a better efficiency;
- Since most of the heat is generated in the stator, it can be dissipated easily;
- The excitation of the permanent magnets is almost independent from manufacturing mistakes, overheating or mechanical damage. So, the reliability of this type of motors is much higher.

There are many types of permanent magnet motor's assemblies with respect to rotor configuration. The magnets can either be mounted on the surface or inside the rotor. The first ones have the advantage of requiring fewer magnets, reducing its weight and price. The second ones allow higher speeds and have higher flux density. Besides that, they can be classified by their flux direction: it can be either radial or axial. Radial flux is the most

common and axial type motors are used when a higher power density and acceleration is required.

Combining the advantages of permanent magnets motors with induction motors it is possible to obtain the hybrid permanent magnet motor. With a construction similar to induction motors, this type of motors operates with less quantity of copper of the stator windings, creating magnetic poles with less winding. This allows a reduction of the weight, less cooling requirement and less problems related to overheating and high starting currents. Besides that, it makes possible the ease of speed control of a DC motor without losing the reliability and efficiency of a permanent magnet motor. However, this type of motors is usually more expensive.

It should be emphasized the Switched Reluctance motor (SRM). This type of motors, very little explored yet, begins to emerge in automobile market, especially but not exclusively for in-wheel solution as presented in [12]. Its operation is similar to a step-motor's operation: the control is based on sequentially inject current in the correct stator winding in order to make rotor spins. This allows a precise control over the rotor's position. However, these motors still have the disadvantage of high purchase price and high weight, as well as control instrumentation, thus needing more development to become commercially interesting.

2.2. System Requirements

Nowadays, one of the biggest aspects to have in consideration when buying a new car is its safety. However, comfort and economy are also two important aspects to take into account. So, an electric vehicle with high autonomy and whose safety is not inferior to that in conventional (internal combustion engine) vehicles would be the ideal solution. This may be possible in a near future if a new technology is considered: regenerative braking. Regenerative braking consists in reuse the energy, usually wasted in the form of heat when the vehicle decelerates, to recharge the batteries.

In this scope some issues emerge: what happens when the batteries are full and the driver brakes? What happens to the energy in an emergency situation, such as the need of stop the vehicle in a very short amount of time? How will the system respond in a situation of repeated braking and acceleration?

Briefly, a system that regenerates energy in an EV demands two main requirements: safety and efficiency, by this order of priority:

- 1) It is necessary that the vehicle stops in a few seconds, if necessary, even at high speed, independently of the battery conditions. This probably implies the existence of an auxiliary mechanical brake.
- 2) It is also necessary that the energy regeneration is done in the most efficient way, always keeping the batteries in an optimum state of charge, which can be ensured by a good battery management system, as well as with a good traction controller.

The system should be capable of remain in duty even if the conditions are not ideal, for example if any dispensed component ceases to be operational. It is expectable that the

vehicle can continue to brake even if the entire electronic braking system fails. Lastly, the usage of kinetic energy should be balanced to ensure that the energy consumed by the braking system itself would not be higher than the energy to be stored, in the case that the vehicle is travelling at low speeds. Besides that, there are aspects like size and weight of the components that should be in consideration not so much by the buyer but mainly by the producer.

2.3. Electronic Power Converters (EPC)

The main concept regarding regenerative braking in EVs is the ability of bidirectional flow of the current. With this in mind it is easy to understand that one of the most important elements of the system is the electronic power converter. It must have two essential characteristics: it has to be capable of working with a control method that allows the bidirectionality referred before, and it has to be robust enough so the vehicle does not need more maintenance than the expected one for a normal (ICE) vehicle.

Thus, it is made a research of what is currently used in the subject of EPC applied to electric or hybrid vehicles and the results are presented next. It is noteworthy the fact that there are two EPCs responsible for the interface battery-motor: one that manages the conditions and state of charge of the batteries, that would be a DC-DC converter which will ensure the interface between batteries and the DC bus; and other that manages the power flow to the motor, responsible for accelerate or decelerate it, which will be a DC-AC converter because the motor works with AC current. Designing the controller for this EPC becomes the aim of this dissertation.

2.3.1. “High Efficiency” Converters

Fig 2.4 shows several topologies of converters used since the first years of development of EPC. The circuit in a) is a buck/boost converter, which reached the operation frequency limit in the 80's. In order to extend the frequency range and improve its power density, it was designed the circuit in b). However, the existence of excessive current and voltage peaks led to the development of another topology, presented in c): ZVT (Zero Voltage Transition). After this, it started to use “snubbers” to suppress (“snub”) voltage and current transients in circuit b) and a new topology emerged, d). To a higher boost ratio, they started to be used topologies with coupled inductors, as shown in e). Finally, designed to be used in applications to withstand power in the order of 100kW, the circuit in f) emerged.

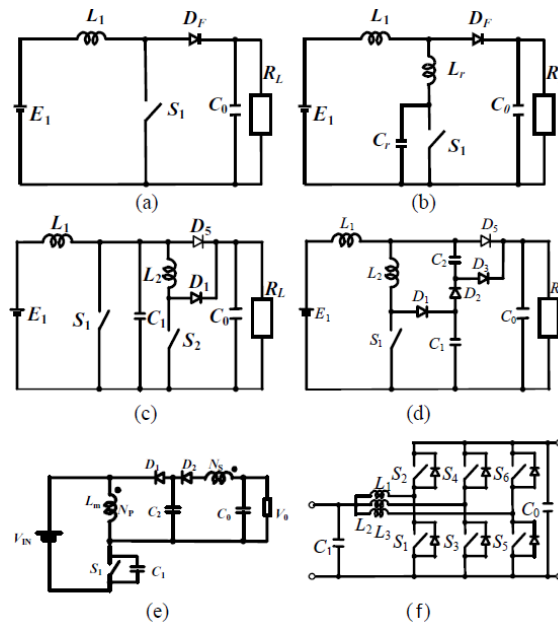


Fig 2.4 - Several high efficiency switching converters' topologies [3].

In order to improve the efficiency of the basic circuits shown before, new topologies were designed. They are shown in Fig 2.5 and described next.

The circuit in Fig 2.5 a), “C-Bridge”, was designed to an application of 8kW and 96% of efficiency at 25kHz of switching frequency. Later, circuit b) was obtained: “*Quasiresonant Regenerating Active Snubber (QRAS) Chopper Circuit*”. It could achieve ZCS (Zero Current Switching) at turning ON and ZVS (Zero Voltage Switching) at turning OFF and reuse the energy of the snubber. Its efficiency is 97.5% and it was obtained for 8kW at 25kHz. This efficiency was later improved to 98.5% using a schottky diode. The topology shown in c), named “*Snubber Assisted Zero Voltage and Zero Current Transition (SAZZ)*” implements ZVZCT (Zero-Voltage Zero-Current Transition) at turning ON and ZVS at turning OFF, using less components than QRAS topology. It was obtained 97.8% of efficiency with 8kW at 100kHz. The operation principle of this topology was applied to a bidirectional circuit, shown in d), which reached 96.6% of efficiency in boost mode and 97.4% in buck mode, working with a base power of 25kW.

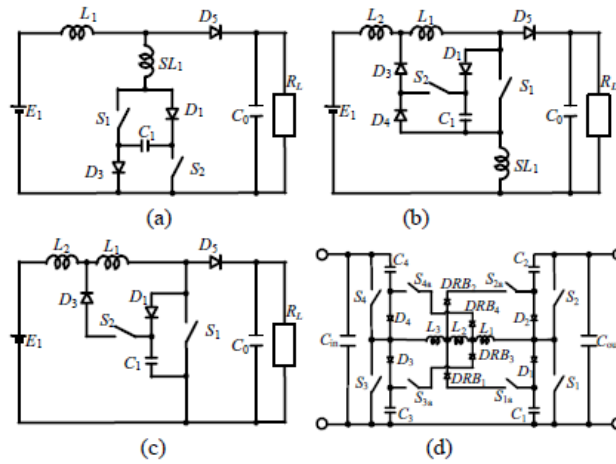


Fig 2.5 - Improved high efficiency converters topologies: unidirectional (from a to c) and bidirectional (d) [3].

2.3.2. DC/DC ZVS Bidirectional Converter with *Phase-Shift* + PWM

This topology consists in a DC/DC bidirectional converter, composed by a current fed half bridge and a voltage fed half-bridge, ensuring a balance in voltage variations in the transformer through C_{a1} and C_{a2} capacitors shown in Fig 2.6. Using PWM control in S_1 and S_2 transistors, the magnitudes of V_{ab} and V_{cd} are adjusted as there are variations in the input and output voltages, which allows to achieve ZVS in a high range of loads. The application of Phase-Shift allows controlling the magnitude and direction of the power flow.

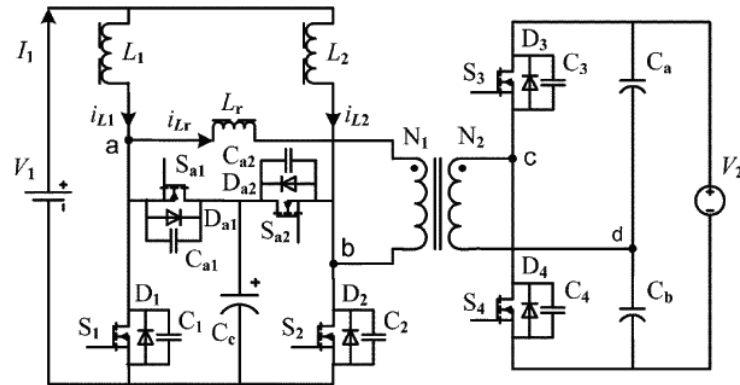


Fig 2.6 - DC/DC ZVS Bidirectional Converter [4].

A further analysis of this topology will not be done as it is not the aim of this document. More information about these topologies is available in [4].

2.3.3. Improved DC/DC *buck/boost* Bidirectional Converter

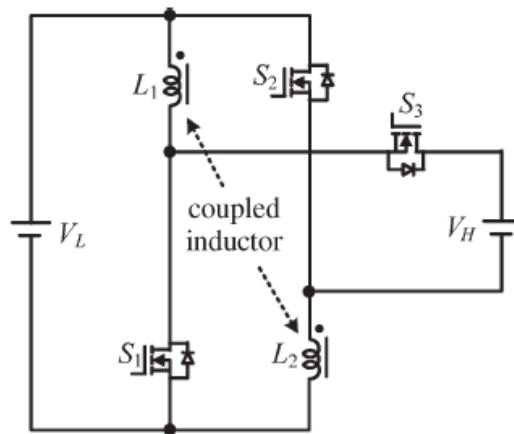


Fig 2.7 - Improved DC/DC buck/boost bidirectional converter [5].

This converter consists in a buck/boost converter in which the inductor is divided in two, sort of a transformer with two windings with equal number of turns. With appropriate control it is possible to make the turns operate in parallel at the charge and in series at the discharge, achieving a bigger step-up gain. Likewise, to buck mode, the turns operate in series at the charge and in parallel at the discharge, achieving a bigger step-down gain. To the same conditions, this converter has a smaller commutation current than the traditional one [5].

There are other topologies of converters that will not be discussed in this document because of their commonness which will not bring any added value to this document, or because of their lack of specificity regarding the application at issue [13].

2.3.4. Isolated Full Bridge Converter

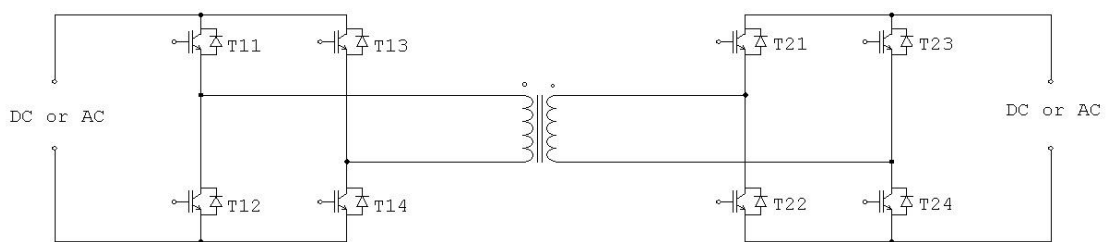


Fig 2.8 - Isolated full bridge converter.

This topology is very used in applications where bidirectional flux of energy is required but with isolation. Having two full bridges in each side of the transformer allows more and better types of control, permitting the usage of this topology to DC/DC, DC/AC, AC/DC and AC/AC applications. Despite the range of possible applications, each one requires a different and specific control. It can be either a voltage or current control, and the transistor's signal generation can be by *hysteresis*, *PWM* or by *space vector modulation* (SVM). The last one consists in sending the signal to the transistors according to the present state of the motor

(given by its variables) and the reference given (e.g.: State 1 -> T1 e T4 ON; T2 e T3 OFF). More information about SVM is given in section 4.2.2.2. This topology may also be used in three-phase applications, rather than single-phase as shown in Fig 2.8.

2.3.5. Three-phase Inverter

Considering the propose of this project, which is designing a controller for the traction of a synchronous motor through the interface DC bus-motor, considering the freedom of control and simplicity of the topology, a three-phase inverter will be used. It is also possible to be used a Braking Chopper before the inverter, as shown in Fig 2.9. This chopper, composed by a transistor and a power resistance in series, will allow the dissipation of the energy in the form of heat if the BMS decides that the batteries could not be charged anymore and the vehicle needs to decelerate. This heat could even be reused for the heating system of the vehicle.

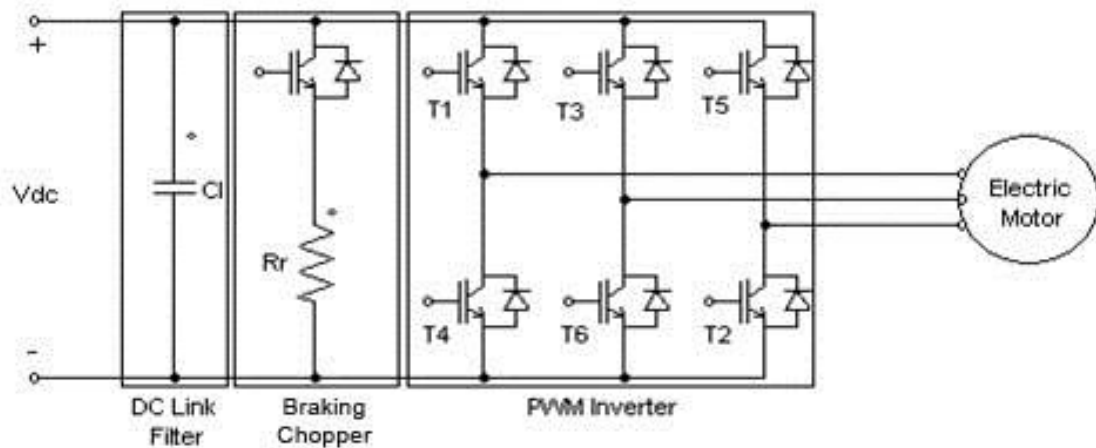


Fig 2.9 - Three-phase inverter to be used, with braking chopper and DC Link filter.

2.4. Types of Control

Motor's control can be performed in several forms. The most common types can be gathered in two main groups: scalar control and vector control. In permanent magnets motors, the most used scalar control is constant V/f . However, due to the poor results obtained in transient state, control imprecisions and phase control limitations, this type of control is becoming less used.

To overcome the obstacles imposed by the scalar control and achieve higher performances, vector control is adopted. Here, two main approaches are known: Direct Torque and Flux Control (DTFC), also called Direct Torque Control (DTC), and Field-Oriented Control (FOC). Both DTC and FOC are strategies that allow torque and flux to be decoupled and controlled independently. Unlike FOC, in DTC there is no current loop in the control

scheme. Instead, torque and flux are measured or estimated and the control loop is closed by the inverter's control signals from this data [14]. Besides that, the results obtained with DTC show that it has a better dynamic response than FOC, despite the last one having better steady-state performance. However, DTC depends on motor parameters which, in certain applications, is a counterpart with high relevance. [15]

Field-Oriented Control can be direct or indirect. Since there is no common agreement in the literature in how to distinguish between them, it is assumed that indirect FOC is based on the estimation of the flux position through stator currents and voltages and motors parameters, whereas direct FOC measures the rotor flux position, usually by Hall sensors. However, rotor flux cannot be sensed directly which means that some calculations must be done after acquiring the sensor's signal. This leads to inaccuracies, especially when the motor's speed is low and the stator resistance voltage drop dominates in the stator voltage equation. It is then preferred to use a sensorless system, eliminating those inaccuracies and providing a cheaper and more robust solution. This is the approach of the control design developed in this work and discussed in the present document.

There are also current control strategies called Trapezoidal (Six-Step) Current Control and Sinusoidal Current Control. These differ by the form of the current injected in the motor: the first one tries to inject rectangular current waveforms and is usually implemented in BLDC motors. The goal is to feed the appropriate phase of the stator in order to maintain a rotating field. The phase shift between stator and rotor fluxes must be controlled in order to produce the required torque. Sinusoidal Current Control is similar to the previous, except the currents generated are sinusoidal instead of rectangular. In this type of control there is no direct control over the torque produced making it appropriated to applications where there's no load variations.

In order to properly design the control over the motor, a reference frame should be chosen. Usually the dq reference frame is chosen to apply the vector control in synchronous machines. The dq reference frame is assumed to be rotating with an angular speed equal to the rotor electrical angular speed (or stator rotating field angular speed, which in synchronous machines is the same). Therefore, all the quantities represented in it are constant at steady-state. A representation of stator voltage and current vectors as well as rotor flux vector is shown in Fig 2.10. This situation represents a virtual motoring situation, in which stator current vector leads the air-gap flux vector. The figure is merely representative and intends to display the different relations between the vectors, so their modules must not be considered.

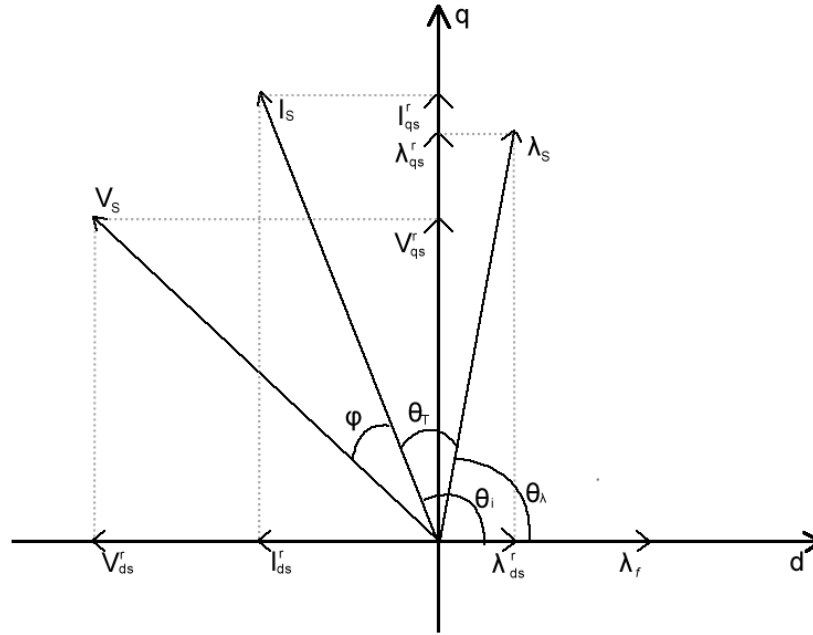


Fig 2.10 - Representation of λ_s , I_s and V_s , as their dq components and angles relations at a random point of operation. Modules must not be considered.

Regarding dq frame, it is important to refer the Park Transformation, or dq0 Transformation, responsible to convert the components of a quantity (like voltage or current) in the three-phase stationary reference frame into two-phase components in a rotating frame. It is given by:

$$P = \frac{2}{3} \begin{bmatrix} \cos(\omega_e t) & \cos(\omega_e t - \frac{2\pi}{3}) & \cos(\omega_e t + \frac{2\pi}{3}) \\ \sin(\omega_e t) & \sin(\omega_e t - \frac{2\pi}{3}) & \sin(\omega_e t + \frac{2\pi}{3}) \\ \frac{1}{2} & \frac{1}{2} & \frac{1}{2} \end{bmatrix} \quad (2.1)$$

As the system is symmetric and balanced, the homopolar component given by the last line of the matrix is not considered. So, applying the Park Transformation to the currents as an example, the following is obtained:

$$\begin{bmatrix} i_d \\ i_q \end{bmatrix} = \frac{2}{3} \begin{bmatrix} \cos(\omega_e t) & \cos(\omega_e t - \frac{2\pi}{3}) & \cos(\omega_e t + \frac{2\pi}{3}) \\ \sin(\omega_e t) & \sin(\omega_e t - \frac{2\pi}{3}) & \sin(\omega_e t + \frac{2\pi}{3}) \end{bmatrix} \begin{bmatrix} i_{as} \\ i_{bs} \\ i_{cs} \end{bmatrix} \quad (2.2)$$

Lastly, with respect to methods of electric motoring control used nowadays, five vector control methods commonly applied to drive PMSMs are exposed, with a brief explanation of each [15].

1. Constant Torque angle control

- Torque angle is maintained at 90° turning i_f current component into zero.
- It is used to speeds below rated speed.
- Power factor decreases with the increase of rotor's speed and stator currents.

2. Unit power factor control

- Unit power factor control implies that the VA ratio of the inverter is completely used to inject real power in the motor.
- This type of control is applied controlling the torque angle as a function of motor's variables and is independent of motor's speed.
- The torque angle has to be higher than 90° .

3. Constant air-gap flux linkage control

- The flux that results of stator current dq components and rotor flux, known as mutual or air-gap flux, is kept constant, usually in a value that is equal to the rotor flux.
- The stator voltage requirements are kept low.
- It is a simple method to apply flux-weakening, allowing the motor to operate with speeds above the base speed.
- Torque angle has to be higher than 90° .

4. Maximum Torque per Ampere control

- Precious control method from machine and inverter usage point of view.
- It is done controlling the torque angle.
- Better performance than constant torque angle control, at the expense of higher stator voltages.

5. Flux-Weakening control

- Voltage and current limits imposed by DC bus before the inverter make the motor's feeding also limited. This makes the speed and torque produced by the motor also limited. In some applications is necessary to have higher speeds than the maxim speed permitted by the voltage and current fed to the motor
- In order to increase the speed, air-gap fluxes are weakened making the electromotive force produced by the rotor inferior to the voltage applied.
- Flux-weakening is made to be inversely proportional to the stator frequency

One definition of electromagnetic torque as a function of θ_i is given by [15] and is presented in equation (2.3).

$$T_{em} = \frac{3}{2} \cdot \frac{p}{2} \left[\frac{1}{2} (L_d - L_q) I_s^2 \sin(2\theta_i) + \lambda_f I_s \sin(\theta_i) \right], \quad (2.3)$$

where p is the number of poles, L_d is the d -axis inductance, L_q is the q -axis inductance, I_s is the stator current vector, θ_i is the angle that stator current vector does with d -axis and λ_f is the rotor magnetic flux.

T_{em} is defined as positive to drive the motor if θ_i is positive, whereas if θ_i is negative the torque produced is in the opposite direction of the speed, so the motor is braking. Besides that, the two stator current components are defined as: $i_q = i_T = \text{Stator current Torque component}$ and $i_d = i_f = \text{Stator current Flux component}$. Also, reference [15] defines θ_i as the torque angle. The author of this document gives another definition of torque angle. This concept will be discussed in Section 4.

Through equation (2.3) it is also possible to see that if θ_i is higher than $\frac{\pi}{2}$, i_f becomes negative and consequently the resultant air-gap flux decreases. This is how flux-weakening operation in permanent magnet motors is done. Furthermore, if θ_i is negative, the machine becomes a generator. This is the main issue to the work described in this document.

2.5. Market Research

Electric and hybrid vehicles are becoming an important part of the industry nowadays. However, they are in development stage yet and for that reason it is not easy to find many pure electric vehicles for sale.

Concerning to the electric traction system, more specifically to regenerative braking system, there are known two suppliers: Rexroth from Bosch group, and Continental. There are also some electric vehicles in production that integrate this system, like Tesla, Ford, Nissan, Mitsubishi or Renault.

2.5.1. Selling of the Regenerative Braking System

Rexroth's system, called Hydrostatic Regenerative Braking System (HRB), is specifically designed to applications which, like the name indicates, are based on a hydraulic traction system, as garbage trucks or buses. Its operation is divided in two steps: first the energy is stored in a pressure accumulator when the vehicle brakes, converting kinetic energy into electric energy; the energy is then restored to the transmission system, which operates symmetrically to the step one. In order to control the charge and discharge process, and to protect the accumulator of too much pressure, there is a set of valves that engages or disengages this mechanism. More information about HRB is presented in [16].

Relatively to the solution provided by Continental, it is directed to any hybrid, electric or fuel cell vehicle. When braking pedal is pressed the energy spent on the brakes is converted in electric energy, used to charge the batteries. In addition to this brake there is a traditional mechanical brake which is activated if the deceleration required is not enough. This decision is made by a central controller that analyses the information from several sensors like wheel speed, turning angle, lateral accelerations, etc. Continental also guarantees that this system, if integrated in a vehicle with Electronic Stability Control, performs every stability functions like ABS, TCS, etc. More information about this solution is presented in [17].

2.5.2. Electric Vehicles With Regenerative Braking

When talking about electric vehicles it is almost mandatory to talk about Tesla, the first company to have series production of electric vehicles. Tesla started to sell electric vehicles in a different approach: they produced an electric sport car with high performance, the Roadster. Recently they launched another type trying to embrace other kind of buyers: the sedan Model S. All their models (Roadster and Model S) integrate regenerative braking. According to them, their system reuses braking energy to almost 0 Km/h, also having a

mechanism that does not let the wheels block, like ABS. It also stops regeneration if the batteries are full charged [18].

Ford is another company that is in electric vehicles industry with Ford Focus Electric. This car, rated as most fuel-efficient five passenger vehicle in America, also integrates regenerative braking. Ford claim that their system regenerates up to 90% of the energy normally lost in braking. They also say that there will be a display inside the car showing the amount of energy being reused at each moment [19].

Nissan and Mitsubishi are in this recent market too with the same concept as Ford. Their models, Leaf and i-Miev respectively, are city cars, small and designed to be preferentially efficient rather than have high performances. Leaf integrates a 80kW, 280Nm motor against i-Miev which uses a 67kW, 180Nm. Both cars are available for around 30.000€ [20].

Renault is also “in the race” with a different approach. Their vehicle, Twizy, pretends to revolutionize the urban mobility concept. It will be available in two versions: one with a 5 CV motor (less than 4kW) which has 45km/h of maximum speed: and another version with 20 CV (near 15kW) that reaches 80km/h. The version with less power does not require driving license [20].

2.6. Summary

This chapter presents the literature review within the scope of electric vehicles. First the system overview is presented allowing a better understanding of this document purpose. Then the requirements for the controller’s design is presented where is emphasized the robustness of the system and the need of an auxiliary mechanical brake to assure the vehicle’s safety. Some recent topologies of electronic power converters are presented and briefly described, finalizing with the three-phase inverter to be used in this work. Then, several types of control are presented and described, and the dq reference frame is explained. It is settled that this is the reference frame to be used because in steady-state the motor’s quantities are represented as constants. Some PMSM control methods known are then described. Finally a market research with relation to regenerative braking system selling and with electric vehicles in production nowadays is presented.

Chapter 3

Permanent Magnet Synchronous Motor

3.1. Introduction

With the discovery of new magnetic materials and their large availability comes the possibility to produce new and better kinds of motor technology, making possible the evolution in electric mobility. In an attempt to overcome the obstacles that DC motors present, which were the most used electric motors until 1950's, emerged the permanent magnets synchronous motors. They do not require neither rotor windings nor external electric sources to produce excitation in the rotor, becoming smaller, lighter and more powerful than DC motors. They also dispense the use of brushes or slip rings, which makes them more robust and suitable for high speed operations. Furthermore, PMSMs allow the control of their power factor. This feature allows them to be used, for example, to make power factor correction like capacitors.

Synchronous motors with permanent magnets are built by a rotor with permanent magnets and a multi-phase, typically three-phase winding stator, which is fed by an external inverter. These motors can be divided in two groups according to the type of the back electromotive force: if it is trapezoidal one the motor is called Brushless DC (BLDC); if it is sinusoidal it is called Permanent Magnet Synchronous Motor (PMSM), which is the object of this thesis. Besides that, these types of motors are called synchronous because the rotor spins at a frequency that is proportional to the rotating field created by stator currents. This leads to the absence of slip speed which is characteristic of induction motors. The rotational force, called torque, is achieved when the fluxes of the rotor (from the permanent magnets) and of the stator (created by the currents) interact. It is known that when these two vectors are 90 degrees from each other, the produced torque is maximum.

In this Chapter it will be discussed the types of PMSM and their advantages and drawbacks, how are they modeled, their operation principle and how they can be controlled, and finally it is described the motor used in this dissertation.

3.2. Types of Permanent Magnet Synchronous Motors

With respect to the direction of the flux, permanent magnets synchronous motors can be classified as: axial flux if the air-gap flux direction is parallel to the rotor shaft or radial flux if the air-flux direction is along the radius of the motor. Usually, axial flux motors have advantages over radial flux motors. For the same conditions and under the purpose of the application described in [21], axial flux motors weight less and consequently have higher torque/mass ratio. They also can be designed to have higher power/weight ratio resulting in less core material. They also have higher efficiency than radial flux motors [21].

Relatively to the arrangement of the permanent magnets, they can be: surface (SPM), surface inset or interior mounted (IPM). Surface mounted permanent magnets motors have the highest air gap flux density but lower structural integrity and robustness. Because of this they are not used in applications that require operating speeds above 3000 rpm. Since the permanent magnets permeability is close to the air permeability, the rotor is isotropic. The interior mounted types of motors are the most robust which makes them preferential to very high speed applications. Surface inset rotors are like SPM but they have an iron tooth between each couple of adjacent PMs. This leads to a slight anisotropy which, in turn, leads to the existence of two torque components: the permanent magnet torque and the reluctance torque. Interior mounted rotors have several flux barriers per pole, as shown in Fig 3.1. In this case, the rotor has three flux barriers per pole. Higher number of flux barriers per pole leads to higher rotor anisotropy. Here, the torque reluctance component is higher, hence the IPM rotor exhibits a high torque density and it is well-suited for flux-weakening operations, up to very high speeds.

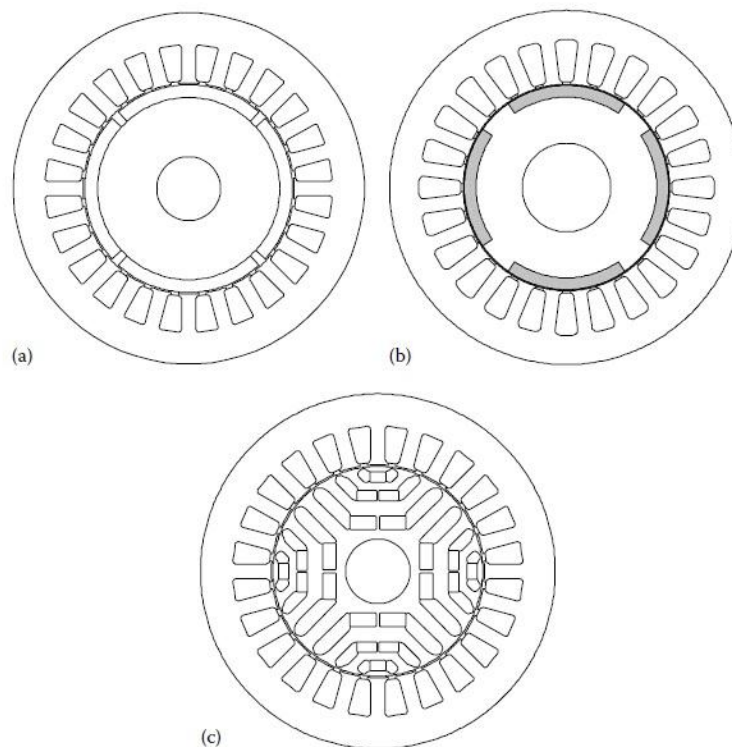


Fig 3.1 - Rotor arrangements of PMSM: a) surface mounted (SPM), b) inset surface mounted and c) interior mounted (IPM) [6].

Even on the subject of IPMs, they can be distinguished according to the direction of the magnetization of the PMs as: Tangentially magnetized and radially magnetized. An illustration of both types is shown in Fig 3.2. Tangentially magnetized rotors create an air gap flux as the sum of two adjacent magnets. In radially magnetized rotors, the PM surface is lower than the pole surface, yielding a lower flux density in the air gap. This configuration can be designed with more than one barrier per pole, which leads to high anisotropy. In both configurations the magnets have alternating polarity. IPM motors have magnetic paths with different permeability, through which is possible to develop a reluctance torque.

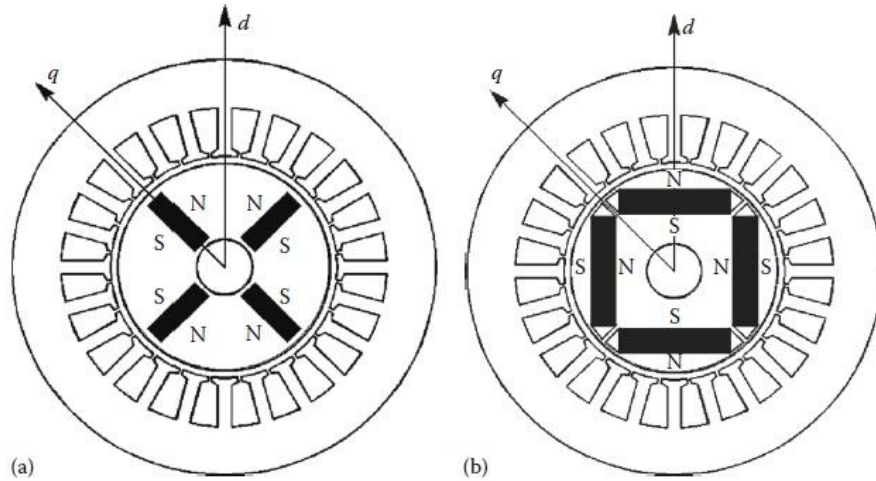


Fig 3.2 - IPM rotor with four poles with a) tangentially magnetized PMs and b) radially magnetized PMs [6].

From the stator windings point of view, as the rotor rotates the magnetic reluctance varies continuously. It changes between two extreme values: the maximum along the d -axis and the minimum along the q -axis. So, two corresponding winding self-inductances can be defined as L_d the min inductance and L_q the maximum.

L_d and L_q are two important parameters of the motor because they are used in motor model equations in order to achieve a proper control - this will be discussed on the next chapter. These inductances depend on the air-gap of flux paths. As said before, the permeability of the magnets are low and approximately the same as the permeability of the air. Thus, SPM motors have $L_d = L_q$ and one can consider that the air-gap thickness is bigger in this case. Similarly, in IPM motors the PM's have lower permeability than the iron (that is, higher reluctance) so the effective air-gap in the magnetic flux path varies according to rotor position. In this case the resulting d -axis inductance is lower than q -axis inductance, yielding $L_d < L_q$. Also, the saliency ratio (or anisotropy ratio) is defined as $\xi = \frac{L_q}{L_d}$.

The phase inductance of the motor L_s can be calculated from L_d and L_q through equation (3.1). As shown, the self-inductance of each phase can be position independent only if L_d and L_q are the same, for example in SPM motors [6].

$$L_s = \frac{(L_d + L_q)}{2} + \left[\frac{(L_d - L_q)}{2} \right] \cos(2\theta) \quad (3.1)$$

where θ is the instantaneous position of the rotor d -axis with respect to one phase. For simplicity usually phase “a” is considered.

The concept of magnetic flux paths and d and q inductances are better understood through the representation presented in Fig 3.3.

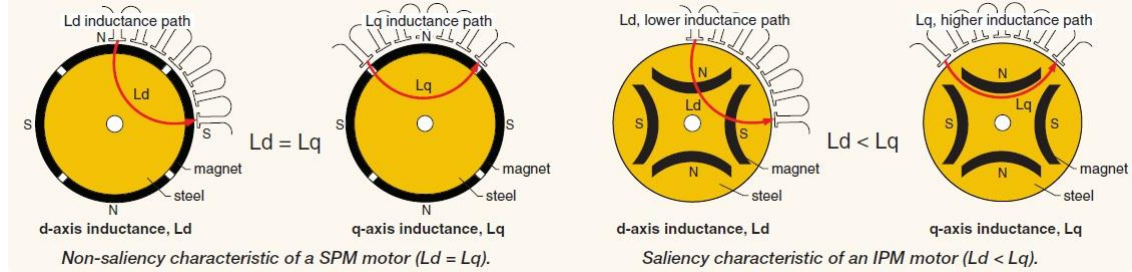


Fig 3.3 - Magnetic flux paths in a) SPM motor and b) IPM motor [7].

3.3. PMSM Modeling

In order to accomplish a simpler way to model the PMSM, the dq reference frame is adopted. That is because the dq frame is rotational with an angular speed equal to the electrical angular speed, that is $\omega_e = \frac{p}{2} \cdot \omega_r$, where p is the number of poles and ω_r is the mechanical angular speed of the shaft. Two reference frames can be chosen: stator and rotor reference frame. For simplicity, the rotor reference frame is adopted. The principle of this model assumes that the rotor flux is aligned with the d -axis, while q -axis is in quadrature - that is leading by 90 electrical degrees. This way there is no rotor flux along q -axis. It is also assumed that the motor's core losses are negligible, so are the magnets fluxes variations due to temperature variations. A representation of the dq axis in a four-pole IPM rotor can be found in Fig 3.2.

However, it is essential to understand where the dq frame comes from. First of all, PMSM is a three-phase machine which is supposed to be balanced, so currents and voltages are 120° from each other. It is much simpler to work on an orthogonal two-phase referential. That transformation is accomplished applying the Clarke-Transformation to the three-phase units as shown in equation (3.2).

$$\begin{bmatrix} X_\alpha \\ X_\beta \end{bmatrix} = \frac{2}{3} \begin{bmatrix} 1 & -\frac{1}{2} & -\frac{1}{2} \\ 0 & -\frac{\sqrt{3}}{2} & \frac{\sqrt{3}}{2} \end{bmatrix} \begin{bmatrix} X_a \\ X_b \\ X_c \end{bmatrix}, \quad (3.2)$$

where X could be voltage, current or any other three-phase unit.

The result is a two-phase orthogonal frame called Alpha-Beta ($\alpha\beta$) frame. The Clarke-Transformation can also be found in a power invariant form, which has a $\sqrt{2/3}$ multiplying factor instead of $2/3$.

The inverse Clarke-Transformation is also known. It is useful to bring the three-phase quantities back so they can be properly applied in the PMSM control. The inverse Clarke-Transformation is presented in equation (3.3).

$$\begin{bmatrix} X_a \\ X_b \\ X_c \end{bmatrix} = \begin{bmatrix} 1 & 0 \\ -\frac{1}{2} & \frac{\sqrt{3}}{2} \\ -\frac{1}{2} & -\frac{\sqrt{3}}{2} \end{bmatrix} \begin{bmatrix} X_\alpha \\ X_\beta \end{bmatrix} \quad (3.3)$$

After applying the Clarke-Transformation it is necessary to rotate this frame synchronously with the rotating field. This way all the units referenced to this frame will be constant in steady state, bringing some huge advantages to the calculus and control of PMSM. This is accomplished applying the transformation described by equation (3.4).

$$\begin{bmatrix} X_d \\ X_q \end{bmatrix} = \frac{2}{3} \begin{bmatrix} \cos(\theta) & \sin(\theta) \\ -\sin(\theta) & \cos(\theta) \end{bmatrix} \begin{bmatrix} X_\alpha \\ X_\beta \end{bmatrix} \quad (3.4)$$

where θ is the electrical angle of the rotor with respect to the stator position.

This transformation generates a two-phase orthogonal rotating frame that is spinning at the same speed that the rotating field is. Then some assumptions can be made: this referential could be aligned with the rotor flux vector, with the stator current vector (rotating field), with phase “a” of the PMSM three-phase fed line, or with any other reference although complicating the analysis. In this document, the d -axis of the desired dq reference frame to work on is aligned with the rotor flux vector.

It is also possible to generate the dq frame directly from three-phase units. That is done applying the Park Transformation, which is given in equation (3.5).

$$\begin{bmatrix} X_d \\ X_q \end{bmatrix} = \frac{2}{3} \begin{bmatrix} \cos(\theta) & \cos(\theta - \frac{2\pi}{3}) & \cos(\theta + \frac{2\pi}{3}) \\ \sin(\theta) & \sin(\theta - \frac{2\pi}{3}) & \sin(\theta + \frac{2\pi}{3}) \end{bmatrix} \begin{bmatrix} X_a \\ X_b \\ X_c \end{bmatrix} \quad (3.5)$$

These three different referential frames are represented in Fig 3.4 like they are considered in this work. The α -axis is aligned with phase a and d -axis is aligned with rotor flux vector, rotating synchronously with it.

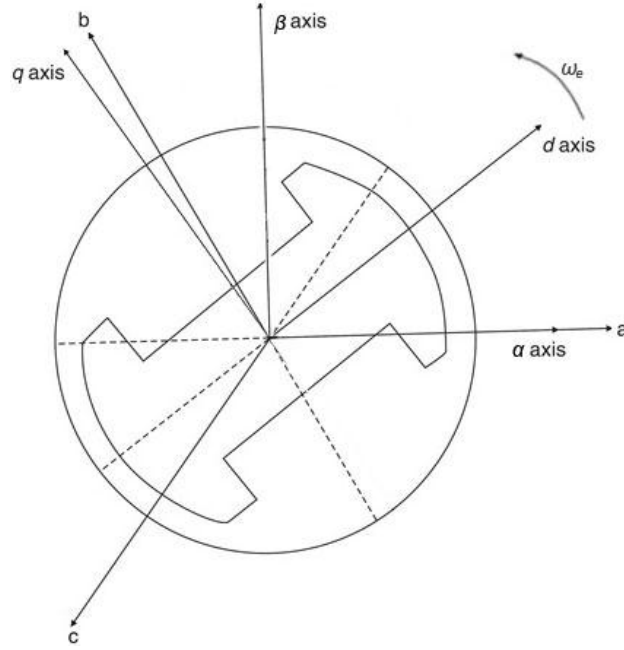


Fig 3.4 - Representation of the three reference frames: three-phase, dq and $\alpha\beta$. d -axis aligned with rotor flux. α -axis aligned with phase-a.

The motor modeling is now ready to be done, assuming that dq frame is used from now on as reference. Therefore, the PMSM stator equations referenced to rotor are represented in equation (3.6).

$$V_s = R_s I_s + \partial \lambda_s + j \omega_e \lambda_s \Rightarrow \begin{cases} V_d = R_s i_d + \partial \lambda_d - \omega_e \lambda_q \\ V_q = R_s i_q + \partial \lambda_q + \omega_e \lambda_d \end{cases} \quad (3.6)$$

$$\begin{cases} \lambda_d = L_d i_d + \lambda_f \\ \lambda_q = L_q i_q \end{cases} \quad (3.7)$$

where R_s is the stator phase resistance, I is the stator current vector, ∂ is the differential operator, λ is the flux, λ_f is the rotor flux, ω_e is the electrical angular speed, L is the inductance, the subscript s refers to the stator and d and q refers to direct and quadrature axis, respectively.

As the permeability of high flux density permanent magnets is almost the same of the air, the magnetic thickness becomes an extension of the air gap by that amount. Then, the stator inductance when the stator winding is aligned with the magnets is called the *direct axis inductance* (L_d). By rotating the magnets by 90 electrical degrees, the stator flux sees the area of the rotor which contains only the iron path. The inductance measured there is called *quadrature axis inductance* (L_q). The direct axis reluctance is greater than the quadrature axis reluctance [15]. This results in an unequal relation between L_d and L_q given by $L_q > L_d$.

The equation (3.6) can be represented in two electric circuits as shown in Fig 3.5.

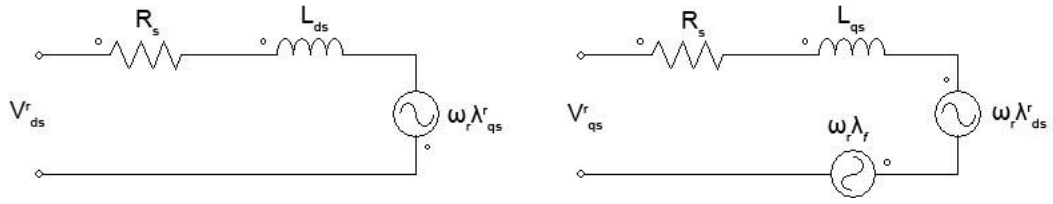


Fig 3.5 - d and q representation circuits of a PMSM.

As shown, the rotor flux is all along the d -axis which produces an EMF along the q -axis. This is an important assumption when talking about the control of PMSM, later on this document.

Now it is possible to define the electromagnetic torque expression as a function of flux and current dq components. The equation is represented in (3.8).

$$T_{em} = \frac{3p}{2} (\lambda_d i_q - \lambda_q i_d), \quad (3.8)$$

where p is the number of poles of the PMSM.

This expression states essentially two things: first, that there is a component that is directly proportional to the torque produced and other that is against the torque. This allows renaming the dq current components for better and easier understanding the rest of this document: i_q is the *Torque-producing component* and i_d is the *Flux-producing component*; Second, that the electromagnetic torque is defined by the cross product between flux and current vector, which means that the d component of one is multiplied by the q component of the other. This allows re-writing the electromagnetic torque expression as in equation (3.9). It is easy to see that T_{em} is maximum when the angle between current and air-gap flux vectors is 90 degrees.

$$T_{em} = \frac{3p}{2} (\mathbf{I}_s \times \boldsymbol{\lambda}_s) = \frac{3p}{2} |\mathbf{I}_s| |\boldsymbol{\lambda}_s| \sin(\theta_T), \quad (3.9)$$

where \mathbf{I}_s is the stator current vector (responsible for the rotating field), $\boldsymbol{\lambda}_s$ is the air-gap flux vector (resultant of the rotor flux and stator induced flux) and θ_T is the torque angle.

Also, using the relations defined in (3.7) it is possible to unfold equation (3.8) in two components: the *fundamental torque component* due to the permanent magnets flux multiplied by the torque-producing current component, and the *reluctance torque component* due to the difference between d and q inductances multiplied by both dq current components. This equation is presented in (3.10).

$$T_{em} = \frac{3p}{2} \left[\lambda_f i_q + (L_d - L_q) i_d i_q \right] \quad (3.10)$$

3.4. Definitions of Torque Angle

The latter equation (3.9) leads this document to a very important concept in this subject: the definition of torque angle. Unfortunately, literature is not consistent in what is, in fact, the torque angle. Many definitions are given for the same angle, and many different angles are defined as the same thing depending on the author. Being aware of this is, of course, a huge problem because it makes impossible to do a quick review of an article without reading the context in which it is inserted and the definitions that the author does. Furthermore, achieving a correct vector control over the motor implies the knowledge of which angle is being taking into account in each case which, in turn, inevitably implies their correct differentiation and definition.

A relevant definition is given in [15] by R. Krishnan. He claims that the torque angle is the angle between stator current vector and rotor flux vector. In fact, this consideration is valid because the electromagnetic torque is still defined as the interaction between two magnetic forces, one created only by the stator current and other created only by the rotor's permanent magnets. This consideration allows re-writing the torque equation as (2.3) presented in Chapter 2.4 and repeated here for convenience.

$$T_{em} = \frac{3}{2} \cdot \frac{p}{2} \left[\lambda_f I_s \sin(\theta_i) + \frac{1}{2} (L_d - L_q) I_s^2 \sin(2\theta_i) \right] \quad (3.11)$$

Now is easy to understand the definitions of dq current components given by Mr. Krishnan and considered valid by the author of this dissertation: i_q being the torque component and i_d being the flux component. In dq reference frame i_d is the projection of I_s over the d -axis ($I_s \cos(\theta_i)$) and i_q is the projection of the same vector over the q -axis ($I_s \sin(\theta_i)$). So the interaction between stator current torque component and rotor flux creates torque, and all the considerations become valid. Moreover, another noteworthy aspect is that for SPM motors L_d and L_q are equal, making the second portion of the equation null, thus controlling the motor's torque only by the influence of i_q . From now on the angle θ_i is considered to be the *stator current angle*.

Another important reference to this issue is made by Mr. Wilamowski [6]. In this book two different angles are called "torque angle". One is the angle between rotor flux vector and stator current vector (the same as before), and the other one is the angle between rotor and stator flux vectors, which is called from now on as θ_λ . The second vector is in fact the air-gap flux vector and this is concluded because of the definitions given in the same book. The author claims that the first angle definition is used in FOC algorithms and the second one in DTC techniques. However, this angle has a direct relation with the stator current angle θ_i , allowing its usage in another control strategy than DTC. Their relation is given by the definitions of stator current and air-gap flux vectors in dq reference frame. Considering the relations shown in (3.12) and (3.13) it is possible to conclude the relations shown in (3.14) and (3.15).

$$i_d = I_s \cos(\theta_i); i_q = I_s \sin(\theta_i) \quad (3.12)$$

$$\lambda_d = \lambda_s \cos(\theta_\lambda) = L_d i_d + \lambda_f; \lambda_q = \lambda_s \sin(\theta_\lambda) = L_q i_q \quad (3.13)$$

$$\cos(\theta_i) = \frac{\lambda_s \cos(\theta_\lambda) - \lambda_f}{L_d I_s} = \frac{\lambda_d - \lambda_f}{L_d I_s} \quad (3.14)$$

$$\sin(\theta_i) = \frac{\lambda_s \cos(\theta_\lambda)}{L_q I_s} = \frac{\lambda_q}{L_q I_s} \quad (3.15)$$

Lastly there is another definition that is quite different from the previous. The approach of the author is in a more physical and mechanical way, concerning the synchronous electrical machines functionality [22]. The torque angle δ , defined in Chapter 2.11 of the mentioned book, is stated to be the angle between the phase voltage V_1 and a virtual - as corresponding to running of the motor without stator supply - voltage defined as the effect of the rotor's magnetomotive force (MMF), E_f . The stator current also creates a flux aligned with it, which induces a voltage lagging by 90° , E_{ar} . The air-gap flux is considered to induce a voltage on the stator, called E_ϕ , which is given as the sum of two other virtual voltages: E_f and E_{ar} . So, if the stator resistance is neglected, as well as all the losses of the motor, then the power that feeds it must be equal to the power generated. Therefore, if this power per phase is defined as the product of line voltage and current times the angle between them (power factor) as in equation (3.16), and the phase reactance, called synchronous reactance (x_d) and defined as the sum of the magnetizing reactance with the leakage reactance, is given, then the torque can be expressed as in equation (3.17).

$$P = |V_1| |I| \cos \varphi \quad (3.16)$$

$$T_{em} = \frac{3P}{\omega_r} = \frac{3}{\omega_r} \frac{|V_1| |E_f|}{x_d} \sin(\delta) \quad (3.17)$$

This approach could be valid in a control implementation and a technique based on it is tested to achieve sensorless operation. However, no good results were obtained. The technique is based on the power balance and is described in Section 4.5.

The author of this dissertation considers the definition of torque angle as the angle between stator current vector and air-gap flux vector, as described in equation (3.9). This consideration is because of the physical behavior of the PMSM. Considering that the electromagnetic torque is created by the interaction between two magnetic fields, it makes perfect sense that it is defined by the multiplication of the module of the vector that represents the stator current - responsible for creating a magnetic field aligned with itself, the module of the vector that represents the air-gap flux - the resultant flux of the interaction between stator and rotor fluxes, and the angle between them. Therefore, when stator current vector is leading air-gap flux by 90° the maximum torque is achieved. This torque angle definition is adopted from now on.

All these relations are graphically represented in Fig 2.10.

3.5. Relations Between Torque Angle, Current and Air-gap Flux

The next conclusions are useful for better understanding the PMSM behavior with respect to air-gap flux and stator current vectors' variations.

Starting from equation (3.9) some conclusions are drawn with respect to the influence of variations in one vector in relation to the others, considering constant torque, that is $\frac{d}{dt}T_{em} = 0$. Therefore, three situations are possible to analyze: current variations, air-gap flux variations and position variations. However, the next analysis is merely theoretical because a complete decoupling of the vectors in question is impossible.

The equation (3.18) is intended to be analyzed. It is the result of deriving equation (3.9) considering constant T_{em} . To do that, the derivative rule defined by $(fg)' = f'g + fg'$ is used.

$$0 = \frac{d}{dt} [|I_s| |\lambda_s| \sin(\theta_T)] \quad (3.18)$$

$$\Leftrightarrow 0 = \frac{dI_s}{dt} \lambda_s \sin(\theta_T) + \frac{d\lambda_s}{dt} I_s \sin(\theta_T) + \frac{d\theta_T}{dt} I_s \lambda_s \cos(\theta_T) \quad (3.19)$$

3.5.1. Torque dependability on $|I_s|$ and $|\lambda_s|$

Since variations in I_s imply variations in λ_s - because the definition of the latter includes the two components of the first - these two conditions are analyzed together. Solving (3.19) in order to I_s leads to equation (3.20).

$$\frac{\frac{dI_s}{dt}}{I_s} = -\frac{\frac{d\lambda_s}{dt}}{\lambda_s} - \frac{\frac{d\theta_T}{dt}}{\tan \theta_T} \quad (3.20)$$

From this equation it is possible to conclude that with the increase of I_s there should be a subsequent decrease of λ_s and/or θ_T . Decreasing θ_T means that the angle between both vectors becomes smaller, meaning that the vectors move closer to each other. This analysis makes sense since theoretically the torque is maximum when both vectors are 90° from each other. If the first consideration for this analysis is that torque is constant, then if there is an increase in stator current, either air-gap flux decreases or the vectors come closer to each other. Since it is physically impossible to decouple I_s and λ_s vectors this conclusion is consistent with physical phenomena.

Moreover it is possible to analyze motor's behavior in two distinct conditions: 1) when $i_d < -\frac{\lambda_f}{L_d} \vee i_d > 0$ and 2) when $i_d < 0 \wedge i_d > -\lambda_f L_d$.

The first condition is when i_d causes the same variations in both current and air-gap flux vectors. This corresponds to the generic conclusion drawn before.

The second condition has two possible behaviors according to the variations in i_d . If it increases then I_s also increases but λ_s decreases. In the other hand, if i_d decreases I_s also decreases but λ_s increases. This is the only situation in which those two vectors have symmetrical behaviors.

3.5.2. Torque dependability on θ_T

Controlling θ_T is perhaps the most appropriate way of controlling the torque in a PMSM. If, somehow, it was possible to directly extract this angle information from the motor, its variations will directly correspond to variations in torque, allowing the control of the motor. However, for extracting θ_T it is first needed to know current and flux vectors, which makes this approach of control difficult to implement.

Through the analysis of the same equation it is possible to conclude what have been said. For constant torque, if a variation in θ_T occurred, air-gap flux and stator current have to compensate by changing their amplitudes.

3.6. Used Motor's Parameters and Simulation

The nominal values and the parameters of the motor that is used in simulation tests are described in Table 3.1 and in Table 3.2, respectively. As said before, this motor is smaller than the CaetanoBus' and its purpose is to test the designed control.

Table 3.1 - Nominal values of the PMSM used in simulation.

Connection	Y
Number of poles	4
Rated Current	160A
Rated frequency	200Hz
Rated power	50kW
Rated torque	80Nm

Table 3.2 - Parameters of the PMSM used in simulation.

Stator Resistance	7.9m Ω
<i>d</i> -axis Inductance	0.23mH
<i>q</i> -axis Inductance	0.56mH
Rotor flux	104mWb

A model of the motor is built based on the equations described before. Using the PSIM ability of running a DLL file through the DLL Block, and using Microsoft Visual C++ 2012 Express software, the model was programmed in C++ code and tested in PSIM.

A simulation for testing the model is done as shown in Fig 3.6. The inverter, on the left side of the figure, is controlled in open-loop by a sine-PWM signal generator. Then, the three-phase voltages are transformed in *dq* voltages through Park Transformation, as explained before, and feed the motor. All the parameters of the motor are established outside the model allowing their modification without the need of changing the code. Moreover, the load torque (T_L) is also available for changing outside the model by a step voltage source, allowing the introduction of a load torque at any instant. The motor's *dq* current components are used as feed-back to calculate the torque, and the rotor angular speed is converted in electrical

angular speed and integrated, so the position of the rotor could be used in Park Transformation.

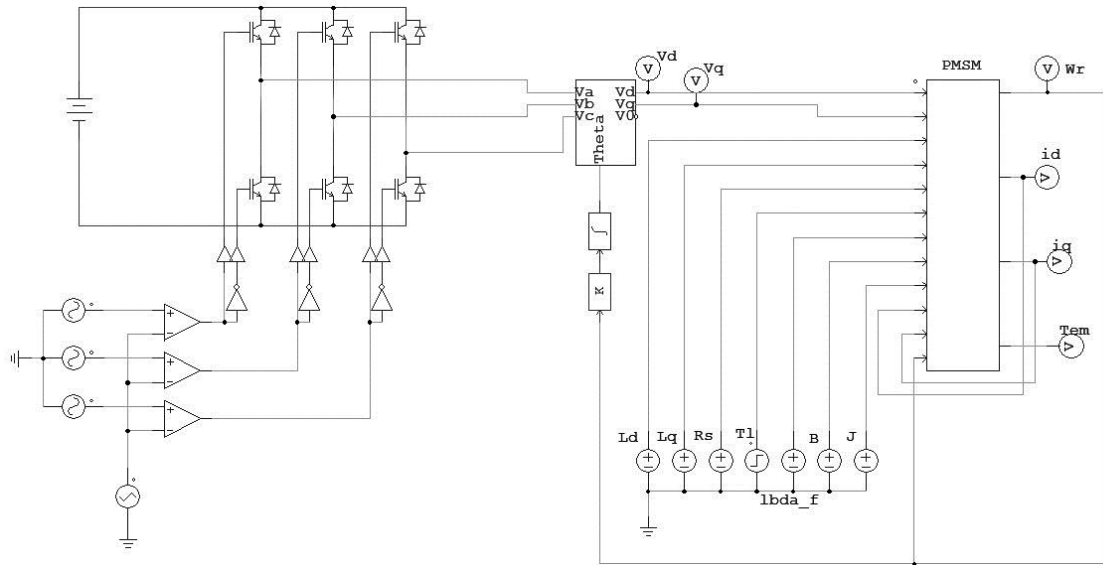


Fig 3.6 - DLL model of PMSM in PSIM software.

Building this model allow the validation of system's equations as well as a better understanding of its behavior and familiarization with PSIM software. However, from this point on, the PMSM block and Park Transformation block of PSIM are used since they satisfy the requirements for this work.

3.7. Summary

A detailed analysis of the permanent magnet synchronous motor is presented in this chapter. Several architectures of PMSMs are presented with respect to permanent magnets arrangement. Then, its mathematical model in dq reference frame is presented and explained, with the relations between three different reference frames. An important analysis to the different definitions of torque angle presented in literature is done, describing each one and assuming for this document purposes that torque angle is between stator current and air-gap flux vectors. A dynamic analysis of torque dependability on stator current and air-gap flux vectors is presented, finalizing with the description of the motor used for this work and its PSIM model created. A DLL model is chosen allowing its designing in C++ language.

Chapter 4

Control of the PMSM

4.1. Introduction

Although making a PMSM to run is not a hard task to do, controlling it is not trivial. In the literature several strategies of control are presented. There are roughly two ways of controlling a motor: scalar and vector control. Vector control allows better control over the behavior of the motor since all its variables are considered (voltage, currents, fluxes, position and speed). This document studies, analyses and compares three methods of vector control: Stator current vector at 90 degrees, Air-gap flux vector at 90 degrees and Maximum Torque Per Ampere (MTPA). These three methods have different characteristics regarding dynamic response and controllability, but particularly with regard to efficiency, which is important considering that the motor is fed by batteries.

Beyond the control methods there is the inverter control technique, which generates the gate signals for the transistors. This could be by Hysteresis, Sinusoidal Pulse-Width Modulation (PWM) or by Space Vector Modulation (SVM). Only the last two have been analyzed and compared due to goals of the work.

In this context, the used controller type must also be considered. Among various types of controllers that are used nowadays, such as PID, Fuzzy, Neuronal-Networks, Sliding-Mode or Adaptive control, only PID is used in this work. Although its performance cannot be the best one, it is linear, simpler and faster to implement than the others and requires less processor usage. This last characteristic is very important since the application of the controller is in an electric vehicle, where robustness and fast response are critical.

Last but not least, two control platforms are analyzed: DSP and FPGA. Although the control of the system is not yet implemented, it is the final objective. Therefore, a study of these two controller platforms is conducted. The performed analysis could be used in future works with respect to this subject.

This Chapter describes each type of control mentioned above, analyses them comparatively and shows the simulation results.

4.2. Control Strategy

Unlike most of the literature already studied, it is implemented a torque control scheme. In this strategy a torque reference is given to the motor, instead of a speed reference as is typically used. This makes a huge difference when the purpose of the system is an electric vehicle application. In this case, it is possible to say that it is the driver who “closes the speed loop” of the control. In other words, the motor accelerates and decelerates according to the torque supplied by the acceleration (or braking) pedal. It is driver’s job to choose if he wants to go faster or slower, and that information is given to the motor by a torque reference as it is done in ICE vehicles. This concept intrinsically avoids the loss of synchronism, one of the biggest problems of controlling this kind of motors. This assumption can be proved by mechanical electromagnetic torque equation as in (4.1).

$$T_{em} - T_L = J \frac{d\omega_r}{dt} + B\omega_r, \quad (4.1)$$

where T_L is the load torque, J is the moment of inertia, B is the friction coefficient and ω_r is the angular speed of the shaft.

Through this equation it is possible to understand that when the motor receives a torque reference (admitting that it can effectively produce that torque) any disturbance to the system will affect only the speed. Once again, if the speed loop of the controller is closed by the driver, he must respond to that disturbance applying more or less torque reference. If the reference of the controller had been speed, at any instant, if there was any disturbance and the torque is already maximum, the motor would lose synchronism, which could lead to system failure. This assumption can be proved by the torque analysis made on Chapter 3 and summarized here: if no more current can be drawn from the source then the current vector is maximum, so it is the air-gap flux vector. The angle between them, torque angle, is then 90° . If any disturbance occurs, like a road bump or some kind of road cavity, then the rotor will be held back and there will be no more power to pull it over again, resulting in the loss of synchronism. Considering the operation with a position sensor, this situation could possibly be predicted and corrected. But with a sensorless system, like it is proposed in this work, that loss of synchronism could be fatal.

Three methods of control are to be discussed: Stator current (I_s) at 90 degrees, air-gap flux (λ_s) at 90 degrees and Maximum Torque Per Ampere. These three methods, although being based on the same concept, have different dynamic responses and are designed under different considerations.

4.2.1. Control Methods

The approach used to control the PMSM is based on a torque reference control. That reference is compared with the calculated motor torque and the error is then brought to zero with a PI which gives the i_q reference. Through system of equations (3.6), V_{q_ref} voltage reference is obtained. At the same time, i_d is calculated by one of the methods described next. V_{d_ref} voltage is then obtained in the same way that V_{q_ref} , and Park-Transformation is applied to generate phase reference voltages, V_{a_ref} , V_{b_ref} , and V_{c_ref} , using the rotor

position signal that comes from the integration of a speed sensor signal. It is important to say that in fact there is a coupling between d and q components (voltages and currents), which means that it is not possible to generate them separately, being one dependent on the other. Therefore, they must be generated simultaneously.

Through equation (3.9) it is clear that the produced torque is maximum when stator current vector is leading air-gap flux vector by 90° . Moreover, for regenerative braking mode, the torque must be negative so being in opposite direction of the speed, working as a generator. This means that the stator current vector becomes lagging the air-gap flux vector, thus making torque angle θ_T negative. In the control strategy described, a negative torque reference is given (by vehicle's braking pedal) which produces a negative i_q reference. The relations between various vectors and their dq components are shown in Fig 2.10.

As discussed in Chapter 3 the torque equation can be written as a function of θ_i as in (3.11). This equation will be analyzed and used in MTPA method discussed on Chapter 4.2.1.3.

4.2.1.1. Stator Current (I_s) Vector at 90 Degrees

In this method, vector I_s is maintained at 90 degrees from the rotor flux vector (which is aligned with d -axis). That way the d - component of I_s is zero. That means I_s is controlled only by i_q . This virtually eliminates the dq coupling issue talked before. The torque expression given in (3.10) becomes:

$$T_{em} = \frac{3}{2} \frac{p}{2} \lambda_f I_q = \frac{3}{2} \frac{p}{2} \lambda_f I_s, \quad (4.2)$$

and torque per stator current is constant and equal to $\frac{3}{2} \frac{p}{2} \lambda_f$.

Normalized electromagnetic torque is then given by:

$$T_{emn} = \frac{T_{em}}{T_b} = \frac{\frac{3}{2} \frac{p}{2} \lambda_f I_s}{\frac{3}{2} \frac{p}{2} \lambda_f I_b} = I_{sn}, \quad (4.3)$$

where the subscript n means normalized.

As shown in (4.2), in this control method, torque is controlled by and directly proportional to i_q . Also, i_q and T_{em} are equal in p.u., making it the simplest method. Motor's equations from (3.6), in steady state become those as shown in system of equations (4.4).

$$\begin{cases} V_{ds}^r = -\omega_e \lambda_{qs}^r = -\omega_e L_q I_s \\ V_{qs}^r = R_s I_s + \omega_e \lambda_f \end{cases} \quad (4.4)$$

However, this method has some issues concerning power factor. It can be seen from Fig 2.10 that power factor can be calculated by equation (4.5) [15].

$$\cos \varphi = \frac{V_{qs}^r}{V_s} = \frac{V_{qs}^r}{\sqrt{(V_{ds}^r)^2 + (V_{qs}^r)^2}} = \frac{1}{\sqrt{1 + \frac{(L_q I_{sn})^2}{\left(1 + \frac{R_s I_{sn}}{\omega_{en}}\right)^2}}} \quad (4.5)$$

This equation shows that power factor decreases with the increase of motor's speed as well as with increasing stator current.

This control has been implemented in PSIM as shown in Fig 4.1.

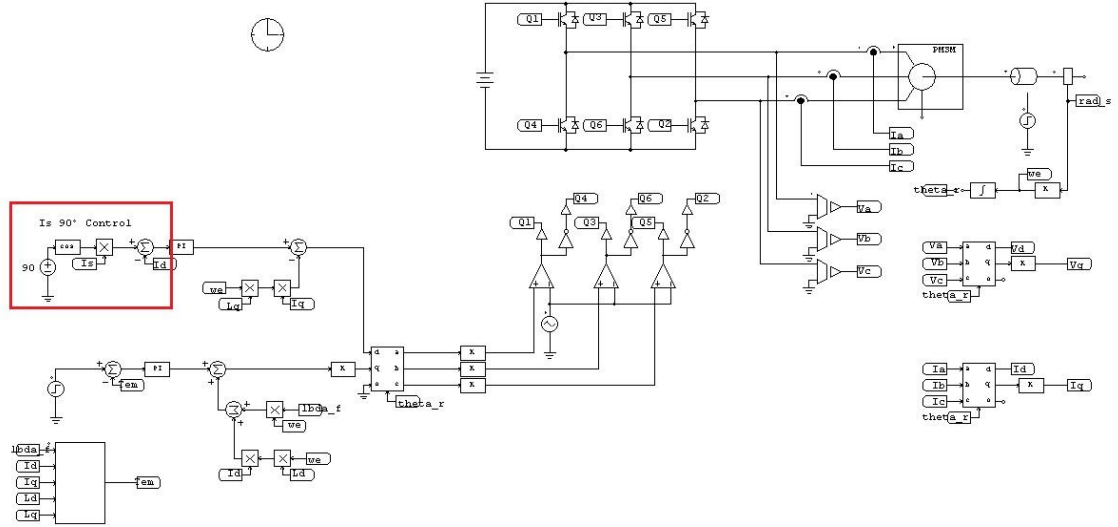


Fig 4.1 - PSIM Control scheme with I_s vector at 90 degrees method.

4.2.1.2. Air-gap Flux (λ_s) Vector at 90 Degrees

Usually, the approach of controlling the air-gap flux is by limiting its amplitude, mostly maintaining it at a constant value and equal to rotor flux. Its main advantage is that, by limiting the air-gap flux linkages, the stator voltage is kept at a low value. Also, by controlling the air-gap flux directly allows a simpler way to achieve flux-weakening operation [15]. However, as in this work no flux-weakening operation is predicted, another approach to air-gap flux control is done: air-gap flux at 90 degrees.

In this control method air-gap flux vector is kept at 90 degrees from the d -axis. As explained before, this flux is the resultant of stator flux linkage created by d and q components and by the rotor flux due to the permanent magnets. Keeping the air-gap flux at 90 degrees implies that i_d must be symmetrical to $\frac{\lambda_f}{L_d}$, turning $\lambda_d = 0$. Physically that means that it is being injected a stator flux component that nulls the effect of rotor flux component.

The module and angle of air-gap flux λ_s in dq reference frame are given by:

$$|\lambda_s| = \sqrt{(\lambda_d)^2 + (\lambda_q)^2} = \sqrt{(L_q i_q)^2 + (L_d i_d + \lambda_f)^2} \quad (4.6)$$

$$\angle \lambda_s = \tan^{-1} \frac{\lambda_q}{\lambda_d} \quad (4.7)$$

This control has been implemented in PSIM as shown in Fig 4.2.

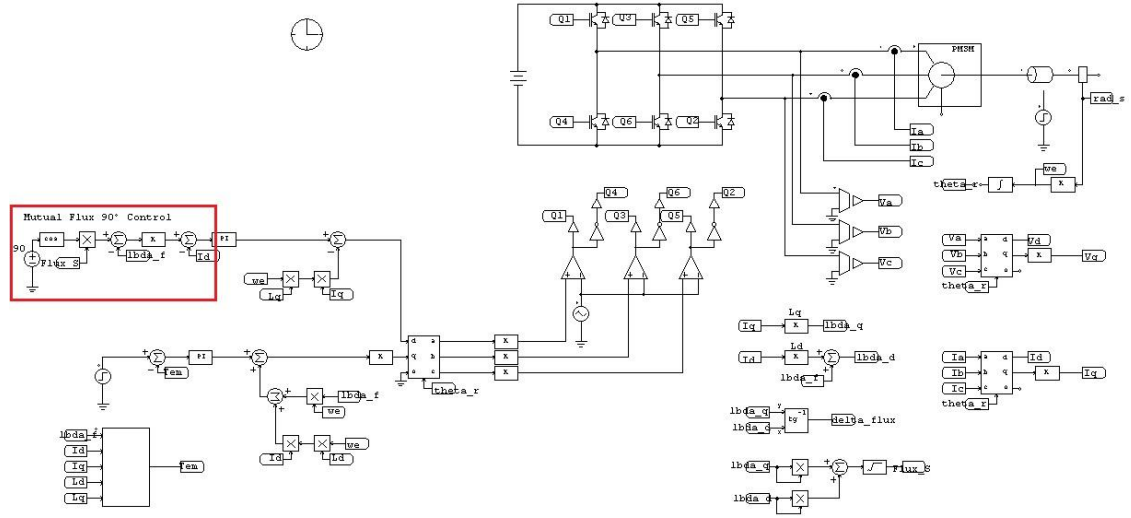


Fig 4.2 - PSIM Control scheme with λ_s at 90 degrees method.

4.2.1.3. Maximum Torque Per Ampere (MTPA)

This method pretends to achieve the best performance results with respect to battery efficiency. The goal is to produce maximum electromagnetic torque with the less current possible. This has repercussions in the voltage required by the inverter. However, in this application, is preferred to have less current than less voltage to the same torque produced.

The mathematical principle behind this method is implicit in its own name. It is necessary to reach a torque per ampere equation and then derive it and equate it to zero to find its maximum or minimum. This last consideration is done evaluating the physical operation of the machine after well understanding its behavior.

Through equation (3.11) it is possible to write an equation in function of torque per ampere as in (4.8).

$$\frac{T_{em}}{I_s} = \frac{3}{2} \frac{p}{2} \left(\lambda_f \sin \theta_i + \frac{1}{2} (L_d - L_q) I_s \sin(2\theta_i) \right) \quad (4.8)$$

Deriving this equation with respect to θ_i , and equate it to zero gives:

$$\frac{d}{d\theta_i} \frac{T_{em}}{I_s} = \frac{3}{2} \frac{p}{2} \left(\lambda_f \cos \theta_i + (\Delta L) I_s \cos(2\theta_i) \right) = 0, \quad (4.9)$$

where $\Delta L = (L_d - L_q)$.

Considering that $I_s = \sqrt{i_d^2 + i_q^2}$ and resolving in order to i_d two solutions are given, presented in (4.10).

$$i_d = -\frac{\lambda_f}{2(L_d - L_q)} \pm \sqrt{\frac{\lambda_f^2}{4(L_d - L_q)^2} + i_q^2} \quad (4.10)$$

Because θ_i needs to be greater than 90° to reduce the air-gap flux, only the negative solution is considered.

Another important conclusion about this method is that it can only be used in motors where $L_d \neq L_q$, like IPM motors. Otherwise it becomes equal to the stator current vector at 90° , that is $i_d = 0$.

MTPA control has been implemented in PSIM as shown in Fig 4.3.

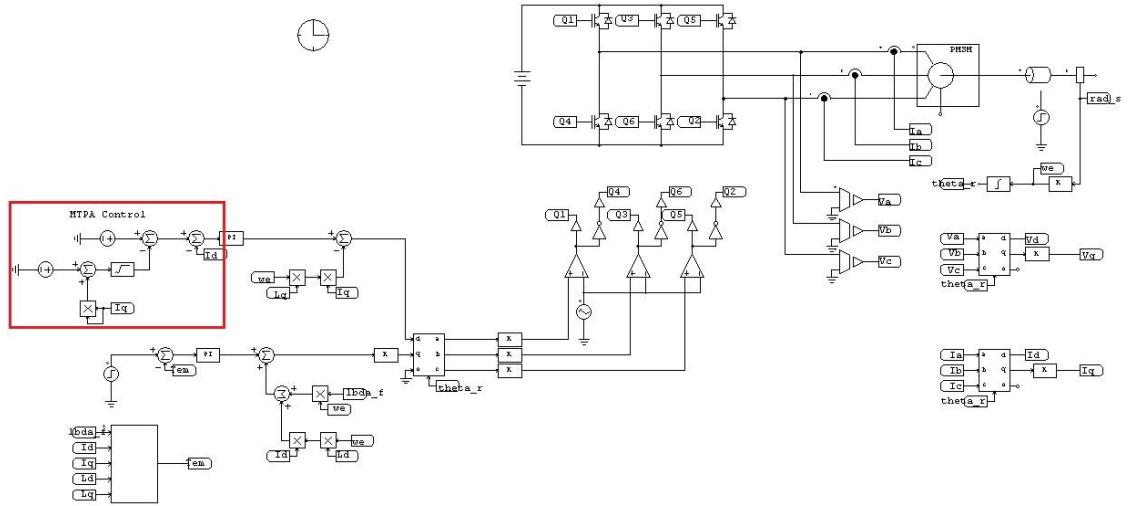


Fig 4.3 - PSIM Control scheme with MTPA method.

The results of these three methods will be discussed later in section 4.4.

4.2.2. Control Signal Generation for the Inverter

4.2.2.1. Sine-wave PWM

Sine-wave pulse-width modulation is a widely used carrier-based modulation technique in power converters. The main reasons are its simple implementation and good power quality. In the other hand there are the losses caused by the high switching frequency required, although there is a tradeoff between that frequency losses and the filters usually required: the higher the frequency the smaller and lighter the filter is, so is its price.

The basic idea behind PWM, is to alternate between the different switching states of the inverter in such a way that the time average of the switched voltage waveform equals the desired reference. Since the output voltage levels of the inverter are fixed, the modulation is performed by changing the width of the pulses, also known as duty cycle [6]. The transistors' gate signals are generated by comparing a reference voltage with a triangular wave signal. The reference is called *modulated signal* and the triangular is the *carrier signal*.

There are two important concepts when talking about sine-wave PWM: *modulation index* and *frequency index*. Modulation index, m_a , gives the relation between modulated and carrier amplitudes and it is defined by equation (4.11). Frequency index, m_f , is presented in (4.12).

$$m_a = \frac{V_{Ref}}{V_{tri}} \quad (4.11)$$

$$m_f = \frac{f_{tri}}{f_1} \quad (4.12)$$

where V_{Ref} is the amplitude of the reference signal, V_{tri} is the amplitude of the carrier signal, f_{tri} is the frequency of the carrier signal and f_1 is the fundamental frequency of the reference signal.

The frequency index is important because it gives the location of the main harmonic. Furthermore, the main harmonic is accompanied by four side harmonics located at $m_f \pm 2$ and $m_f \pm 4$ that appear due to a convolution effect between the fundamental and carrier frequency during the comparison performed by PWM [6].

For single-phase converters there are two types of PWM: unipolar and bipolar. The first ones produce output voltages that switch between zero and a positive voltage, or between zero and a negative voltage. The bipolar PWM produces output voltages that change between positive and negative voltages. Three-phase inverters usually use bipolar PWM, which is the same as single-phase but with references repeated through the three legs of the inverter, with a phase shift of 120 degrees.

4.2.2.2. Space Vector Modulation (SVM)

The Space Vector Modulation logic implies that the transistors' gate signal is given all at once as the inverter was a single device waiting for the input signal. This means that, for each state, 6 signals are generated and applied to the transistor's gates. So, it is necessary to define each transistor, as shown in Fig 2.9. As in Sine PWM, if the upper transistor is on, the corresponding lower transistor is off, otherwise there will be a short-circuit. Now it is possible to create a pattern for each state, which gives 8 possible combinations represented in Fig 4.4. Notice that two of them (V_0 and V_7) produce the same output voltage, that is 0. The switching vectors, line to neutral voltage and line to line voltage are presented in Table 4.1. Note that voltage values are multiplying factors for V_{dc} .

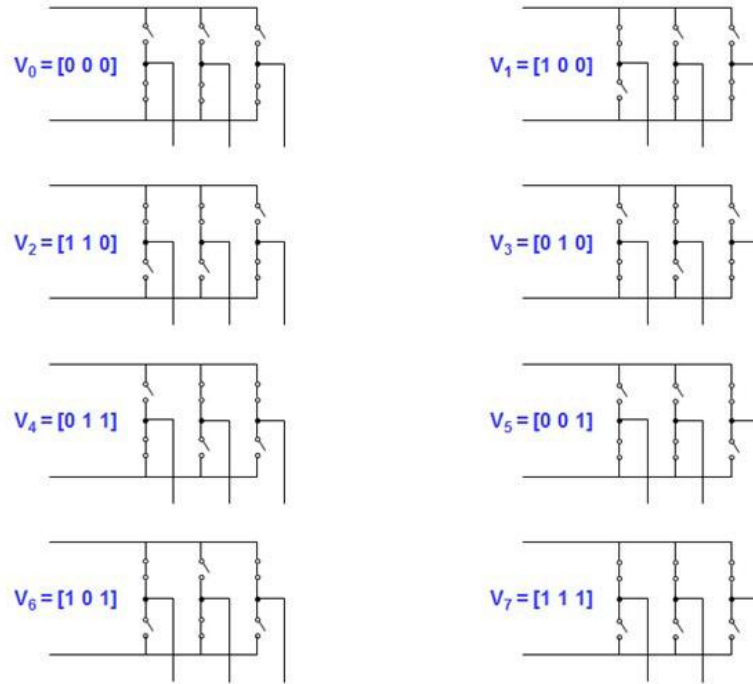


Fig 4.4 - SVM states according to inverter's transistors state.

Table 4.1 - Switching vectors combinations.

Voltage Vectors	Switching Vectors			Line-to-Line voltage			Line-to-neutral voltage		
	a	b	c	a	b	c	a	b	c
V_0	0	0	0	0	0	0	0	0	0
V_1	1	0	0	1	0	-1	$2/3$	$-1/3$	$-1/3$
V_2	1	1	0	0	1	-1	$1/3$	$1/3$	$-2/3$
V_3	0	1	0	-1	1	0	$-1/3$	$2/3$	$-1/3$
V_4	0	1	1	-1	0	1	$-2/3$	$1/3$	$1/3$
V_5	0	0	1	0	-1	1	$-1/3$	$-1/3$	$2/3$
V_6	1	0	1	1	-1	0	$1/3$	$-2/3$	$1/3$
V_7	1	1	1	0	0	0	0	0	0

The principle of the SVM is to generate an output that approximates the voltage reference by a combination of these eight switching patterns. It is also assumed that the vector representation is in stationary $\alpha\beta$ frame, which in turn is divided into 6 sectors, represented by vectors V_1 to V_6 , separated by 60° (creating a hexagon). At each instant, the controller tries to generate V_{Ref} by temporally combining two adjacent vectors.

The creation of SVM can be resumed in 3 steps:

Step 1 - Determine V_α , V_β , V_{ref} (V_s) and the angle of the vector V_s , α ;

Step 2 - Determine the times T_0 , T_k and T_{k+1} ;

Step 3 - Determine the switching sequence;

Step 1

V_α and V_β are determined using the Clarke Transformation, explained in the previous chapter. Then, $V_s = \sqrt{V_\alpha^2 + V_\beta^2}$ and $\alpha = \tan^{-1} \frac{V_\beta}{V_\alpha}$. Comparing α with 6 different angles given by the vectors V_1 to V_6 , the Sector of V_s is known.

Step 2

$\frac{t_0}{T_m}$, $\frac{t_k}{T_m}$ and $\frac{t_{k+1}}{T_m}$ represent the duty cycle of each vector k , being T_m the modulation period. t_0 , t_k and t_{k+1} are given in [6] by:

$$t_k = \frac{3T_m|V_s|}{2V_{DC}} \left\{ \cos(\theta - \theta_k) - \frac{\sin(\theta - \theta_k)}{\sqrt{3}} \right\} \quad (4.13)$$

$$t_{k+1} = \frac{3T_m|V_s| \sin(\theta - \theta_k)}{V_{DC} \sqrt{3}} \quad (4.14)$$

$$t_0 = T_m - t_k - t_{k+1} \quad (4.15)$$

Step 3

The switching pattern chosen can be either with 7 or 5 segments. The difference is whether or not one uses both zero vectors (V_0 and V_7). In terms of output voltage, they are the same. So, for simplicity, and for reduce the number of commutations, it is used the 5 segments technique. Furthermore, as said before, vectors V_0 and V_7 produce the same output voltage so either one can be chosen knowing that:

For V_0 the following relations hold:

- The phase c component of all vectors generated in sector 1 and 2 is always 0.
- The phase a component of all vectors generated in sector 3 and 4 is always 0.
- The phase b component of all vectors generated in sector 5 and 6 is always 0.

In the same way, for V_7 the following relations hold:

- The phase a component of all vectors generated in sector 6 and 1 is always 1.
- The phase b component of all vectors generated in sector 2 and 3 is always 1.
- The phase c component of all vectors generated in sector 4 and 5 is always 1.

Once again to keep it simple, V_0 is chosen.

The sequences are different if it is considered odd or even sectors. That is because it is intended to maintain the pattern symmetrical to the center of T_m . Therefore, the sequences are shown in Fig 4.5 and Fig 4.6 [6].

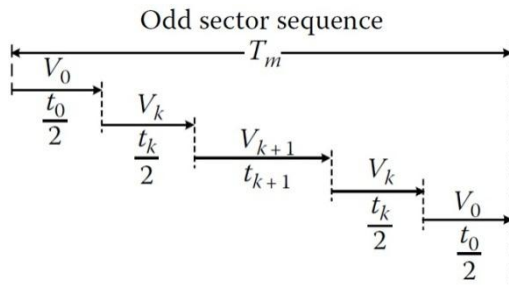


Fig 4.5 - SVM sequence for odd sector.

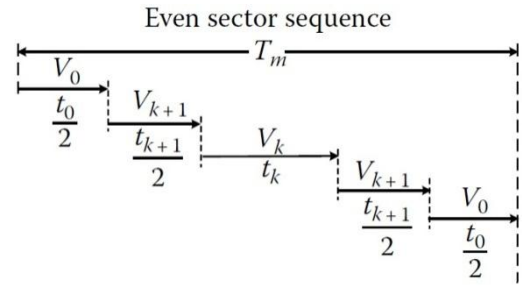


Fig 4.6 - SVM sequence for even sector.

Finally the tables containing the transistors' firing sequences have to be built. There should be one table for each transistor and they should be built considering a sector for each row and the sequence shown above for the columns. The value of each cell is selected making the correspondence between the Sector, the segment and the corresponding transistor signal given by Table 4.1. Notice that tables for transistors 4, 6 and 2 are complementary of tables 1, 3 and 5 respectively. The following table is an example for transistor T1:

Table 4.2 - Example of a SVM table for transistor T1.

	Segment 1	Segment 2	Segment 3	Segment 4	Segment 5
Sector 1	0	1	1	1	0
Sector 2	0	0	1	0	0
Sector 3	0	0	0	0	0
Sector 4	0	0	0	0	0
Sector 5	0	0	1	0	0
Sector 6	0	1	1	1	0

The implementation of SVM in PSIM can be seen in Fig 4.7. The steps described before are highlighted for easier understanding of the model.

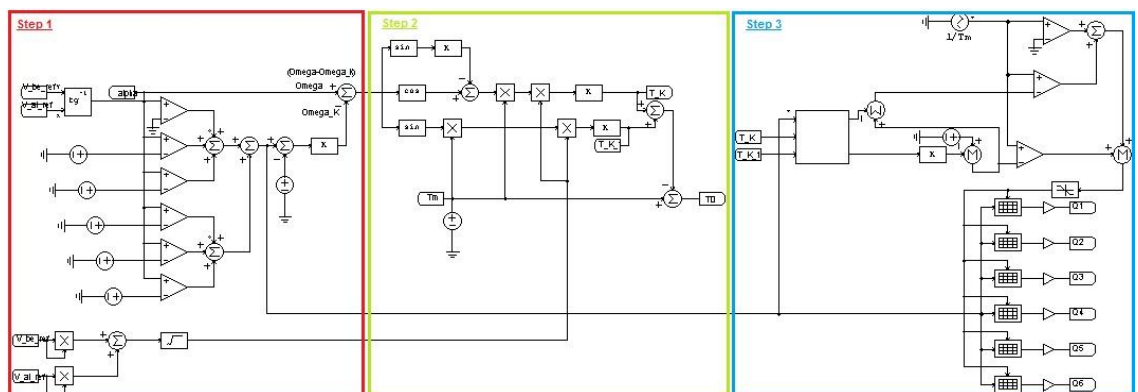


Fig 4.7 - SVM model designed in PSIM with different steps highlighted.

4.2.3. Controllers' Tuning

At this point three methods of control were described as well as two signal generation techniques for the inverter. In this section a brief overview over nowadays most used controller types is done and the PI controllers used for this work are explained. Several controller types are known but the most used are PID (Proportional-Integral-Derivative) or variances like PI, PD, PI+D, etc., Fuzzy Logic or variances like Adaptive-Fuzzy Logic, Artificial Neural Networks (ANN) or variances like Neuro-Fuzzy Networks, and Genetic Algorithms.

Although PID controllers have a general application capability they often do not provide an optimal control. The main reason is because they consist in a feedback system, with constant parameters and without any knowledge of the process. Furthermore, in applications where there is no possibility of having overshoot, like some industry machinery, the gains should be small resulting in poor performance.

Despite this, and considering the requirements of the system, only PID controllers are object of evaluation in this work. That is because of its simplicity and linearity, which simplifies its implementation and turns the control program faster. If the tests conducted with this controller result in a satisfactory performance, the usage of other type of controller is disregarded. Otherwise some more comparison tests should be done in order to evaluate the controller that has the best trade-off between performance, robustness and computational demand.

PID mechanism consists in minimizing the error between a reference value and a measured output of a process by feedback. Mathematically the controller is a sum of a gain, integration and derivation of the error at its input. Heuristically these three values can be understood with respect to time: proportional (P) depends on the present error, integral (I) depends on past errors and derivative (D) predicts future errors. By tuning these parameters through their gains (K_p , K_i and K_d , respectively) it is possible to adjust the dynamic and steady-state response of the controller as wish. So, two main approaches are considered: one called *regulation* whose objective is to stay at a given set point, rejecting any disturbances; and other named *command tracking* which has the objective to perfectly follow (track) the changes in the given reference. Some processes demand one of these approaches while others must be settle with the other. In this case, in which the process is a PMSM vehicle, a balance between them is required because the reference is constantly changing and disturbances are expected to happen. So, this means that there must be a trade-off between the results obtained. Probably a very quick response would have some overshoot and ringing of the signal. No-overshoot and smooth response would be accomplished as a cost of slower response. Moreover, PID controller is typically only used when the process is a second-order one. For simpler systems the derivative component is not considered. Another reason for the absence of the derivative component is the amplification of noise. Any peaks in the input signal of the controller would lead to huge outputs by the derivative gain which would then be accumulated by the integral gain, and the system remains unstable and uncontrollable. Therefore, PI controller is usually used in slower and single-order systems. This is the case of this work, where the largest time constant of the system is defined by the shaft constant of the motor as $\frac{J}{B}$, where J is the moment of inertia and B is the friction coefficient. In the frequency domain it causes the dominant pole, which is the pole that dictates the slower

time response of the system, giving the information of “how fast” should the controller be to have good performance.

The output of a PID controller can be expressed in time domain as:

$$y(t) = K_p e(t) + K_i \int_0^t e(t) dt + K_d \frac{d}{dt} e(t), \quad (4.16)$$

where K_p , $K_i = \frac{K_p}{T_i}$ and $K_d = K_p T_d$ are the proportional, integral and derivative gains respectively, and $e(t)$ is the input error signal. T_i and T_d are the integrative and derivative time constants, respectively.

In the frequency domain PID is known for its Laplace form:

$$Y(s) = K_p + \frac{K_i}{s} + K_d s = \frac{K_d s^2 + K_p s + K_i}{s} \quad (4.17)$$

4.2.3.1. PI Controller Tuning

There are several methods to tune a PI controller. Although most sophisticated techniques are subject of patents and used in simulations software, there are some simpler forms of tuning the PID controllers. The most common ones are: Ziegler-Nichols, Software tools and Manual Tuning. Ziegler-Nichols method is as experience based technique and although it was designed for PIDs, it can be used for PIs and even P controllers. Its procedure goes like this: I and D gains are started as zero and the P gain is increased until the process starts to oscillate, K_{\max} . The period of the oscillation is recorded, P_u . Then, for the controller type chosen, one of the lines of Table 4.3 is chosen and their gains are applied.

Table 4.3 - Ziegler-Nichols method.

Control Type	K_p	K_i	K_d
P	$0.5K_{\max}$	-	-
PI	$0.45K_{\max}$	$1.2K_p/P_u$	-
PID	$0.6K_{\max}$	$2K_p/P_u$	$K_p P_u/8$

Many software tools are available for tuning PIDs. They usually require the mathematical model of the process and some other controller parameters so an Auto-tune can be performed. In Simulink, for example, there is a toolbox (SiSoTool) that allows the user to design the controller as wish. The response to several types of input can be seen and the adjustments can be done in real-time. However, some advanced control skills are needed to achieve good results without consuming large amounts of time.

The first approach to the PIs tuning for this work was done in Simulink as described before. A model of the process was built and SiSoTool toolbox was used to tune the PI gains. A general block diagram of the system is described in Fig 4.8.

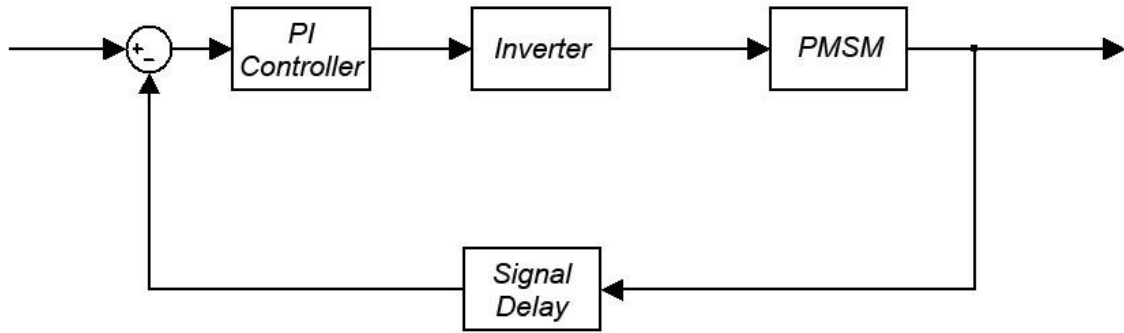


Fig 4.8 - Simplified block diagram of the system.

Briefly describing, a torque reference is given and compared with the calculated torque from the information of the motor's parameters and current. Then the error enters in a PI controller which gives the reference to the inverter's signal which generates the input to the PMSM. In fact, the functionality of the whole system is much more complex than this. For example, there are 2 PI controllers, one for the generation of i_q reference and other for the i_d . These two controllers have to be tuned together because of the coupling between dq components in generation of V_d and V_q references. This is the worst obstacle to the tune of the controller.

The approach to the tune of the PIs is through the frequency model of the PMSM so it could be implemented and tested in Simulink. If a good model could be built, SiSoTool toolbox could be used to adjust the PI gains. To do this, a simplified model of the motor is chosen just considering the “ q sequence” in which the voltage at the input becomes the current through a transfer function of the motor winding, and this current is then transformed in a torque which, through mechanical electromagnetic torque expression, becomes the output of the system as speed. The inverter is considered to be just a gain and a pole equal to half of the commutation period. The signal acquisition delay is also neglected. The implemented system in Simulink can be seen in Fig 4.9.

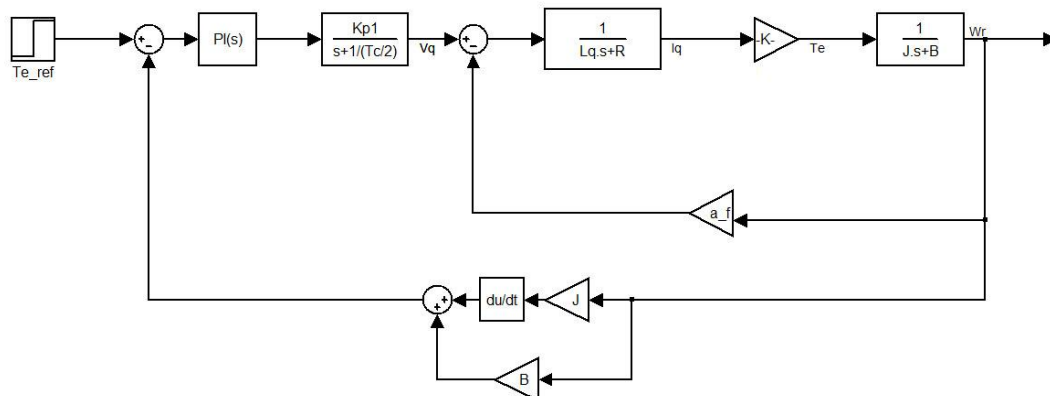


Fig 4.9 - Simplified system implemented in Simulink.

However, this model is not good enough because there is a coupling between d and q components, as said before. The simplifications chosen were too much so the system lost significance and the automated tune of the controller was ineffective.

Although the effort in modeling and testing the system was unsuccessful, this approach allowed a better understanding its functionality. The dq coupling is proved to be a problem that cannot be ignored and that is hard to consider when modeling the system control. Besides that, this approach proved to be impossible to be used to tune the controller in the amount of time available for this work. Therefore, another form of tuning the PI is chosen: Manual Tune.

Manual tuning is an online method that requires advanced control knowledge and skills, as well as fast simulation capabilities. The method consists in evaluating the time constants of the system after which a coherent proportional gain is applied, which would theoretically turn the system stable but with poor performance. This is done with integral and derivative gains being zero. Then, the integral gain is raised to decrease the steady-state error. This should lead to some overshoot or even instability, which should be dealt decreasing the proportional gain. Finally, the derivative gain is added as needed, if needed at all. The influences that increasing each controller parameter independently has in the system response behavior are resumed in Table 4.4 [23].

Table 4.4 - Influence of increasing controller parameter in response behavior.

Controller Parameter	Rise Time	Overshoot	Settling Time	Steady-state error	Stability
K_p	Decrease	Increase	Small Increase	Decrease	Degrade
K_i	Small Decrease	Increase	Increase	Decrease significantly	Degrade
K_d	Small Decrease	Decrease	Decrease	No effect/Small change	Improve if Kd small

Having these effects in mind and performing several tests evaluating their results, both PIs are tuned simultaneously. As said before, there is one PI that regulates i_d for generating V_{d_ref} and another PI that regulates the torque (which is proportional to i_q) for generating V_{q_ref} . The results are shown on Table 4.5 and Table 4.6 and are in the form that is presented in PSIM PI block: a gain K_p and a time constant $T_i = \frac{K_p}{K_i}$. In other words, in PSIM it is impossible to change a single gain without changing the other.

Table 4.5 - I_d PI gains.

K_p	1
T_i	0.01

Table 4.6 - Torque PI gains.

K_p	5
T_i	0.0001

4.3. Controller platform

A controller platform research must be done before any physical implementation of the system. Nowadays, the development of faster, smaller and better micro-processors allows that many different approaches could be considered in a vehicle application. Having in mind the initial requirements of the system to be controlled, and the controller itself, an appropriate platform should be chosen in order to suit perfectly to the situation. In this way, three main platforms are considered in vehicles applications, based on: general purpose or specific micro-controllers, DSPs (Digital Signal Processors) and FPGAs (Field-Programmable Gate Array). DSPs and FPGAs based platforms are emerging in this industry quite recently and for that reason their characteristics will be compared in this section.

A DSP is designed to be used in signal processing applications where functions like signal convolution, Fourier Transform or finite impulse filters are needed. It is also intended to be small, with low power consumption and cheaper. Usually it is programmed with C language and fixed- and floating-point is used. The main advantage over the micro-controllers widely used in vehicles applications is that it combines high-speed performance with peripheral circuits, memory and optimized CPU in a single chip [10]. Because of this, the DSP's programming becomes much simpler than FPGA's which is an advantage. Concerning the motor drive, the usage of DSPs opened horizons to other level of performance, allowing a more complex, precise and faster control over the motor dynamics. However, DSP's have a big drawback: the processing is sequential. This architecture turns the DSP in a non-deterministic platform with relation to time, which can be a problem when one of the main issues in vehicles applications is the safety. For example, if some process takes more time to finish, the whole system is delayed.

With respect to FPGA, it is a structure of thousands of logic cells and interconnections that are rearranged in order to perform the control algorithm that the programmer designs. A representation of this architecture is presented in Fig 4.10. The language used to program the FPGA is Verilog or VHDL. There are two basic kinds of FPGAs: SRAM-based reprogrammable and OTD (One Time Programmable). The SRAM FPGA is the most common and can be reprogramed many times. It needs a system memory to store the data so it can be reprogrammed each time it is powered up. The OTD FPGA uses anti-fuses (contrary to fuses, connections are made, not melted) to make permanent connections in the chip. It does not require a system memory to download the program, however if a change to the program is needed to be done after programming it, the chip has to be substituted [24].

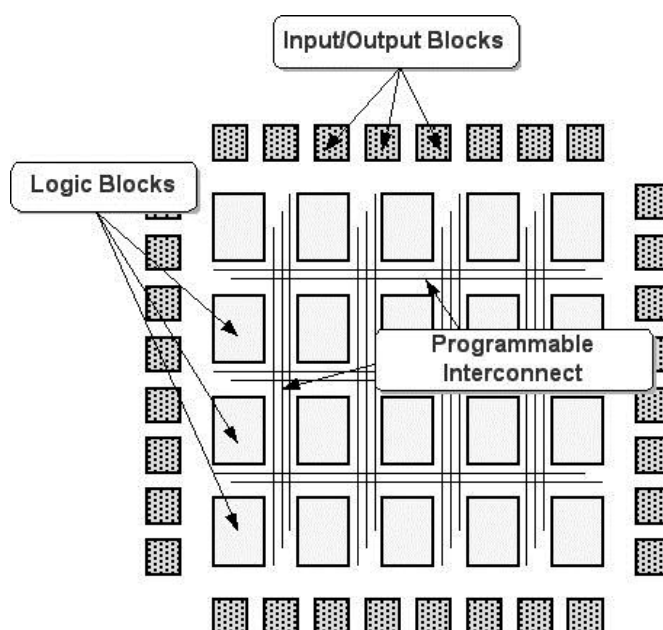


Fig 4.10 - Representation of FPGA architecture.

Unlike the DSP, in FPGA, more than the software, mainly the hardware is programmed. That makes the FPGA programming much more complex than the DSP. This is an obvious disadvantage because the same program would take much longer to program in the FPGA than it would take to program in the DSP. However, this also becomes a very important feature because it makes possible to design many blocks and multi processors capable of running in parallel. This guarantees deterministic latency, which is, once again, critical in functional and safety concerns.

In FPGA the main program could be running in a high speed loop while another high-level safety algorithm could be running in parallel assuring the correct operation of the whole system. This is not possible with the sequential processing of a DSP. FPGA also has an advantage compared to the DSP because it provides a higher sampling frequency. This is important because, in this application, currents and voltages must be measured constantly and with precision. Hereupon, FPGA would be a great choice in the subject of this project.

However, as application specific micro-controllers are being developed nowadays, especially in vehicles applications, some considerations should be done in this regard. A micro-controller is an embedded circuit that contains the main elements to make possible its programming as well as the execution of some type of control. They are the processor, the memory and some inputs and outputs which may include analog-to-digital converters (ADC), serial-port communication (or any other type of communications), interrupts, etc. They are usually much smaller than the DSP or FPGA and consume less energy, though they do not have the same processing capability of the other two. Because of that, and because they are cheaper than the DSP or FPGA, vehicles production companies usually integrate several micro-processors, each one for each purpose among all electrical requirements of the vehicle.

4.4. Partial Results Analysis

In this section the partial results obtained from the methods described before are presented and analyzed. This analysis pretends to be comparative and some conclusions will be drawn. The same test pattern of input is used for all the strategies, thus allowing a better comparison. The simulation runs for 2 seconds of the process. The pattern is described as following: with no load in the motor, the torque reference starts in 0 and rises to 50Nm in 0.3s. It stays there for more 0.2s, when a torque step of 20Nm is introduced (thus reaching 70Nm), staying there for 0.5s. At the second 0.6 a constant load torque of 50Nm is applied to the motor and remains until the end of the simulation. At the second 1.0, and during a transient time of 0.1s, a braking torque of -50Nm is applied and maintained until 1.5s. There, the torque reference is brought to 0Nm and is raised to 70Nm in the remaining 0.5s of the simulation.

This pattern pretends to simulate the starting of the vehicle in a plane surface (although it is known that there is always a load torque due to the vehicle weight and ground friction) with a smooth and constant increase of the acceleration pedal, followed by a quick stroke to the maximum torque available by the pedal length (the match between this pedal position and the torque signal sent to the controller should be limited for safety purposes) predicting a road rise. Next the vehicle enters that ramp so the load torque is increased. The driver is then on an emergency situation and apply full brake until the vehicle is completely stopped. Then the braking pedal is released and another throttle ramp is applied. As the vehicle is in a ramp, and assuming it cannot go backwards just for simulation purpose, it does not start moving until the torque produced is higher than the load torque imposed by the ramp. A graphical representation of this pattern could be seen in Fig 4.11 as well as the expected speed behavior described.

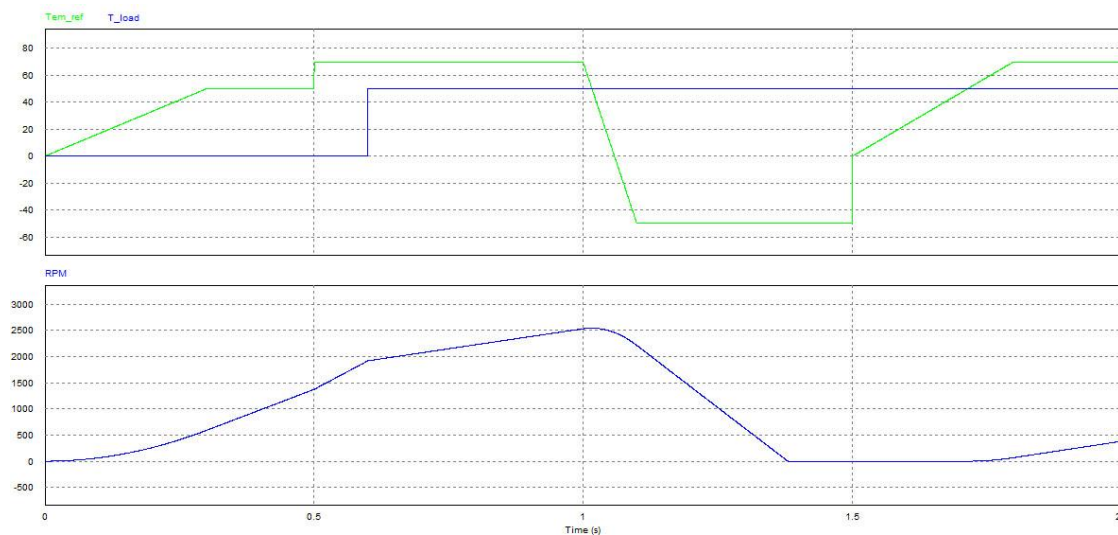


Fig 4.11 - Torque reference and load torque pattern. Expected speed behavior.

4.4.1. Stator current vector angle (θ_i) at 90 degrees with sine-PWM

This method is implemented like shown in Fig 4.1. A torque reference is given which then generates i_q reference which, in turn, generates V_q reference. At the same time, I_s is calculated and maintained at 90° from the d -axis (rotor flux vector). This turns into an i_d reference by multiplying a co-sine function with I_s module. This reference generates V_d reference which, together with V_q reference, are transformed into three-phase sinusoidal quantities through inverse Park Transformation and compared with a triangular waveform at 5kHz. The simulation time step is $1\mu s$.

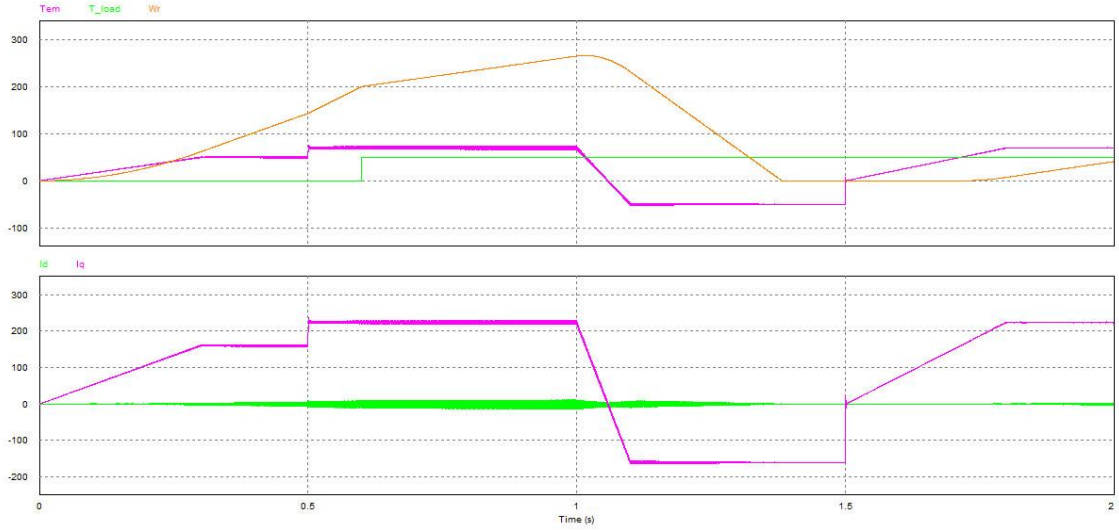


Fig 4.12 - Results for I_s at 90° with sine-PWM. Top graphic: torque produced, load torque and rotor angular speed; Bottom graphic: i_d and i_q .

The results show that this method has a good dynamic response and that the torque produced is following its reference independently of the load torque. Moreover, the rotor speed behavior is the expected in relation with the torque variations. The delays with relation to torque changes are due to the inertia of load, which is 0.1kg.m^2 . It is possible to see that the control tries to bring i_d to zero thus making torque directly proportional to i_q , as it is supposed to be in this method. This assumption can be confirmed analyzing the stator current vector angle θ_i in Fig 4.13. It stays in 90° during motoring action and -90° during generator (braking) action, despite torque and speed variations. It is also possible to see that when a negative torque reference is given, the θ_i angle becomes lagging θ_λ angle, turning θ_T angle negative and confirming what is explained before about torque and torque angle. Furthermore, on the bottom graphic the modules of I_s and λ_s can be seen. λ_s module is multiplied by 1000 making possible its visualization comparatively to I_s , since L_d and L_q are very small. It is noteworthy that torque can only be negative due to θ_T because $|I_s|$ and $|\lambda_s|$ can never be negative by their definition. Also, $|I_s| = 0 \Rightarrow |\lambda_s| = \lambda_f$, which means that air-gap flux is only due to rotor's PMs when stator current is zero.

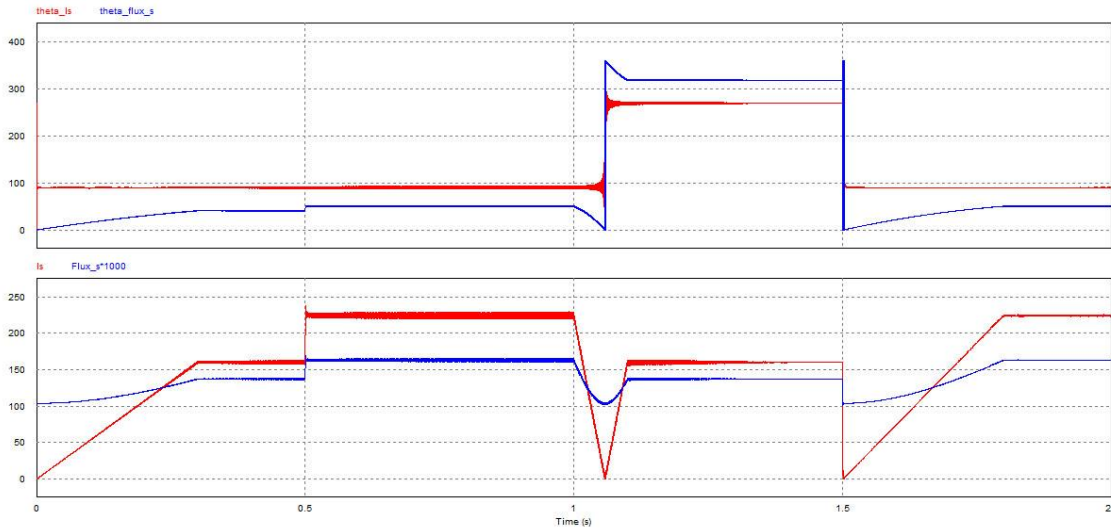


Fig 4.13 - Results for I_s at 90° with sine-PWM. Top graphic: stator current angle θ_i and air-gap flux angle θ_{λ} ; Bottom graphic: I_s and λ_s (x1000) modules.

4.4.2. Air-gap flux vector angle (θ_{λ}) at 90 degrees with sine-PWM

In this method, the air-gap flux vector is maintained at 90° from d -axis. The simulation conditions are the same as before.

At first sight, the results with this method look much like the previous one: the torque produce is proportional to i_q and the speed variations are pretty much the same. However, with a careful analysis, it is possible to see that in this case i_d current is not zero. Instead it is such to make air-gap flux d - component zero, that is $i_d = -\frac{\lambda_f}{L_d}$. Furthermore, the ripple of the torque is less with this method which is an advantage.

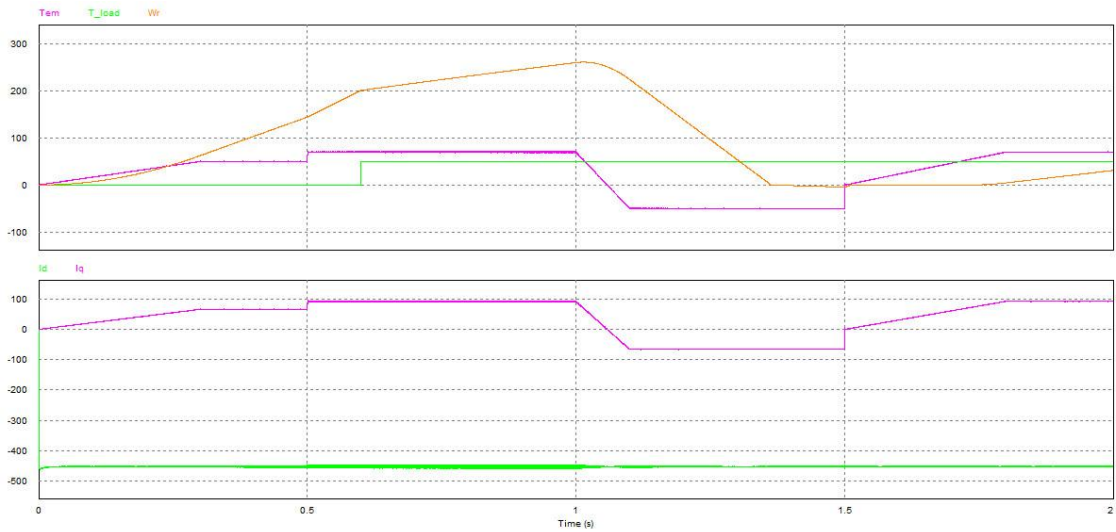


Fig 4.14 - Results for λ_s at 90° with sine-PWM. Top graphic: torque produced, load torque and rotor angular speed; Bottom graphic: i_d and i_q .

Analyzing the angles of stator current and air-gap flux vectors in Fig 4.15 is possible to conclude that this method is working properly because θ_λ is maintained at 90° , or -90° when braking because i_q current becomes negative. Another remarkable aspect is the amplitude of I_s . It is almost twice that in the previous method and it stays almost constant along the simulation. The author claims that this is because of the i_d needed to maintain λ_d at zero. Also, as i_d does not produce torque directly, some more i_q current must be used, thus creating a very large I_s . Although this method has less torque ripple and almost constant stator current, the amount of current needed is a huge drawback in an application like electric vehicles.

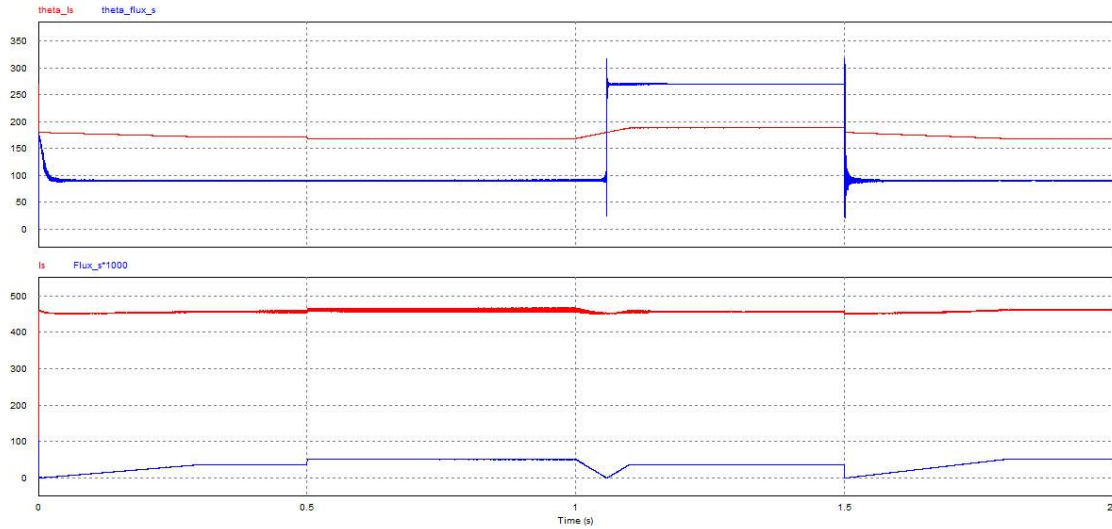


Fig 4.15 - Results for λ_s at 90° with sine-PWM. Top graphic: stator current angle θ_i and air-gap flux angle θ_λ ; Bottom graphic: I_s and λ_s (x1000) modules.

4.4.3. MTPA with sine-PWM

The last method concept is based on using the less current possible to a given torque reference. The same situation, with same parameters, is evaluated.

There are two very important things to analyze here: one is the behavior of stator current vector in relation to the air-gap flux vector. The other is the behavior of dq current components in relation to each other. Previously in this document it was assumed that the torque should be maximum when θ_T is 90° . In this case, since the current must be the minimum possible and, as shown in the previous method, the air-gap flux vector is very small in amplitude, θ_T should be close to 90° .

As it is possible to see through Fig 4.16 the torque ripple is between the first and the previous methods. However, the differences are not noteworthy. On the other hand, the dq current components behavior is significant. They are such that make the stator current be the less possible, so their behavior in relation to each other is not easily predicted. Nevertheless, it is possible to see that, despite the method used, the torque produced is always directly proportional to i_q . This method also introduces a slight i_q overshoot on step

transitions. Although it is not relevant having in consideration its amplitude and duration, in section 4.4.4 it is possible to see that it does not exist.

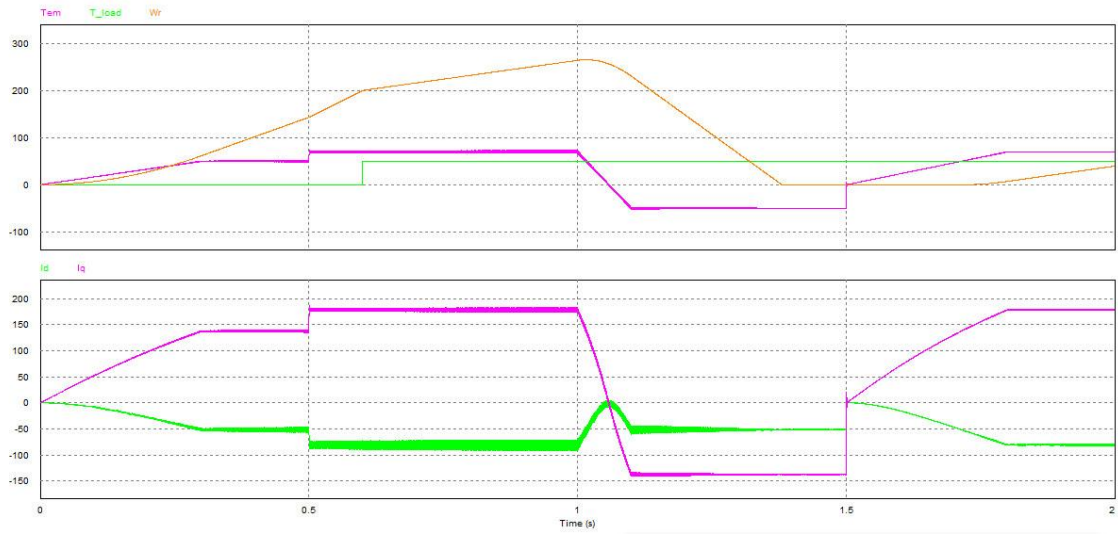


Fig 4.16 - Results for MTPA with sine-PWM. Top graphic: torque produced, load torque and rotor angular speed; Bottom graphic: i_d and i_q .

The results in Fig 4.17 show that the torque angle is less than but close to 90° . Furthermore, the module of I_s is smaller than the other methods along all the simulation, as it is supposed.

This leads to the conclusion that, in the present application of an electric vehicle, the MTPA method is the best choice because it has approximately the same dynamic results with respect to torque than the other two methods, but it uses less current, which is priority in this case.

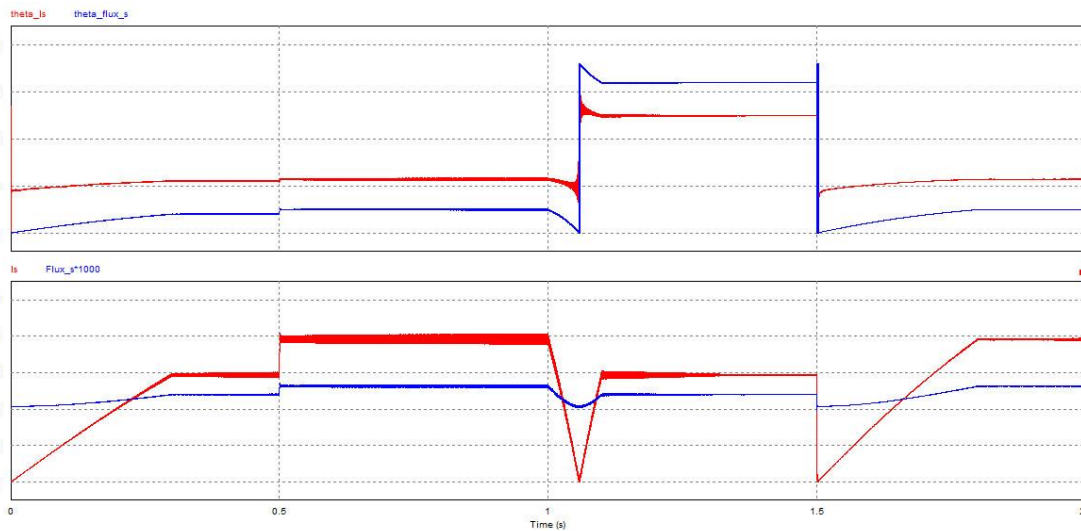


Fig 4.17 - Results for MTPA with sine-PWM. Top graphic: stator current angle θ_i and air-gap flux angle θ_λ ; Bottom graphic: I_s and λ_s (x1000) modules.

4.4.4. MTPA with SVM

Since MTPA has the best overall performance, it is chosen to compare the two signal generation techniques discussed before: sine-PWM and SVM. The same conditions are settled including the frequency of SVM that is 5kHz.

It is possible to see through Fig 4.18 and Fig 4.19 that the torque ripple is almost inexistent (about 0.4%), and the current and flux vectors have less ripple too. Moreover, there is no current overshoot in any case tested unlike with the sine-PWM method. This is expected since SVM method has a better dynamic response than sine-PWM.

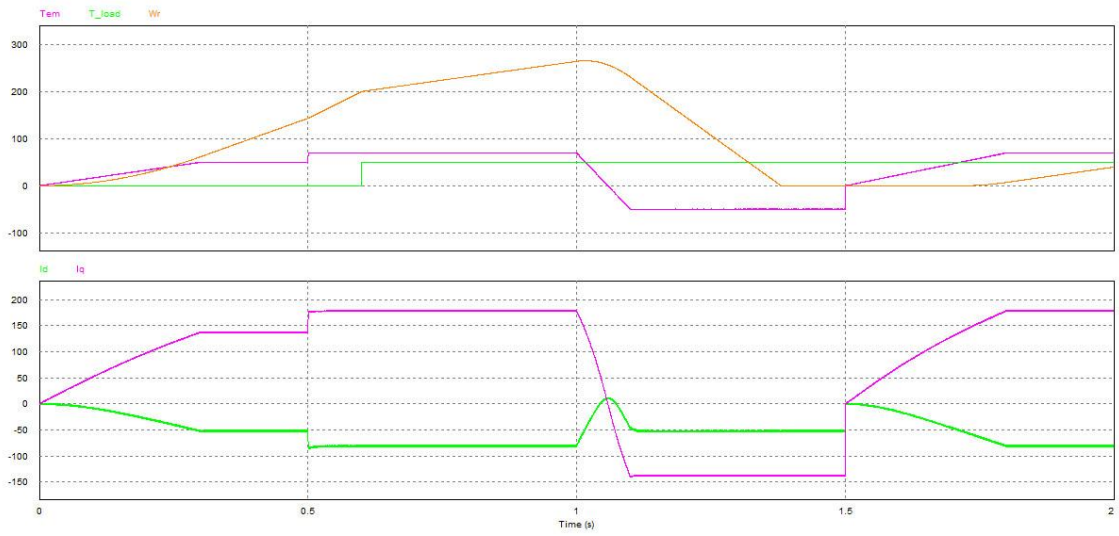


Fig 4.18 - Results for MTPA with SVM. Top graphic: torque produced, load torque and rotor angular speed; Bottom graphic: i_d and i_q .

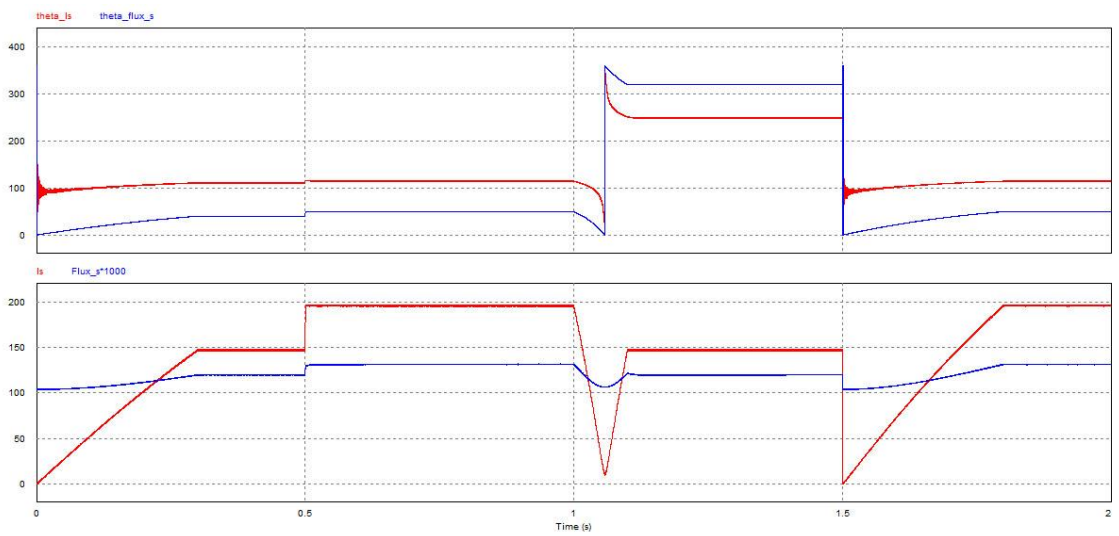


Fig 4.19 - Results for MTPA with SVM. Top graphic: stator current angle θ_i and air-gap flux angle θ_λ ; Bottom graphic: I_s and λ_s ($\times 1000$) modules.

Despite the better results obtained with SVM, as the application of this control is an electric vehicle, the differences in motor's dynamic response are not considerable. There are more important issues to deal with like safety and system robustness that are more easily achieved with a simple system rather than a complex one. Thereby, a system with sine-PWM signal generation is not discarded for this application. Its frequency could be adjusted to the controller platform chosen, so the higher frequency can be settled without harming the system performance.

4.5. System Behavior Based on Power Balance

For a better understanding of the motor's operation and the results obtained, a power analysis is made. With permanent magnet synchronous motors it is possible to force them to consume/produce reactive power, either with lagging or leading power factor. This is because of the vector control, which allows a precise and instantaneous control over the voltage and current that fed the motor.

In the control method used (MTPA) active and reactive power are not directly controlled. Instead, the method tries to reduce the current required by the motor, "ignoring" the power factor. The consequence is that, depending on the operating conditions the motor could be absorbing or injecting active or reactive power, if that's the case in which the motor uses less current for the torque demanded.

4.5.1. Power definitions

Before any considerations about the power flow it is necessary to clarify the definitions about power concepts. Since the motor used is a PMSM the currents and voltages waveforms are nearly perfect sinusoidal. To simplify, any distortions that could occur are not considered, so the waveforms are considered to be always perfectly sinusoidal.

The basic concept behind active and reactive power is that they result from the product between the root mean square (RMS) values of voltage and current affected by the co-sine and sine values of the phase shift between these units, respectively. Active power is defined as the power effectively used by the loads in an electric system, and non-active power represents the remaining power components in the same system.

The following considerations about the various theories written with respect to the power definitions are presented in [25].

Nowadays two main theories are references to power definitions:

- One developed by Budeanu in 1927 in which voltages and currents are defined in frequency domain;
- The other, developed by Fryze in 1932 where voltages and currents analysis are done in time domain.

Nevertheless, as this is a controversy issue, many other researchers devoted their work to this subject and consequently many theories were published over the decades. For example, Darrieus said that reactive energy is the difference between magnetic energy and electric energy of the circuits. Pillet applied this concept to voltages and currents, in frequency domain, with the restriction that these quantities should be periodic and with average value being zero. For Filipsky only active power has significance, whereas reactive power results from mathematical manipulations between apparent and active power.

In the 80's, Akagi proposed a new definition of power for three-phase systems: p-q Theory, or Instantaneous Reactive Power Theory. He based himself in the interest of knowing the instantaneous values of the power, thus having no requirements in periodicity or past registers of voltage and current values. Subsequently other theories have emerged in order to generalize the Instantaneous Reactive Power theory. Those theories are based on the usage of spatial vectors to represent instantaneous values of voltage and current. The scalar product and vector product of these vectors allow obtaining active and reactive power, respectively.

4.5.2. Mathematical Expressions

For now on, in this subchapter, the uppercase letters are RMS values and lowercase letters to instantaneous values.

In a single-phase electric system with AC voltages and currents, a power source produces an instantaneous voltage defined as:

$$v(t) = \sqrt{2} V \sin(\omega t) \quad (4.18)$$

If an inductive and linear load is applied, the current is defined as:

$$i(t) = \sqrt{2} I \sin(\omega t - \varphi), \quad (4.19)$$

where V and I are the RMS values of voltage and current, respectively, ω is the angular frequency of the fundamental component and φ is the phase shift between voltage and current.

Instantaneous power is then defined by instantaneous variation rate of the electric energy $W(t)$ from the source to the load:

$$p(t) = \frac{dW(t)}{dt} = v(t) \cdot i(t) \quad (4.20)$$

When this rate is negative, the energy flows from the load to the source. This is exemplified by the power expression in a purely resistive load, $p(t) = R[i(t)]^2$, which is always positive, indicating that the power flows from the source to the load.

Active power is the mean value of the instantaneous power in a finite time period defined by:

$$P = \frac{1}{kT} \int_{\tau}^{\tau+kT} v(t)i(t)dt, \quad (4.21)$$

where T is the time through the measuring is done, τ is the initial instant of the measurement and k is a positive integer number.

In sinusoidal circuits, this power represents the active power transferred to the load and is defined as in (4.22). It is also determined that the reactive power is complementary and defined as in (4.23).

$$P = VI \cos \varphi \quad (4.22)$$

$$Q = VI \sin \varphi \quad (4.23)$$

This shows that the reactive power is related with the energy exchange between the source and the load, caused by the phase difference between voltage and current.

Apparent power is obtained by the product of RMS values of voltage and current and can also be calculated through power triangle shown in Fig 4.20.

$$S = VI = \sqrt{P^2 + Q^2} \quad (4.24)$$

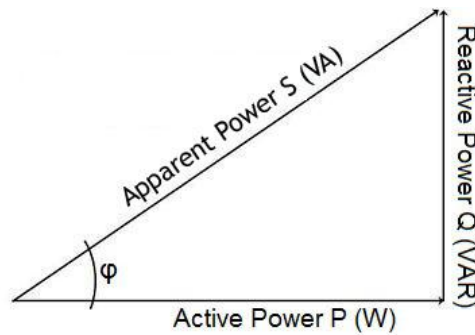


Fig 4.20 - Power Triangle

Finally, power factor is obtained by the quotient between active and apparent power as following:

$$F_p = \frac{P}{S} = \cos \varphi \quad (4.25)$$

Moving to three-phase system, all the considerations done above are adapted easily. Considering k each of the three-phase waves, instantaneous voltage is given by:

$$v_k(t) = \sqrt{2} V_k \sin \left(\omega t - \frac{2\pi}{3} (k - 1) \right), k \in \{1, 2, 3\} \quad (4.26)$$

And instantaneous current is given by:

$$i_k(t) = \sqrt{2} I_k \sin\left(\omega t - \varphi_k - \frac{2\pi}{3}(k-1)\right), k \in \{1,2,3\} \quad (4.27)$$

Instantaneous power in a balanced three-phase system is given by the sum of the instantaneous power in each phase as in (4.28).

$$p(t) = \sum_{k=1}^3 v_k(t) \cdot i_k(t), k \in \{1,2,3\} \quad (4.28)$$

Substituting the voltage and current expressions given before and admitting a symmetric and balanced three-phase system, it is possible to write the following relations:

$$P_T = \sum_{k=1}^3 P_k = 3VI \cos \varphi \quad (4.29)$$

$$Q_T = \sum_{k=1}^3 Q_k = 3VI \sin \varphi \quad (4.30)$$

$$S_T = \sum_{k=1}^3 S_k = 3VI \quad (4.31)$$

4.5.3. P-Q Theory

As said before, P-Q Theory was developed by Mr. Akagi in the early 80's. This theory is valid only in three-phase systems, either balanced or unbalanced, with or without harmonic distortion.

The singularity of this theory is that it uses the Clarke Transformation (3.2) in voltages and currents to calculate instantaneous active and reactive power.

Since this theory can be represented in the complex plane, it is usual to find in the literature *real power* instead of *active power*, and *imaginary power* instead of *reactive power*. Applying this definition of complex power to voltage and current vectors allow the writing of those vectors as:

$$\mathbf{v}_{\alpha\beta} = v_\alpha + jv_\beta \quad (4.32)$$

$$\mathbf{i}_{\alpha\beta} = i_\alpha + ji_\beta \quad (4.33)$$

Thus, the complex power can be defined by (4.34) where the first part is the active or real power and the second part is the reactive or imaginary power.

$$\mathbf{s} = \mathbf{v}_{\alpha\beta} \mathbf{i}_{\alpha\beta}^* = (v_\alpha i_\alpha + v_\beta i_\beta) + j(v_\beta i_\alpha - v_\alpha i_\beta) \quad (4.34)$$

It is now possible to say that instantaneous active (p) and reactive (q) power in a balanced three-phase system without neutral conductor are given by:

$$\begin{bmatrix} p \\ q \end{bmatrix} = \begin{bmatrix} v_\alpha & v_\beta \\ -v_\beta & v_\alpha \end{bmatrix} \begin{bmatrix} i_\alpha \\ i_\beta \end{bmatrix} \quad (4.35)$$

Furthermore, it is possible to transform the reactive power expression back to a three-phase reference frame with inverse Clarke Transformation, which shows that it is obtained by the cross product between currents and voltages of different phases, proving that this power does not contribute to the energy transferred from the source to the load, being a “fictitious” power.

$$q = v_\beta i_\alpha - v_\alpha i_\beta = \frac{1}{\sqrt{3}} [(v_a - v_b)i_c + (v_b - v_c)i_a + (v_c - v_a)i_b] \quad (4.36)$$

Later, two researchers (Ferrero and Superti-Fuga) proposed an analysis based on p-q theory but in the dq reference frame, that is applying the Park Transform (3.5) to voltages and currents. This results in an apparent power given by (4.37) which has the advantage to be represented in a rotating reference frame without losing significance. All the considerations done before are also valid in this approach.

$$s = v_{dq} i_{dq}^* = (v_d i_d + v_q i_q) + j(v_q i_d - v_d i_q) \quad (4.37)$$

This theory brought the possibility of new control methods and better analysis of the operational behavior of electric systems, namely in electric motors.

4.5.4. Power Control

Using the concepts discussed before it is possible to design a control scheme that permits a type of sensorless control over the PMSM. Reading only voltages and currents that fed the motor it is possible to estimate the torque that is been produced by the motor by equation (4.38).

$$T_{em} = \frac{P + \text{friction} + \text{winding} + \text{core loss}}{\omega_r} \quad (4.38)$$

where P is the electrical power effectively converted in mechanical power and ω_r is the rotor angular speed.

Ignoring the losses caused by friction and winding and assuming that core losses are given by $P_{winding} = RI^2$, electromagnetic torque can be expressed as:

$$T_{em} = \frac{P + P_{winding}}{\omega_r} \quad (4.39)$$

This approach has two main issues: first, although a position sensor is not required, it is impossible to apply this concept without any rotor speed information. Second, the power is calculated using the voltage measured, which is commutated at the inverter's high frequency. This means that is necessary to add a filter in this estimation, introducing delays and phase shifts that must be considered and harm the system robustness.

Thus, this approach has been tested in PSIM as shown in Fig 4.21. First it is necessary to analyze the frequency of both voltage and current waves so a proper filter should be

designed. Then a dynamic gain is designed to compensate the signal attenuation caused by the filter. Active and reactive powers are calculated based on equations from the system (4.35). Reactive power could later be used for enhancing the control. Finally the torque is calculated by subtracting the core losses to the power calculated and dividing the result by the rotor speed. The average value of this result is then calculated.

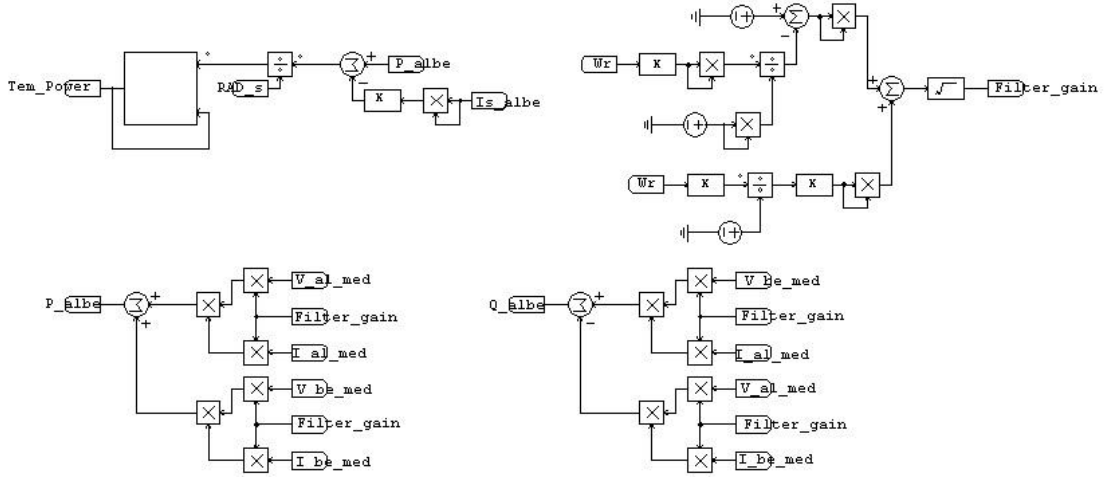


Fig 4.21 - Sensorless control based on power balance. Top left: Electromagnetic torque calculus; Top right: Dynamic filter gain; Bottom left: Active power calculus; Bottom right: Reactive power calculus.

To better understand the dynamic gain designed it is important to first understand how a low-pass filter works. The transfer function of a first-order low-pass filter is given by:

$$G(s) = k \cdot \frac{\omega_c}{s + \omega_c} \xrightarrow{k=1} \frac{1}{\frac{s}{\omega_c} + 1}, \quad (4.40)$$

where ω_c is the cut-off frequency of the filter.

Control theory says that the gain and phase of (4.40) are given by (4.41) and (4.42), respectively. The Bode diagram according to equation (4.40), with a cut-off frequency of 5Hz, can also be seen in Fig 4.22. Remember: $\omega_c = 2\pi f_c$ and $X_{dB} = 20\log(X)$.

$$|G(j\omega)|_{dB} = -20\log\left(\sqrt{1 + \left(\frac{\omega}{\omega_c}\right)^2}\right) \quad (4.41)$$

$$\angle G(j\omega) = -\tan^{-1}\left(\frac{\omega}{\omega_c}\right) \quad (4.42)$$

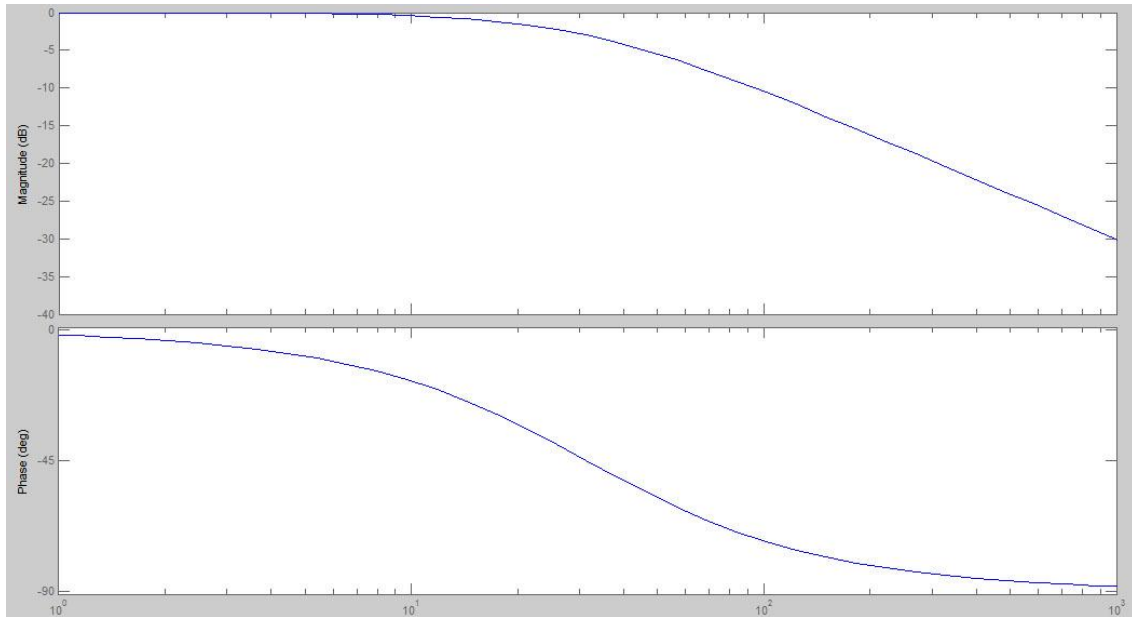


Fig 4.22 - Bode Diagram of a first-order low-pass filter. $f_c = 5\text{Hz}$.

However, to achieve better filtering, a second-order low-pass filter is chosen instead. This filter has the following transfer function:

$$G_{2nd}(s) = k \cdot \frac{\omega_c^2}{(s + \omega_c)^2} \xrightarrow{k=1} \frac{\omega_c^2}{s^2 + 2\xi\omega_c s + \omega_c^2} \quad (4.43)$$

Once again, it is known that the gain and phase of (4.43) are calculated through (4.44) and (4.45), respectively. The Bode diagram that represents this filter with $\omega_c = 2\pi \times 5 \cong 31,4 \text{ rad/s}$ is presented in

$$|G_{2nd}(j\omega)|_{dB} = -20 \log \left(\sqrt{\left(1 - \frac{\omega}{\omega_c}\right)^2 + \left(2\xi \frac{\omega}{\omega_c}\right)^2} \right) \quad (4.44)$$

$$\angle G_{2nd}(j\omega) = -\tan^{-1} \left(\frac{2\xi \frac{\omega}{\omega_c}}{1 - \left(\frac{\omega}{\omega_c}\right)^2} \right) \quad (4.45)$$

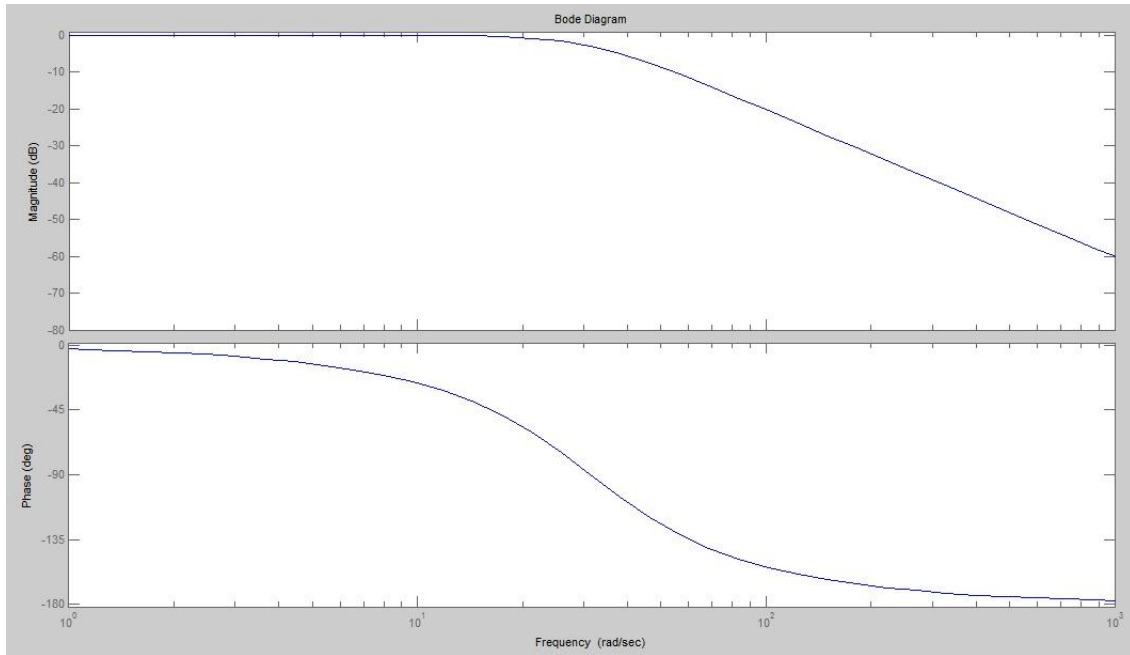


Fig 4.23 - Bode Diagram of a second-order low-pass filter. $f_c = 5\text{Hz}$.

This control analysis allow the filter designer to know essentially two things: first, if it is intended to have the same signal amplitude of the input at the output, as in this case, the gain of the filter must be amplified by a gain that varies with the frequency of the input signal, since it introduces attenuation. Second, as it is intended to calculate power and thus two quantities are needed (voltage and current), both have to be filter (despite the current signal being already sinusoidal) so their phases are affected by the same phase shift, thus not interfering in the calculus. With this in mind, the power and consequently the torque are calculated as shown in Fig 4.21.

Although this technique seems to be very promising, it did not give good results in the motor control. The author claims that the main reason for that is the startup at zero speed. Since there is no rotor speed, the torque calculated when the system starts it is theoretically infinite. More, there are motor losses that are not considered, what could cause inaccuracies harming the control. Finally, since the motor has a wide speed range and it depends on the current frequency, the low-pass filter needs to be designed with a very low cut-off frequency. Although a dynamic gain is designed to compensate the attenuation, at high frequencies it loses accuracy, again harming the control robustness. Therefore there will not be presented any simulations results with this technique.

4.6. Summary

The control of the PMSM is presented in this chapter. The strategy, consisting in a torque reference scheme, is described and 3 different methods are discussed: stator current vector at 90° , air-gap flux vector at 90° and Maximum Torque Per Ampere. Then, two different signal generation techniques for the inverter are presented: Sine-PWM and SVM. SVM design is

explained and due to its dynamic characteristics it is considered the best. Three different controller platforms are then presented: DSP, FPGA and specific application micro-controller. Their main characteristics are exposed and because of DSP sequential processing architecture, it is discarded for a possible vehicle application. Among the other two platforms, FPGA is considered the best because of its processing abilities and parallel architecture. Four tests were performed, one for each method and another one for MTPA with SVM. The aim of the last test is to compare sine-PWM with SVM and MTPA method is chosen because it has the best overall performance. It is proved that SVM has better dynamic performance than sine-PWM and for that reason is chosen for a future implementation of this system. Finally the system behavior based on power balance is discussed. P-Q theory is described in order to allow the system analysis in dq frame. This approach is used as a position sensorless technique, although without good results. Its implementation is described but due to the lack of valid results, none are presented.

Chapter 5

System Sensorless Control

5.1. Introduction

Controlling a permanent magnet synchronous motor usually requires knowing the rotor position to perform an effective stator current vector control. This implies the purchase of sensors which can be expensive. Besides that, considering a vehicle application, more wiring is needed which decreases the robustness and reliability of the system, increases the need of maintenance and the inertia of the vehicle and introduces noise problems. Usually this sensor is a shaft-mounted optical encoder, resolver or Hall sensors. Furthermore, the rotor speed is also frequently required implying the usage of another sensor.

In order to overcome this problem some new control techniques have emerged based on a sensorless approach. They consist in estimating the rotor position and speed in order to accomplish the same results that are obtained if a sensor is used. These techniques can roughly be divided in the following categories which will be discussed in this chapter:

- Back-EMF estimators
- State observers
- Sliding-mode observers
- High-frequency signal injection
- PLL-based estimators

5.2. Sensorless Techniques Comparison

This section pretends to briefly describe some sensorless techniques used to control a PMSM. Although sensorless control is a very recent technique, several solutions are available in the literature [26]-[40]. Most of them require some kind of startup assistance in order to achieve proper control of the system. Others are not feasible in vehicles applications. Some of the techniques described could be put together so better results could be achieved. An example of this is presented in [26] where Back-EMF estimation is combined with High-frequency signal injection in a hybrid vehicle application.

Back-EMF estimators, State observers and Sliding-mode observers were tested in PSIM without any good results. However, one of the previous techniques proved to be worthwhile and it has been implemented with good results: PLL-based position and speed estimator. Its description and design is detailed on 5.2.5.

5.2.1. Back-EMF Estimator

For this kind of sensorless estimation two stator line voltages and currents measurements are required. Then, the third line voltage and current is calculated and the Clarke Transformation is applied to obtain α and β voltage and current components in the stationary frame. The stator flux vector module and angle are calculated knowing the α and β components of the flux, which are estimated by the expression:

$$\lambda_{\alpha\beta} = \int v_{\alpha\beta} - R_s \cdot i_{\alpha\beta} dt, \quad (5.1)$$

where $\lambda_{\alpha\beta}$ is the flux, $v_{\alpha\beta}$ is the voltage, R_s is the stator phase resistor, $i_{\alpha\beta}$ is the current and the subscript $\alpha\beta$ refers to α and β components, respectively.

The module and angle of the flux vector is then given by:

$$|\lambda_s| = \sqrt{(\lambda_\alpha)^2 + (\lambda_\beta)^2} \quad (5.2)$$

$$\angle \lambda_s = \tan^{-1} \frac{\lambda_\beta}{\lambda_\alpha} \quad (5.3)$$

The rotor position is assumed to be given by the angle of stator flux and the speed by its first derivative. This obviously affects the performance of the controller because the results critically depend on the accuracy of the estimated flux components which, in turn, depend on the accuracy of the measured voltages and currents and the integration algorithm chosen. In addition, this estimation consider that the speed variations are negligible thus ignoring the rotor flux component for the $\alpha\beta$ flux estimation. Although many drift compensations have been reported, the pure integration in the software or hardware circuits can still be problematic at low frequencies, where the stator voltage becomes very small and are dominated by the ohmic voltage drops [27].

5.2.2. State Observer

State observers are other name to closed-loop estimators. That is, estimation of unknown parameters based on motor's measurements, with the use of estimation error to adjust the response of the estimator [28]. State observers are a very common way of applying sensorless control over PMSM. They usually consist in estimate rotor position by variations in motor's parameters, as inductance variations due to magnetic saturation, which are noticed through mathematical calculations knowing motor's model equations. The INFORM technique ("INDirect Flux detection by On-line Reactance Measurement") was proposed by Schroedl [29] and is based on real-time inductance measurements using saliency and saturation effects. During a short time interval, the "complex INFORM reactance" is calculated for estimating

flux angle. However, this technique must be combined with observer techniques to work properly in whole speed range [30].

Other observers known for PMSM sensorless control are Extended Luenberger Observer (ELO) and Extended Kalman Filter (EKF). ELO is applicable to non-linear, time-variant and deterministic systems. EKF is a recursive optimum-state estimator, able to provide optimum filtering of the noises in measurements if the covariances of these noises are known. It is an optimal stochastic observer what makes it a viable candidate for the on-line determination of the rotor position and speed of PMSM. “However, none of the practical industry applications of EKF-based sensorless PMSM control has been reported due to the technical difficulties, which may include: 1) detailed dynamic model of PMSM with initial rotor position; 2) formulation of the EKF model in closed form; 3) discrete-time model of the overall controlled system and details of power electronics circuitry and implementation; 4) complex methods for correcting the rotor flux variations; 5) initial speed position convergence; 6) computational expense, specific design, tuning criteria and so on” [27].

5.2.3. Sliding-mode Observer

Among the existing sensorless approaches, sliding mode observer has been recognized as one of the best techniques due to its advantages in robustness to disturbances and low sensitivity to parameter variations.

Briefly, sliding mode observer techniques are based on the state variables of the PMSM. A sliding surface is defined as well as two limits for that surface, creating a hysteresis window. The controlled variable is intended to track that surface and slide along it within the limits imposed.

Some variations of sliding-mode observers are presented in literature [31]-[34]. Yoon-Seok Han presented a technique that uses Lyapunov functions for determining the adaptive law for the speed and stator resistance estimator. This technique showed good results with respect to variations in stator resistance [31]. Elbuluk investigated a sliding mode observer for estimating the rotor position and speed of PMSM considering motor's parameters variations. Instead of directly using filtered switching signals by a low-pass filter, an observer is designed to undertake the filtering task for the estimated back-EMF. It is stated that the observer has the structure of an extended Kalman filter and is expected to have high filtering properties. However, no experimental results are presented [33]. In other article ([34]) Elbuluk claims that the sliding mode technique applied is robust to motor's parameters variations. The results show a parameter detuning of 200% with good results.

5.2.4. High-frequency Signal Injection

High-frequency injection sensorless techniques basically consist in injecting a high-frequency voltage signal in any phase of the motor assuming that is the direction of the rotor flux vector (or d -axis) and measure the current. The current will be highest when the inductance is lowest, that is through the L_d axis. Similarly, the measured current will be lowest when the inductance is higher, meaning that's the direction of L_q axis. Of course that this is only valid in motors where $L_d \neq L_q$, otherwise this technique must not be considered

valid. Once motors' parameters are known, the measurement of these currents and L_d and L_q extraction can align the supposed reference frame with the real rotor position and therefore a sensorless system is achieved.

However, these techniques require high precision and fast measurement, and fast signal processing capability, which inevitably will increase the complexity and cost of control system. Furthermore, the injected high frequency voltages may also cause more torque ripple, shaft vibration and audible noises. Due to the constraints of the maximum PWM switching frequency and the geometry of rotor, such techniques usually work to some specific motors in the limited operating speed range, i.e., only at standstill and low speeds [27].

5.2.5. PLL-based Estimator

This technique, based on [8], pretends to estimate rotor position and speed by synchronizing the estimated reference frame with the real rotor reference frame, which has the rotor flux vector aligned with the d -axis. This is achieved estimating the back-EMF vector created by the rotor's PMs and bringing its d - component in the estimated reference frame to zero. That assumption means that the rotor's back-EMF vector is aligned with the actual q -axis, and consequently the rotor flux vector is aligned with d -axis, as it is supposed to be. Fig 5.1 represents this logic in the vector form. The circumflex accent means that the unit referred is estimated and the angle between the reference frames is defined by $\tilde{\theta}_r = \theta_r - \hat{\theta}_r$.

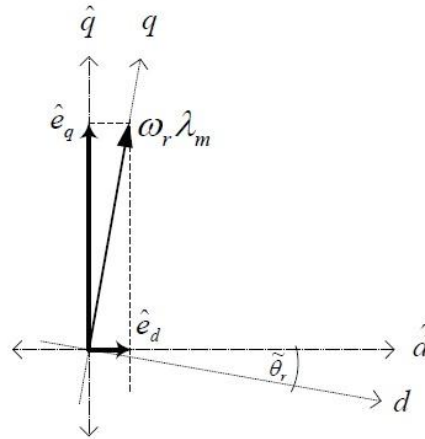


Fig 5.1 - PLL-based estimator logic [8].

From Fig 5.1 it is possible to establish the following geometrical relationship:

$$\hat{e}_d = \omega_r \lambda_f \sin \tilde{\theta}_r \quad (5.4)$$

$$\hat{e}_q = \omega_r \lambda_f \cos \tilde{\theta}_r \quad (5.5)$$

To estimate the d - and q - components of back-EMF in the estimated reference frame, motor's equations are used:

$$\hat{v}_d = R_s \hat{i}_d + L_s \frac{d}{dt} \hat{i}_d - \hat{\omega}_e L_s \hat{i}_q - \hat{e}_d \quad (5.6)$$

$$\hat{v}_q = R_s \hat{i}_q + L_s \frac{d}{dt} \hat{i}_q + \hat{\omega}_e L_s \hat{i}_d + \hat{e}_q \quad (5.7)$$

The estimator logic is described as following: \hat{e}_d is compared with a reference (that is zero) and the error enters in a PI controller. The output of the PI is the estimated speed which is then integrated in order to obtain the estimated position. The position is used to correctly apply the Park Transform to the three-phase voltages and currents that are being measured from the motor. Their d - and q - components, and the estimated angular speed, are then used to calculate the back-EMF dq components as described before. So, when $\hat{e}_d = 0$, means that the error is zero and that the position estimated is actually the real one. This means that the speed from which the position is calculated is also accurate, indicating that the two frames are overlapped.

This technique of estimating the rotor's position can be used since standstill without any other auxiliary system for starting the motor. However, until enough speed to generate measurable back-EMFs is developed, the estimation has some imprecisions. This could be a problem or not, depending on the transmission rate used in the vehicle. If the motor could reach about 80 rad/s in less than a second, the driver does not even notice the oscillations that occur in the first milliseconds. These results are analyzed later in this chapter.

5.2.5.1. PLL Controller Design

According to [8], since the calculation of the back-EMFs should be the fastest element in the sensorless control scheme, it can be approximated by its gain:

$$G_{obs}(s) = \frac{\hat{e}_d(s)}{\hat{\theta}_r(s)} = -|\hat{e}_{dq}| = -\sqrt{\hat{e}_d^2 + \hat{e}_q^2} \quad (5.8)$$

As shown in (5.8), the d - component of the back-EMF \hat{e}_d has a negative signal with respect to the rotor position $\hat{\theta}_r$, so the PI controller must have negative gain to compensate for this. By replacing (5.4) and (5.5) into (5.8) the gain of the estimator becomes proportional to the rotor speed according to the following relation:

$$G_{obs}(s) = -\omega_r \lambda_f \quad (5.9)$$

By inserting a linearization gain before the PI, as shown in (5.11) it is possible to cancel the speed-dependent gain nature of the PLL and to tune the PI with positive gains. The gains of the PI, K_p and K_i , can be obtained after the transfer function of the PLL linearized is known. According to [8] they can be calculated by:

$$\begin{cases} K_p = 2\xi\omega_{pc} \\ K_i = \omega_{pc}^2 \end{cases} \quad (5.10)$$

where ξ is the desired damping factor and ω_{pc} is the desired bandwidth of the rotor position controller.

The linearization gain is then given by:

$$G_{lin}(s) = -\frac{1}{\sqrt{\hat{e}_d^2 + \hat{e}_q^2}} \cong -\frac{1}{\hat{e}_q} \quad (5.11)$$

This approximation is valid assuming that \hat{e}_d is controlled to zero and reaches that value in a short amount of time. Considering this brings a big computational advantage of not having a square root. From the controller platform point of view, this could represent the saving of several micro-seconds, which could be critical.

Good results with this technique are achieved with Matlab Simulink working with PSIM via SimCoupler. This interface lets both simulation platforms run simultaneously allowing, for example, the implementation of the power system in PSIM and all the control in Simulink. Because PSIM is much better in dealing with power systems, and Simulink has many advantages over PSIM in terms of user interface simplicity, pre-built optimized function blocks and some toolboxes created specifically for some controller platforms (like DSP or FPGA), having the possibility of join this two virtual environments in one single system (simulation) is pretty useful.

The PLL-based sensorless logic described before is implemented in Simulink using SimCoupler to interact with PSIM where the power stage is, and the control over the motor is accomplished. The usage of Simulink to implement the control could be an advantage later when the program needed to be programmed in FPGA, because of the toolboxes that Xilinx provide for Matlab. Also, Simulink provides various types of resolving the differential equations that represent the model, whereas PSIM only allows the change in integration fixed time-step parameter, using the trapezoidal rule integration method. Simulink provides many solver types, either for Fixed Time-step as for Variable Time-step. Although each solver apply a different numerical method to solve the ODEs (Ordinary Differential Equation) of the system, many of them are variants of Runge-Kutta method. So, as at first sight it is not necessary a method that is more accurate, the solver chosen for this application is “ode4 Fourth-Order Runge-Kutta” with a Fixed-Step time of 0.1 μ s. More information about the Simulink solver is available in [41].

5.3. Sensorless Control Results

The results obtained with sensorless control are pretty satisfactory. Although they are not as good as with the use of a speed sensor (as expected), the control actually behaves as it should and the motor operation can be assured according to what has been said before in section 4.2.

The PI gains were adjusted as the PI's of torque and i_d in the previous control. As the input of the PLL PI is the error of a back-EMF and the output is supposed to be an angular speed, according to (5.4) the proportional gain should be around the inverse of the value of rotor's permanent magnets flux, times the number of pole pairs. The integral gain should be at least 10 times bigger, so the practical experience says. Thus, these gains were adjusted by analysis of the system behavior among various tests. The gains used are described in Table 5.1 and the PLL-based sensorless speed and position estimator implemented in Simulink is shown in Fig 5.2.

Table 5.1 - Sensorless PLL PI gains.

K_p	60
K_i	1500

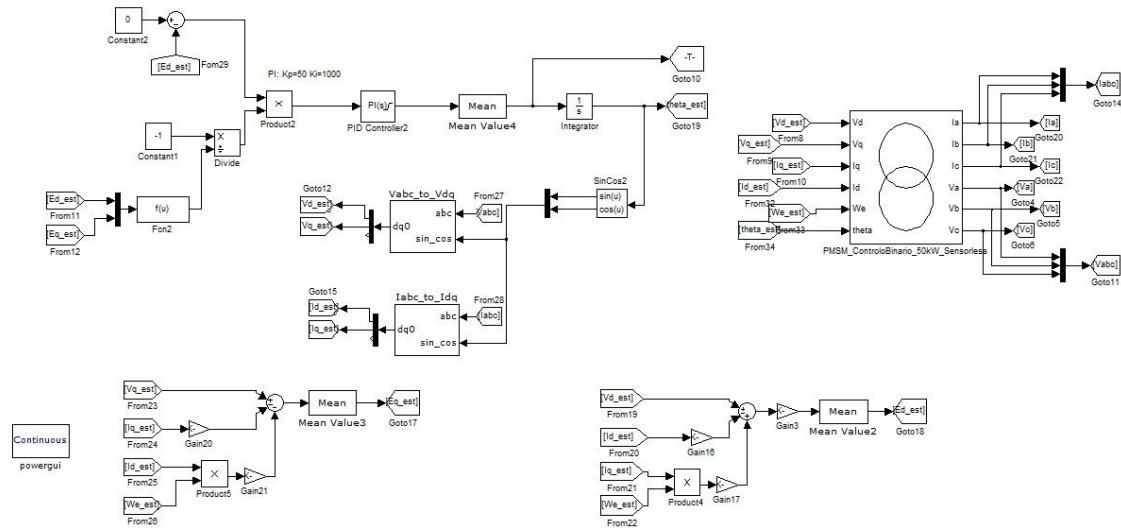


Fig 5.2 - PLL-based sensorless speed and position estimator implemented in Simulink.

In Fig 5.2 it is possible to see the PLL-based logic in the upper left corner, with the error measurement, the linearization gain, the PI controller which generates the rotor electrical angular speed and its integration to generate rotor position. This position is then used to generate dq components to be used in e_d and e_q estimation, represented by the two blocks on the bottom. The speed and position estimated, as well as dq voltage and current components, are sent to PSIM through SimCoupler block on the right of the Fig 5.2, which also receives three-phase measured voltages and currents to be converted.

To demonstrate the correct operation of the motor with the control method described and with sensorless PLL-based technique, a complete test is designed. The motor starts with an increasing torque reference and without load so the speed can increase. Then, it is introduced a constant torque load to the motor with a torque equal to reference torque so the speed can become constant. Then, the load torque increases again to simulate the initiation of road ascension or an obstacle on the road, and consequently the speed decreases. The torque reference rises to compensate this and the speed rises again. The torque is then set to zero, to simulate a complete pedal lifting, and it is possible to see the speed decreasing to zero.

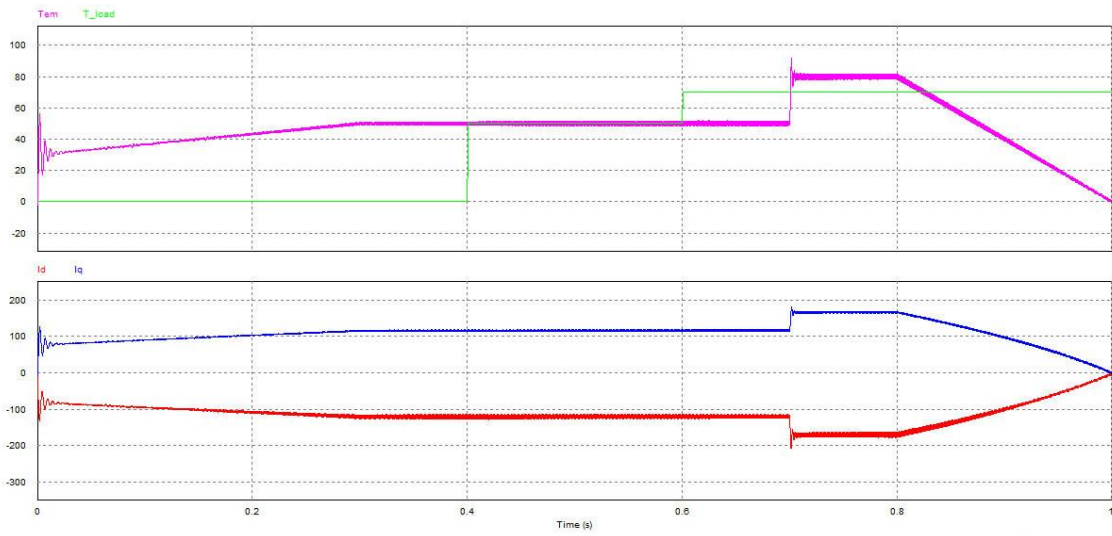


Fig 5.3 - Sensorless operation. Top graphic: Torque produced and load torque. Bottom graphic: i_d and i_q .

Fig 5.3 shows the correct operation of the motor without measuring its rotor position or its speed. The PLL-based sensorless technique described before is proved to be working properly. The method used is MTPA which is proved by the i_d and i_q dynamics. It is important to notice that, despite the controller is working correctly, there is much more overshoot in the transient stages than with rotor position measurement, as well as more ripple in both torque and current. These results are expected since with sensorless operation there is always some delay resultant of the estimation process, as well as small imprecisions in relation to the real rotor position and speed. These differences, although small, are determinant for the best system behavior. Fig 5.4 shows the estimated and measured (not used for the control, just for comparison purposes only) rotor electrical speed and position. It is noteworthy the imprecisions in speed estimation in the first instants of the simulation. This is when the motor is at standstill and at low speeds. Although this estimation error seems very relevant, since it occurs in a very short amount of time it is completely imperceptible for the vehicle's driver.

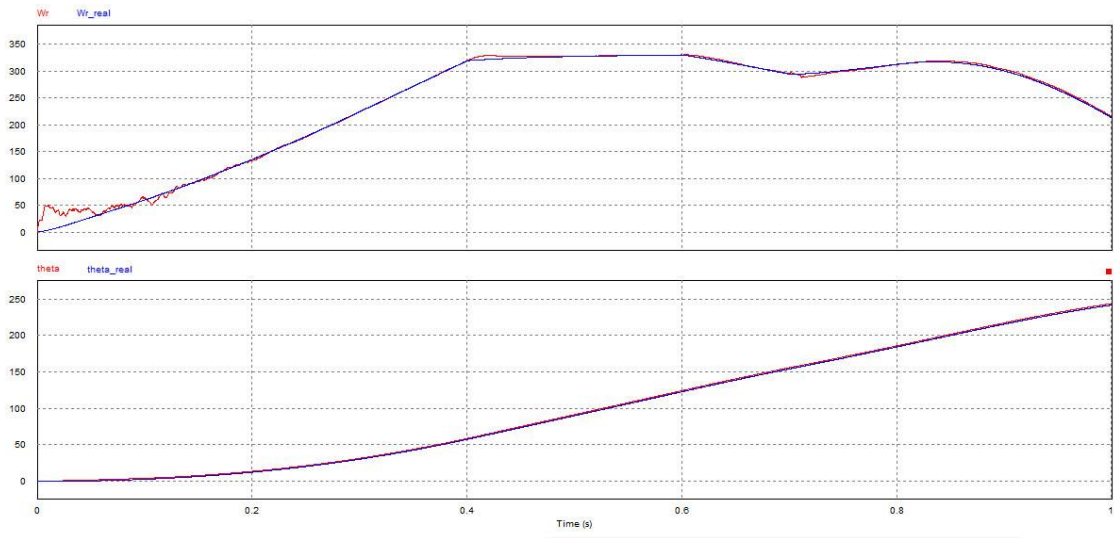


Fig 5.4 - Sensorless operation. Top graphic: Rotor electrical angular speed (W_r - estimated; W_{r_real} - measured); Bottom graphic: Rotor electrical position (θ - estimated; θ_{real} - measured).

5.4. Summary

Several sensorless techniques for controlling the PMSM are presented. They are divided in five categories: back-EMF estimators, state observers, sliding-mode observers, high-frequency signal injection techniques and PLL-based estimators. Each of these categories is described and discussed. Due to the results obtained in PSIM, only PLL-based estimator is further analyzed in this document. Its implementation is explained and the results obtained with Co-Simulation between PSIM and Simulink are discussed. The system proved to be controllable with positive torque reference without any position or speed sensor, validating the estimator operability in this range.

Chapter 6

System Validation

6.1. Introduction

In this Chapter a validation of the system is done. Having in considerations what has been said so far, a detailed analysis about regenerative braking and dynamic performance of the sensorless traction control system is done. Also, several considerations about a future implementation of the work here described are drawn. Finally, some suggestions about what could possibly be done to enhance this work are given.

6.2. Regenerative Braking

A simulation of a real road situation is done in Chapter 4 which included a braking intervention, with negative torque reference. However, that system is using a speed sensor, from which the position information is taken. In Chapter 5 a validation of sensorless system control is done, again trying to simulate a real road situation, but this time without applying a braking torque. That test is performed here and the results are analyzed.

Before the description and analysis of the simulation results, an important remark must be done. As said in section 5.2.5.1 the solvers available for simulation in Simulink are variants of Runge-Kutta method. As it turns out, this mathematical method is not sufficient to perform an accurate simulation with the requirements of this system. Although the system works fine when positive torque reference is given, with sensorless operation in Simulink and all the power and control stages in PSIM, for negative torque reference that does not happen. The author considers that the conditions imposed by the system when calculating the dq components of the back-EMFs at low and negative torque (which means that i_q is also very small or negative) introduce discontinues or undefined solutions, that Runge-Kutta method cannot deal with. As the author in [42] states: “Runge-Kutta is a mathematical integration method based on Euler’s method, which is not recommended for practical use for mainly 2 reasons: the method is not very accurate when compared to other, fancier, methods run at the equivalent step size, and neither is it very stable”. Moreover, when talking about other methods for resolving ODEs, as Bulirsch-Stoer or predictor-corrector methods, the author

creates an analogy saying that “Those methods are the high-strung racehorses. Runge-Kutta is for ploughing the fields”. For these reasons, the exactly same PLL-based estimator designed in Simulink is transposed to PSIM. This system, with the speed and position estimator designed in PSIM as shown in Fig 6.1, is analyzed in this chapter.

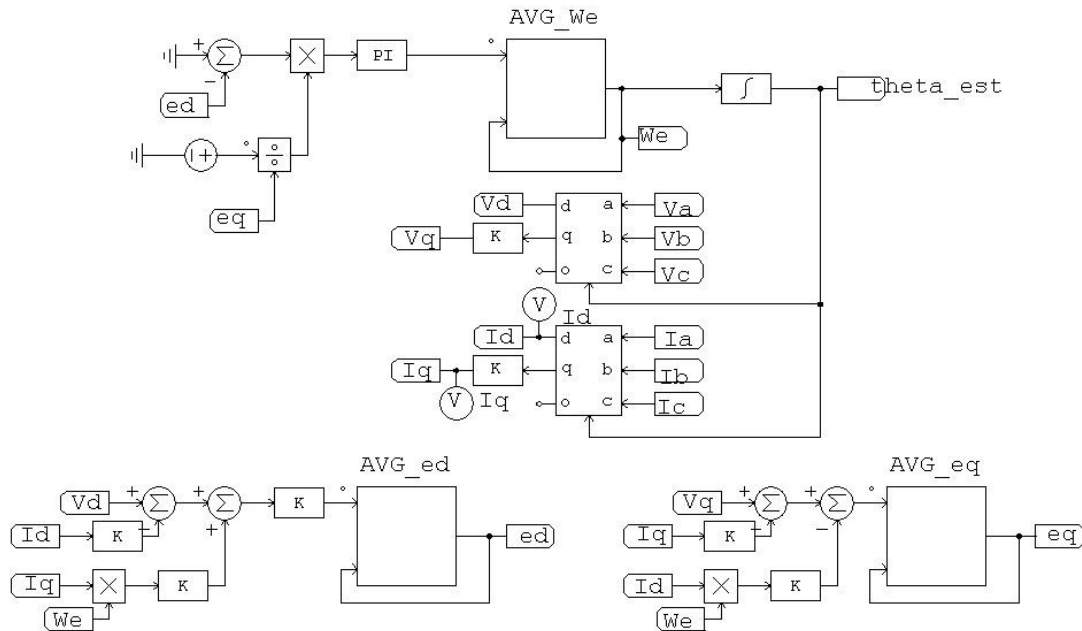


Fig 6.1 - PLL-based speed and position estimator implemented in PSIM.

The C-Blocks presented are used to calculate the average value of their input by using a sliding-window technique. It consists in saving the last X values of the input (being X the amount of samples defined by user) and dividing that sampled values by X. The output is updated each X samples, maintaining its value until another cycle is completed.

The situation that has been tested is described as follows: the motor starts from standstill without load torque and achieves the reference of 70Nm with the speed rising accordingly. At 0.3s the torque decreases to 50Nm and a load is introduced at 0.4s with a constant torque of 50Nm (same as the reference given). The speed is expected to become constant. The same load is maintained until 0.6s. At 0.5s a braking torque is applied, of -50Nm. It remains there until second 0.7, where “the braking pedal” is released slowly. The motor keeps running because of the inertia since no other force is applied to it from the moment that “braking pedal” is released. The torque and current results can be seen in Fig 6.2. As expected there is a small error between calculated and effective electromagnetic torque because of the error in speed estimation.

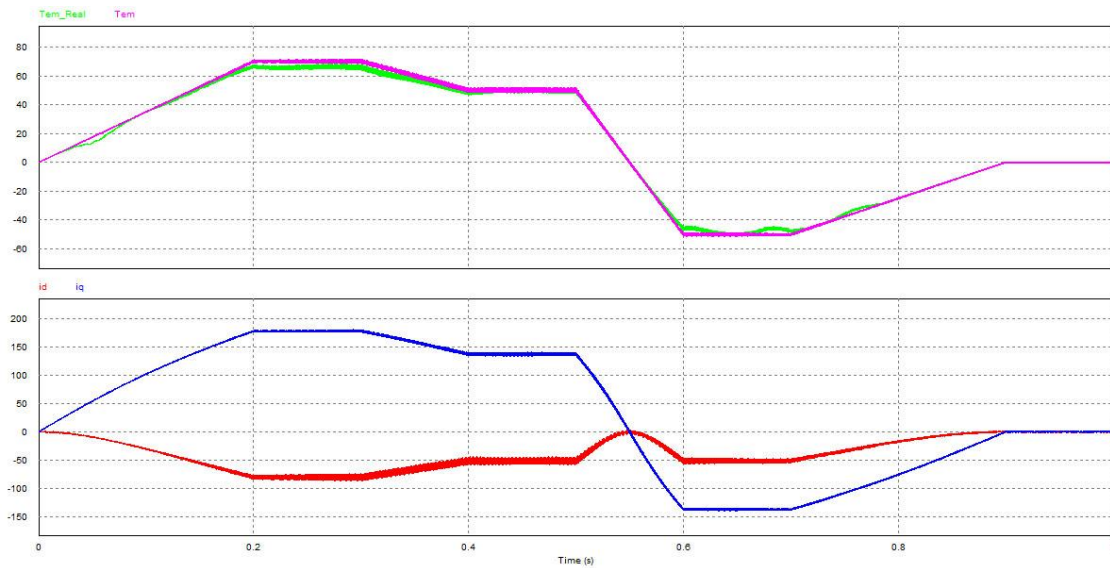


Fig 6.2 - Sensorless operation with regenerative braking. Top graphic: Torque calculated (T_{em}) and torque produced (T_{em_Real}). Bottom graphic: i_d and i_q .

As for the speed and position estimation, the results are presented in Fig 6.3. As shown, there is the same speed estimation error at low speeds that is present with the sensorless algorithm designed in Simulink. But despite that, the result does not affect the stability of the system, neither the position estimation. There are also some estimation imperfections every time the speed has an accentuated change. That would not occur in a physical application like an electric bus because the inertia is such that does not allow quick speed changes thus preventing this singularity from happening. It is also remarkable the result obtained for the position estimation. In the maxim error registered is of 0.4% at 6.014s. The detailed error is presented in Fig 6.4.

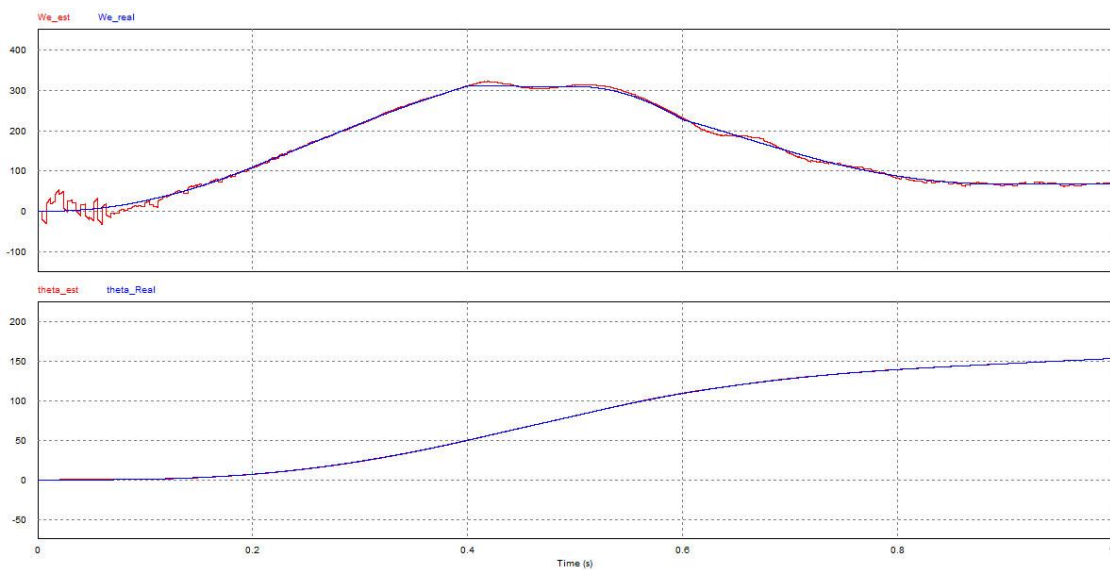


Fig 6.3 - Sensorless operation. Top graphic: Rotor electrical angular speed (W_r - estimated; W_{r_real} - measured); Bottom graphic: Rotor electrical position (θ - estimated; θ_{real} - measured).

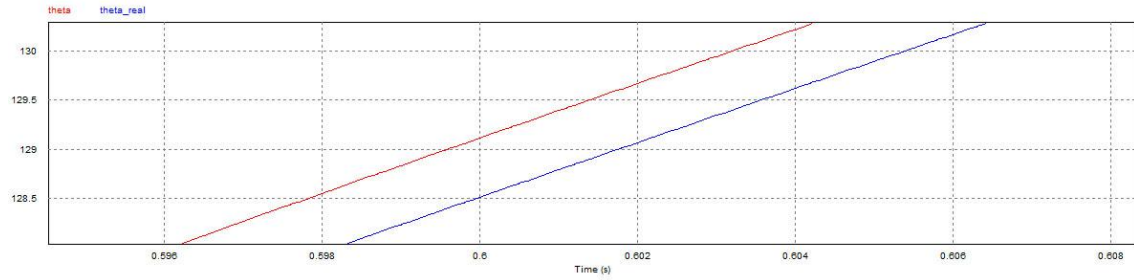


Fig 6.4 - Detail of the estimated position error.

It is important to make sure that the current is actually flowing from the motor to the DC-bus when the motor is braking. To do that a current probe is used in DC-bus. As the current on DC-bus is not filtered and only its average value is important to analyze at this time, a C-Block to calculate its average value is used as described before for the speed and back-EMF components. The result is shown in Fig 6.5.

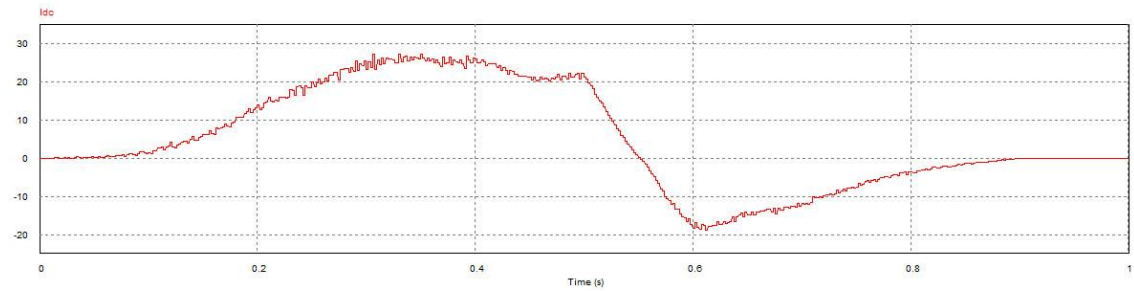


Fig 6.5 - DC-bus average current I_{dc} in traction and braking, with sensorless operation.

It is important to notice two things in this figure. The first is that the DC-bus current inverts direction according to the torque produced. That means that the current is flowing from the motor to the DC-bus when a negative torque is applied, thus effectively achieving energy regeneration while braking. Another important aspect is the fact that the current is null when no torque and no load is applied to the motor. In the situation simulated only the inertia is considered from 0.9s to the end. In this case, the motor maintains the speed but no regeneration is performed because the torque reference is zero. This also can be seen as if the inverter is an open circuit, thus the current flowing is zero. As the rotor is spinning, a back-EMF is induced at the terminals of the motor, which is wasted since there's no current flowing.

To achieve a better performance and to extend at the maximum the battery range, the energy generated when the vehicle is running and there is no braking nor acceleration torque must be harnessed. Conceptually this is done giving a negative torque reference when none of the vehicle's pedals are pressed and the speed is rising, indicating that the vehicle is going down. Mathematically this behavior can be understood by electromagnetic torque mechanical equation presented in (4.1) and repeated here for convenience.

$$T_{em} - T_L = J \frac{d\omega_r}{dt} + B\omega_r \quad (6.1)$$

In a descending ramp the load torque can be considered the rotating force that the wheels do in the motor shaft due to gravitational force. As this force is in the same direction of the speed, load torque T_L becomes positive. In order to maintain the speed, a negative electromagnetic torque should be generated, thus taking advantage of the motor kinetic energy. A high-level algorithm should be implemented in order to evaluate the speed and the driver's reaction, deciding whether or not a negative torque should be generated and how much should it be. It must also be considered the power-torque relation given by (6.2). The rotor speed must be taken into account when considering regeneration because the power generated could not be enough to compensate the inverter's operation.

$$T_{em} \cdot \omega_r = P \quad (6.2)$$

The situation here described is tested and its analysis is presented in the next section.

6.3. System Performance Detailed Analysis

This section pretends to analyze the system performance in terms of dynamic response. Also, a regenerative stage when there is no braking input is tested, as described in the previous section.

Torque and dq current components behavior have already been analyzed, as well as speed and position estimation and even DC-bus current when driving and braking the motor. Next, a detailed analysis of current and torque ripple, current and air-gap flux vectors' angles, and back-EMF is done.

With relation to torque and current, a detailed figure of their ripple is shown below. Also, a comparison between sine-PWM and SVM is performed with the results being displayed in Fig 6.6 and Fig 6.7. The commutation frequency is set to 10kHz and simulation time-step is set to $0.1\mu s$ to avoid loss of definition and control inaccuracies.

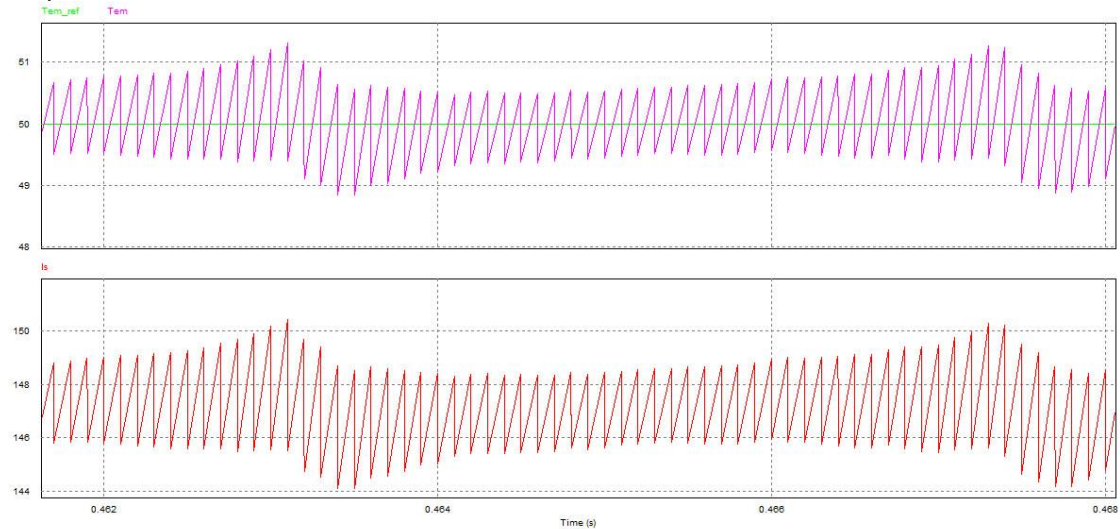


Fig 6.6 - Ripple detail of (top) torque and (bottom) stator current, with sine-PWM at 10kHz.

As shown in Fig 6.6, the maximum torque ripple with sine-PWM at 10kHz is about 2,5Nm and the average is about 1Nm, which is not much ($\cong 3\%$) considering the torque effectively produced of 50Nm. With respect to stator current, the maximum existent ripple is of about 6A and the average ripple is about 2,5A. Once again, relatively to the effective current, the ripple is no considerable ($\cong 2,5\%$), although the ideal goal is 0% ripple.

As for SVM, the results presented in Fig 6.7 show almost the same results: a torque ripple of about 2Nm and a stator current ripple of about 6A in the worst case and about 2,5A in the better case, making an average of about 4A of ripple.

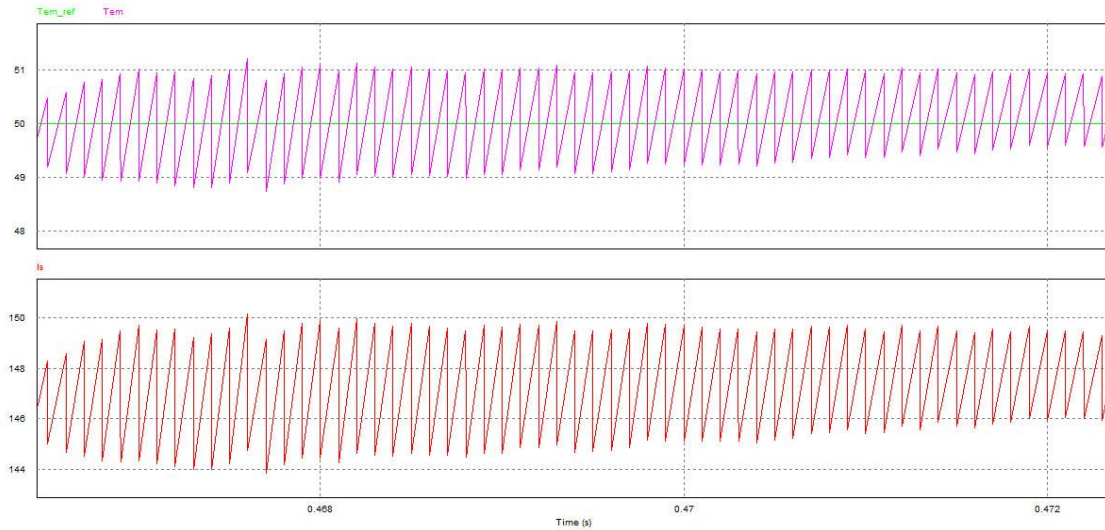


Fig 6.7 - Ripple detail of (top) torque and (bottom) stator current, with SVM at 10kHz.

An unexpected conclusion can be drawn from these results: the SVM has the same results as the sine-PWM with respect to torque and current ripple when the system is working sensorless. It is settled before that the inverter's signal generation would be done with SVM because the results obtained justified the choice. However, in this case, that does not happen. The reason for that may be the fact that in sensorless operation it is needed a lot more processing abilities that may interfere with the SVM routine. Since SVM require much more computation than sine-PWM to be performed correctly, and since the speed and position estimation also introduce delays and errors in the system, those may be the reasons why these two techniques almost do not distinguish themselves with respect to ripple generation. However, using a controller that has high processing performance, like the FPGA, the results could be different, and SVM should have better results than sine-PWM. Moreover, SVM has a better DC usage (about 15% more than sine-PWM) that could be useful in a vehicle application like this one because it can deliver more power to the motor with the same battery capacity. This leads to the usage of less current which decreases the inverter losses, increasing system's efficiency.

With relation to the angles of the current and air-gap flux vectors, they can be seen in Fig 6.8. It is possible to see the variations in both of them as the torque requirements change, as well as the changes in the angle *between* them. Remember: that angle, θ_T , is the torque

angle. It can be observed in more detail in Fig 6.9 for positive torque and in Fig 6.10 for negative torque.

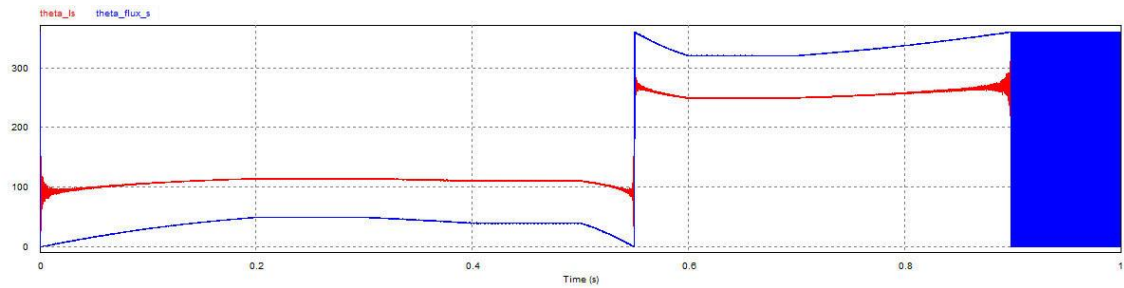


Fig 6.8 - Stator current vector angle θ_i and air-gap flux vector angle θ_λ .

The final blur presented in the figure is because the angles are calculated using the arctangent function. When dq components are zero, the result becomes undefined and simulation result is that of the last instants of Fig 6.8.

It is important to notice that torque angle changes with torque necessities. Although the control method does not control this angle directly, it is inevitable that it changes according to torque requests. However, since the control method used is MTPA, as explained before it tries to use the less current possible to a given torque reference. So, as both current and air-gap flux vectors depend on dq current components, the changes in their amplitudes are directly proportional to each other and consequently the torque angle does not react exactly as expected, that is becoming bigger when more torque is needed. In fact, the torque produced is maximum when torque angle is 90° . However, it does not mean that that's the situation in which less current is used for a given torque. As shown, the torque angle is less when torque reference is 70Nm than when it is 50Nm, but the current is the minimum in any case, and that's what that matters in a vehicle application. Fig 6.9 and Fig 6.10 show the detail of the torque angle for positive and negative torque, respectively.

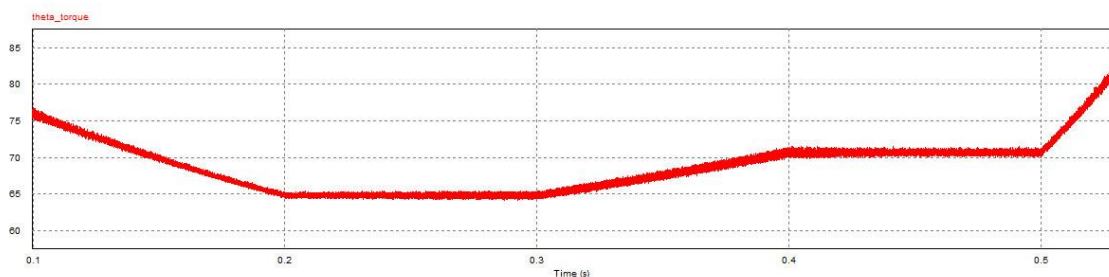


Fig 6.9 - Torque angle detail for positive torque.

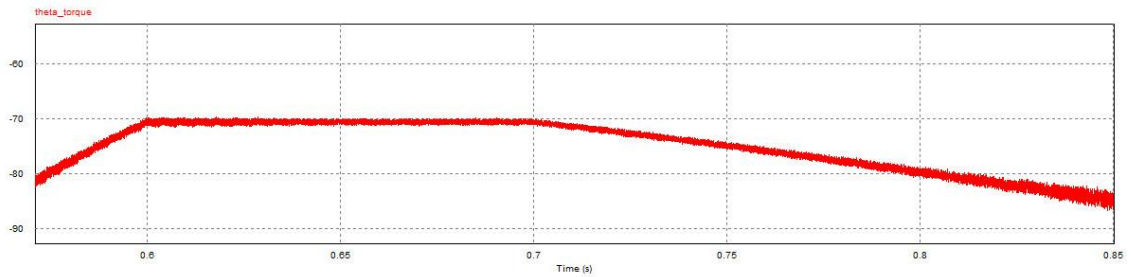


Fig 6.10 - Torque angle detail for negative torque.

The last analysis done to the test performed in the beginning of this chapter is to the back-EMF produced by the motor. As expected it is proportional to the speed of the rotor, and it gives an idea of the amount of power that can be used in regenerative braking. This information could be used in a high-level algorithm that would decide whether or not the regeneration is feasible. Fig 6.11 shows the average by sliding-window of the motor's back-EMF.

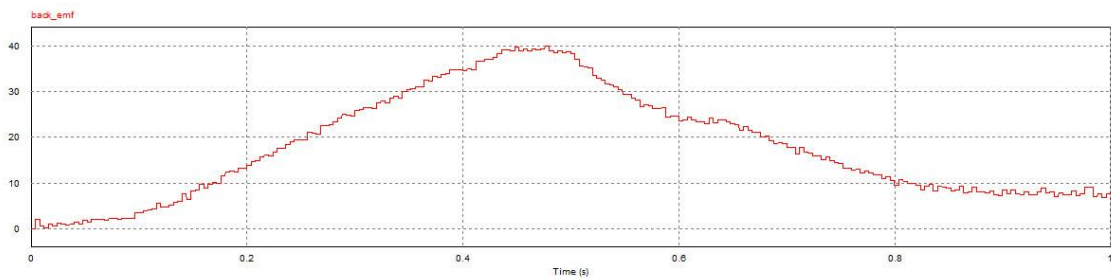


Fig 6.11 - Back-EMF produced by the motor.

The last test performed is to reuse the energy when the vehicle is descending and the driver is not braking. This could be used like a cruise-control feature, available in most of the vehicles nowadays, but with the capability of maintaining the speed not only when the speed is decreasing but also when it is rising. In other words, when the driver does not press any pedal and the vehicle is accelerating, the vehicle's traction control designed could generate a negative braking torque to maintain the speed and reuse some energy to recharge the batteries.

This test is performed and the results of torque produced, load torque, rotor speed and DC-bus current is shown in Fig 6.12. It is important to notice that when the load torque is negative (simulating the vehicle descending) and the motor torque is zero, there is no reusable current and the rotor speed rises. When the motor torque matches the load torque, since it is negative, the back-EMF generated by the rotor is used to generate current flowing from the motor to the DC-bus, charging the batteries.

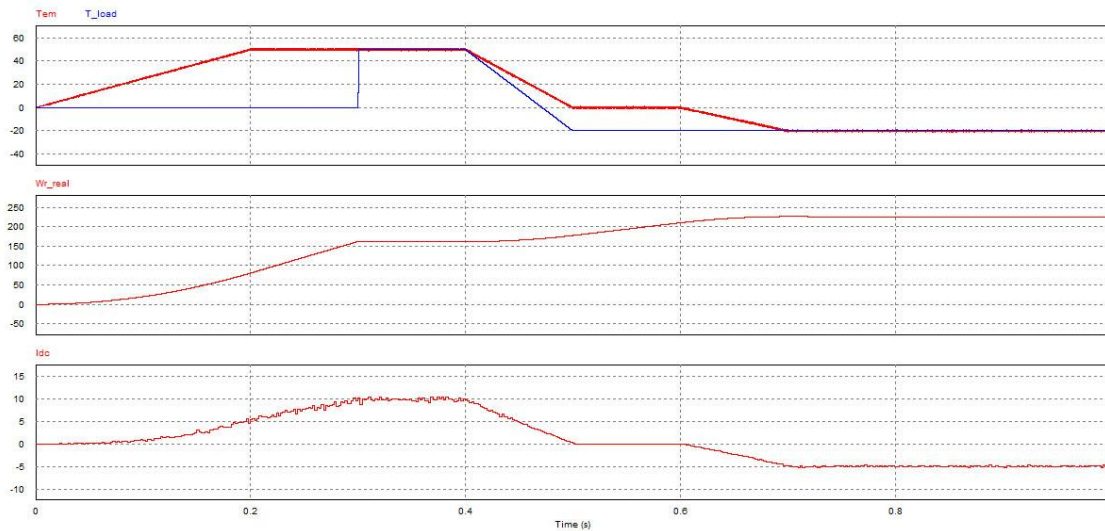


Fig 6.12 - Regenerative feature like cruise-control. Top: torque produced and load torque; Middle: rotor angular speed; Bottom: DC-bus current.

6.4. Hardware Implementation

The final purpose of the work described in this document is to be implemented in CaetanoBus' electric urban bus. But before that, a prototype should be built in order to validate the correct operation of the system in a physical scenario.

Although this implementation could not be achieved, a study of possible implementation solutions is conducted. As described in section 4.3 the most suitable controller platform is the FPGA based one due to its parallel processing abilities and good performance. However, since it works with a fixed-point architecture, the implementation of complex mathematical functions inherent to this controller are very difficult.

Taking advantage of FPGA capability of creating software processor cores called MicroBlaze that could be programmable by C language, this approach is chosen as the best for the purpose of this work. Then, the processing logic is described like this: the processor core created runs the main controller program which contains the logic described in section 4.2.1 as well as the inverters signal generation by SVM described in 4.2.2. The high-level program logic could be implemented in hardware, by VHDL programming, as well as the signals acquisition using FPGA ADCs. The inputs are simultaneously read by processor program in MicroBlaze and high-level logic implemented in hardware, and the data processed at the same time in both programs is shared. At the end of each program the outputs are settled.

Although this approach is theoretically the ideal one, there is an alternative to FPGA that is the microcontroller. It has the advantage of not needing hard previous configuration that FPGA requires and all its programming is usually done in C language. Before choosing any microcontroller solution, as the IGBT inverter module is already given (Fig 6.14), a driver must be chosen. Among several possible manufacturers like International Rectifier, Floeth, Powerex and Concept, and having in consideration the characteristics of the inverter's IGBTs



Fig 6.14 - Infineon IGBT driver module for HybridPACK™1.

6.5. Summary

As the control strategy and methods have already been discussed and their results presented, as well as with sensorless control with positive torque reference, the last test remaining is the validation of regenerative braking without speed or position sensors. This test was only possible with the implementation of sensorless technique in PSIM. That is because of the integration method of Simulink - Runge-Kutta - which is not capable of dealing with some singularities existent when a negative reference torque is given. The simulation results are presented and discussed, proving the successful operability of the system in several load conditions. A detailed analysis of torque, current and flux is also performed. Lastly, a possible solution for controller platform, inverter and drivers to physical implementation of the system is presented.

Chapter 7

Conclusion

7.1. Final Conclusions

In this dissertation a sensorless control technique over a permanent magnet synchronous motor is designed, intended to be applied in an electric urban bus. The design procedure is described and the simulation results are analyzed and discussed.

Initially a research over several electric traction components was done. The research included an analysis of the vehicle's components and the different possibilities for each component. Among them are electric motors for which a comparison between several different types is done. The permanent magnet synchronous motor is chosen due to its higher power density, low size and weight and higher efficiency. The requirements of the system are settled. Then, several types of electronic power converters are described, essentially for the DC-DC conversion. The last one is a three-phase converter that could be used as a DC-AC converter, and it is chosen to this application due to its simplicity and bidirectional power flow ability. Two main control strategies are described: scalar and vector control. Due to its better characteristics, vector control is chosen to this work, so two approaches are studied: DTC and FOC. Due to parameter changes robustness, FOC is chosen to be used. Several methods to apply FOC are described as well as their main characteristics. The rotational dq referential is explained and chosen to be the base of this work because, in steady-state conditions, the motor's quantities are constant. Finally, a brief enunciation of two electronic regenerative braking systems for sale is done, as well as the main electric vehicles in production nowadays.

Next a detailed analysis to the types of permanent magnet synchronous motors and their modeling is done. Their physical operation is explained and mathematical equations in dq referential frame are described. A noteworthy analysis of the torque angle is accomplished, allowing a better comprehension of the various definitions given in the literature, summarizing them and explaining the assumptions that turn valid each definition. The angle between air-gap flux and current vectors is considered to be the torque angle in this document. A brief dynamic analysis of PMSM is done and the chosen motor's parameters are described. Finally, the model described is designed in PSIM and its implementation is explained.

The core of this dissertation is the control design described in Chapter 4. First it is described the strategy of control that is based on a torque reference. Then, three different methods are explained and implemented in PSIM so they could be tested. Two control signal generation techniques for the inverter are described: sine-wave PWM and Space Vector Modulation. Due to its better dynamic and steady-state results, SVM is chosen as the best technique. Then, the basic operation of proportional-integral controllers chosen is detailed and their tuning is explained. Two PIs are used for this work, one that regulates the i_d current and other for the torque (which is proportional to i_q current). Three possible controller platforms are described: DSP, FPGA and micro-controller. It is decided that, in a possible future implementation, FPGA is the best having in consideration the requirements of the system. Also, a specific micro-controller for vehicles application could be a good choice. The results obtained with the three methods are showed and analyzed and because of the better results obtained from MTPA, it is chosen to compare sine-PWM and SVM control signal generation. It is concluded that SVM has better results and for that reason it is chosen to be used in this work. Lastly, the system behavior based on power balance is done with the intention of implementing a possible sensorless solution. Regardless of the good theoretical results, the simulation tests are not conclusive and for that reason this approach is discarded.

The power balance sensorless approach led the way to other techniques of controlling the motor without the need of measuring its speed and position. So, a study of several different strategies used nowadays is done and among the options available in the literature, the one that seemed perfect for the purpose of this work is the PPL-based speed and position estimator. For that reason it is chosen to be implemented. The detailed analysis of this technique is done and the results of its implementation in Simulink (working simultaneously with PSIM by SimCoupler Module) are tested. The results for several positive torque references are analyzed. It is concluded that this approach allow the control of the PMSM and with good dynamic responses.

Finally a system validation is done with detailed analysis of current and torque waveforms, as well as back-EMF generated, current and air-gap flux vectors' angles, and DC-current to prove the ability of regenerative braking. The possibility of regenerating energy in a descending road even without braking is tested successfully. This approach allows an even better range extender for the batteries. In the end, the pretended hardware implementation is described, explaining the principle of operation of FPGA as well as the inverter and drives chosen.

Although this work does not include a physical implementation to validate in laboratory the results obtained, the tests performed in simulation environment were exhaustive, covering several possible real situations (but with time intervals much shorter than the real ones, which guarantee the correct operation of the system in slower tests) and allow the conclusion that it is possible to implement the control designed in a real motor with good results. Furthermore, it is possible to conclude that the method used, MTPA, is the most appropriate for a vehicle application since the current used for the same torque is minimum, giving the higher battery range comparatively to other control strategies. Also, the results obtained with sensorless operation allow the conclusion that it is the better approach to the PMSM control since it has the same overall performance that a system with speed and position sensors, with the advantage of need less wiring and electrical equipment.

The development of this work allowed consolidating the knowledge acquired during the course, with emphasis in power electronics, movement control, signal processing and controllers design. It also improved some soft-skills like the ability of project management, self-discipline, advanced skills in simulation software and writing in foreign language.

7.2. Future Work

In this section several suggestions of possible expansions to the work here described are presented.

- Accomplish a practical implementation of this control in a real PMSM. As already described, the best solution would be with a FPGA controller platform.
- Implement the high-level algorithm to deal with regenerative and emergency braking. In this case, the algorithm should apply the mechanical brake rather than the electrical brake, wasting the kinetic energy but stopping the vehicle safely.
- Apply power balance approach here described to control the motor without rotor position sensor. Several signal filtering techniques should be tested to achieve the best results.
- Have in consideration the permanent magnets' magnetic saturation limits to perform a more realistic simulation and to stipulate more accurately the limits of the controller and possible dynamic adaptation.
- Try different controllers other than PI in order to achieve better dynamic response. A possible alternative would be an artificial neural-network that could auto-adapt to driver's behavior.

References

- [1] C.C. Chan, "The State of the Art of Electric and Hybrid Vehicles", *Proc. IEEE*, Vol. 90, No. 2, February 2002.
- [2] Comparing motor-control techniques. Available in <http://www.ecnmag.com/Articles/2009/10/Comparing-motor-control-techniques/>. Access in January 12, 2012.
- [3] A. Kawamura et al. "State-of-the-Art High Power Density and High Efficiency DC-DC Chopper Circuits for HEV and FCEV Applications", *13th Int. Power Electronics and Motion Control Conference*, 2008.
- [4] Huafeng Xiao and Shaojun Xie, *Member, IEEE*, "A ZVS Bidirectional DC-DC Converter With Phase-Shift Plus PWM Control Scheme", *IEEE Trans. Power Electron.* Vol. 23, No. 2, March 2008.
- [5] Lung-Sheng Yang and Tsorng-Juu Liang, *Senior Member, IEEE*, "Analysis and Implementation of a Novel Bidirectional DC-DC Converter", *IEEE Trans. Ind. Electron.*, Vol. 59, No. 1, January 2012.
- [6] Bogdan M. Wilamowski and J. David Irwin, *The Industrial Electronics Handbook - Power Electronics and Motor Drives, 2nd Edition*. Taylor and Francis Group, LLC 2011.
- [7] Jun Kang, Ph.D. "Control Engeneering - Yaskawa". Available in [http://www.yaskawa.com/site/dmdrive.nsf/link2/NKOE-84VL6B/\\$file/PR.ControlEngineering.05.pdf](http://www.yaskawa.com/site/dmdrive.nsf/link2/NKOE-84VL6B/$file/PR.ControlEngineering.05.pdf). Access in May 23, 2012.
- [8] Rolando P. Burgos et al. "Design and Evaluation of a PLL-Based Position Controller for Sensorless Vector Control of Permanent-Magnet Synchronous Machines", 2006 © IEEE.
- [9] Infineon Technologies AG, "Hybrid Kit for HybridPACK™1: Evaluation Kit for Applications with HybridPACK™1 Module," vol. V2.5, 2012-03-30, 2012.
- [10] Ricardo Soares, "Traction Control for Hybrid Electric Vehicles", to be published in July 2012.
- [11] F. P. Lopes, "Estudo e Comparação de Diferentes Métodos de Controlo de Motores Síncronos com Ímanes Permanentes," M.S. thesis, Dept. Electro. Eng., FEUP, Porto, Portugal, 2008.
- [12] Howard C. Lovatt et al. "Design Procedure for Low Cost, Low Mass, Direct Drive, In-Wheel Motor Drivetrains for Electric and Hybrid Vehicles", 2011 © IEEE.
- [13] Mohammad Kabalo et al. "State-of-the-Art of DC-DC Converters for Fuel Cell Vehicles", Transport and Systems Laboratory (SeT) - EA 3317/UTBM.
- [14] Direct Torque Control versus Field Oriented Control. Available in <http://yantrabazaar.com/Documents/DTC%20VS%20Field%20Oriented.pdf>. Access in January 26, 2012.
- [15] R. Krishnan, *Electric Motor Drives - Modeling, Analysis, and Control*. Prentice Hall 2001.

- [16] Hydrostatic Regenerative Braking System HRB - Bosch Rexroth AG. Available in http://www.boschrexroth-us.com/business_units/brm/en/products_and_solutions/hydraulic-systems/hrb-system/index.jsp. Access in January 10, 2012.
- [17] Continental Automotive - Regenerative Brake System. Available in http://www.conti-online.com/generator/www/de/en/continental/automotive/themes/passenger_cars/chassis_safety/ebs/extended_functions/brems_systeme_en,tabNr=.html. Access in January 10, 2012.
- [18] The Magic of Tesla Roadster Regenerative Braking |Blog| Tesla Motors. Available in <http://www.teslamotors.com/blog/magic-tesla-roadster-regenerative-braking>. Access in January 10, 2012.
- [19] 2012 Ford Focus Electric Vehicle (EV). Disponível em <http://www.ford.com/electric/focuselectric/2012/>. Access in May 21, 2012.
- [20] Veículos elétricos - portal dos motociclos e carros elétricos. Available in <http://www.veiculoselectricospt.com>. Access in May 21, 2012.
- [21] Yilmaz Kurtuluş, *Comparison Of Axial Flux And Radial Flux Brushless Dc Motor Topologies For Control Moment Gyroscope Wheel Applications*, M.S. thesis in Middle East Technical University, Turkey, 2009.
- [22] G. McPherson, *An Introduction to Electrical Machines and Transformers*. New York : John Wiley & Sons, 1981.
- [23] Kiam H. Ang, Gregory Chong, *Student Member, IEEE*, Yun Li, *Member, IEEE*, "PID Control System Analysis, Design, and Technology". IEEE Trans. Control Sys. Technol., Vol. 13, No. 4, July 2005.
- [24] *Xilinx Programmable Logic Design: Quick Start Guide*. Available in http://www.xilinx.com/support/documentation/boards_and_kits/ug500.pdf. Access in May 2, 2012.
- [25] Joaquim R. Monteiro, "Conversão Matricial Trifásica no Condicionamento do Trânsito de Energia Elétrica," Ph.D. dissertation, Dept. Elect. Eng., FEUP, Porto, February 2010.
- [26] Oskar Wallmark, *On Control of Permanent-Magnet Synchronous Motors in Hybrid-Electric Vehicle Applications*. Chalmers University of Technology, Göteborg, Sweden 2004.
- [27] Song Chi, M.S.E.E, "Position-sensorless control of permanent magnet synchronous machines over wide speed range," Ph.D. dissertation, The Ohio State University, Ohio, USA, 2007.
- [28] Peter Vas, *Sensorless Vector and Direct Torque Control*. Oxford University Press, 1998.
- [29] Manfred Schroedl, *Member, IEEE*, "Sensorless Control of AC Machines at Low Speed and Standstill Based on the 'INFORM' Method," 1996 © IEEE.
- [30] P. Thiemann et al. "New Sensorless Rotor Position Detection Technique of PMSM Based on Direct Flux Control", IEEE Proc. 2011 Int. Conf. Power Eng., Energy and Electrical Drives, Torremolinos (Málaga), Spain. May 2011.
- [31] Yoon-Seok Han et al. "Sensorless PMSM Drive with a Sliding Mode Control Based Adaptive Speed and Stator Resistance Estimator", IEEE Trans. Magn., Vol. 36, No. 5, September 2000.
- [32] Vadim I. Utkin, "Sliding Mode Control Design Principles and Applications to Electric Drives", IEEE Trans. Ind. Electron. Vol. 40, No. 1, February 1993
- [33] Malik Elbuluk and Changsheng LI, "A Sliding Mode Observer for Sensorless Control of Permanent Magnet Synchronous Motors", 2001 © IEEE.

- [34] Malik Elbuluk, Changsheng LI, "Sliding Mode Observer for Wide-Speed Sensorless Control of PMSM Drives", 2003 © IEEE.
- [35] Marwa Ezzat et al. "Sensorless Speed Control of Permanent Magnet Synchronous Motor by Using Sliding Mode Observer", 11th Int. Workshop on Variable Structure Systems, Mexico, 2010.
- [36] Babak Nahid-Mobarakeh, *Member, IEEE*, et al. "Back-EMF Estimation-Based Sensorless Control of PMSM: Robustness With Respect to Measurement Errors and Inverter Irregularities". IEEE Trans. Ind. Appl., Vol. 43, No. 2, March/April 2007.
- [37] Jun Sung Park et al. "State Observer with Stator Resistance and Back-EMF Constant Estimation for Sensorless PMSM", 2010 © IEEE.
- [38] Chunyuan Bia et al. "Sensorless DTC of Super High-speed PMSM", Proc. IEEE Int. Conference on Automation and Logistics, China, 2007.
- [39] Hao Zhu et al. "A Simplified High Frequency Injection Method For PMSM Sensorless Control", 2009 © IEEE.
- [40] Matti Eskola, "Speed and Position Sensorless Control of Permanent Magnet Synchronous Motors in Matrix Converter and Voltage Source Converter Applications", Ph.D. dissertation, Tampere University of Technology, Tampere, 2006.
- [41] MathWorks Help - Solver Pane. Available in <http://www.mathworks.com/help/toolbox/simulink/gui/bq7cmisp-1.html#bq9mhyj-1>. Access in May 2, 2012.
- [42] William H. Press et al., "Integration of Ordinary Differential Equations," in *Numerical Recipes: The Art of Scientific Computing*, 3rd ed. New York, Cambridge University Press, 2007, ch. 17, sec. 1.
- [43] Infineon Technologies AG, "EICEDRIVER® 1ED020112-FA Single IGBT Driver IC", Version 1.0 April 2008, 2012.
- [44] CT-Concept Technologie AG, "2SC0108T2Ax-17 Preliminary Data Sheet", Version from 05-11-2009, 2012.
- [45] M. K Syed and Dr. Bv S. Ram, "Instantaneous Power Theory Based Active Power Filter: A Matlab/Simulink Approach", J. Theoretical and Applied Inform. Technology, © 2005-2008 JATIT.
- [46] Jussi Puranen, "Induction Motor Versus Permanent Magnet Synchronous Motor In Motion Control Applications: A Comparative Study," Ph.D. dissertation, Lappeenranta University of Technology, Lappeenranta, Finland, 2006.
- [47] Ying-Shieh Kung et al. "Simulink/ModelSim Co-Simulation of Sensorless PMSM Speed Controller", IEEE Symp. Ind. Electron. And Applicat., Langkawi, Malaysia, 2011.
- [48] Giuseppe Acciani et al. "Time Domain Analysis Of Switching Circuits By Using The Simulink-Based Co-Simulation", 2009 © IEEE.
- [49] Cheng-Hu Chenl et al. "Regenerative Braking Control for Light Electric Vehicles", IEEE PEDS, Singapore, 2011.
- [50] M.K Yoong et l. "Studies of Regenerative Braking in Electric Vehicle", Proc. IEEE Conference on Sustainable Utilization and Development in Engineering and Technology, Malaysia, 2010.
- [51] Andong Yin et al. "Control of Hybrid Electric Bus Based on Hybrid System Theory", 2011 © IEEE.
- [52] Haitao Min et al. "Experiment Study and Control Strategy Simulation On Powertrain For an Electric Bus", Int Conference Electron. & Mech. Eng. Inform. Technology, 2011.